

# For Reference

NOT TO BE TAKEN FROM THIS ROOM

Ex LIBRIS  
UNIVERSITATIS  
ALBERTAEANAE







THE UNIVERSITY OF ALBERTA

Release Form

NAME OF AUTHOR ..... BRENT A. BERRY .....

TITLE OF THESIS ..... CONTAINMENT OF OIL SLICKS .....

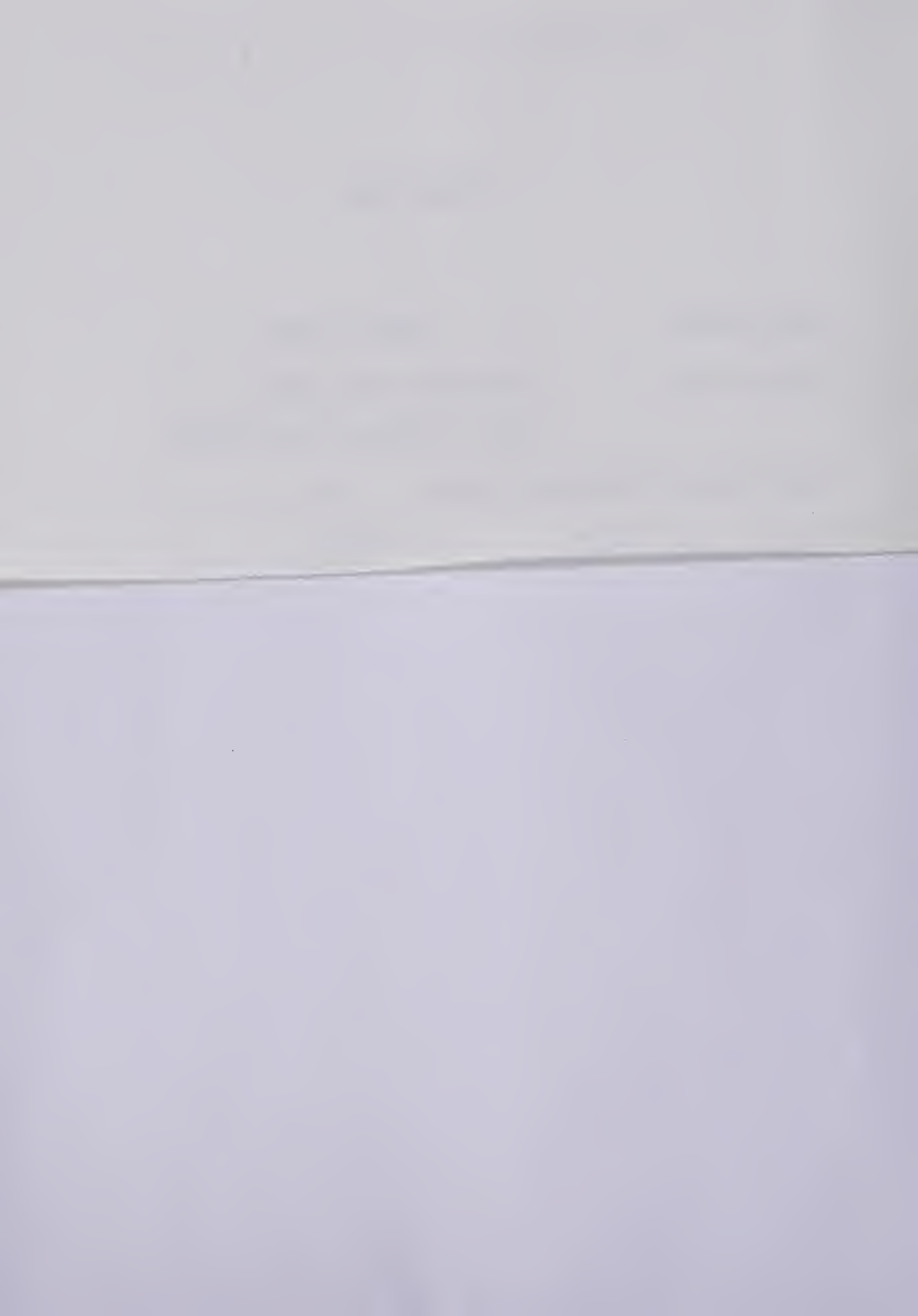
..... UNDER ICE COVERS BY USE OF BOOMS .....

DEGREE FOR WHICH THESIS WAS GRANTED M. Sc. ....

YEAR THIS DEGREE GRANTED 1981 .....

Permission is hereby granted to THE UNIVERSITY OF  
ALBERTA LIBRARY to reproduce single copies of this  
thesis and to lend or sell such copies for private,  
scholarly or scientific research purpose only.

The author reserves other publication rights, and  
neither the thesis nor extensive extracts from it may  
be printed or otherwise reproduced without the author's  
written permission.



THE UNIVERSITY OF ALBERTA

CONTAINMENT OF OIL SLICKS  
UNDER ICE COVERS BY THE USE OF BOOMS

by



BRENT A. BERRY

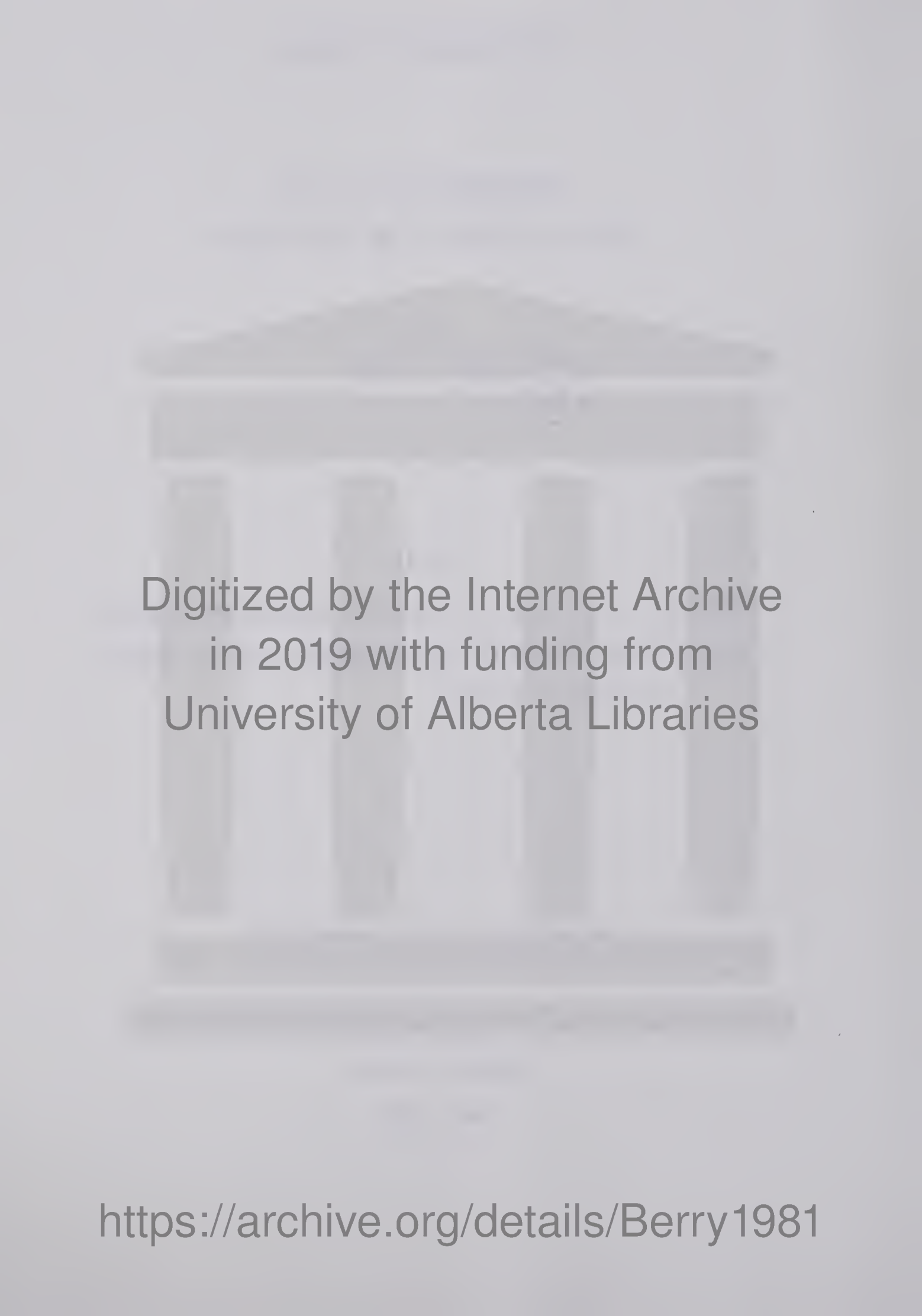
A THESIS

SUBMITTED TO THE FACULTY OF GRADUATE STUDIES AND RESEARCH  
IN PARTIAL FULFILMENT OF THE REQUIREMENTS FOR THE DEGREE  
OF MASTER OF SCIENCE

DEPARTMENT OF CIVIL ENGINEERING

EDMONTON, ALBERTA

FALL 1981

A faint, grayscale background image of a classical building, possibly a temple or a large library, featuring four prominent columns supporting an entablature. The building is set against a backdrop of soft, diffused light, creating a hazy, ethereal atmosphere.

Digitized by the Internet Archive  
in 2019 with funding from  
University of Alberta Libraries

<https://archive.org/details/Berry1981>

THE UNIVERSITY OF ALBERTA  
FACULTY OF GRADUATE STUDIES AND RESEARCH



## ABSTRACT

The influence of a solid ice cover on the general behaviour of a fixed volume oil slick retained by a boom has been studied. A series of experiments have been conducted for both ice free and ice covered oil slicks encompassing a range of Froude Numbers. The study addressed deviations in profile shape, internal oil velocities, and interfacial waves between ice free and ice covered oil slicks. An analytical model describing the internal oil velocity distribution has been developed. The addition of an ice cover was found to increase the oil slick thickness, decrease the oil slick length, and suppress the growth of interfacial waves.



## ACKNOWLEDGEMENTS

The author wishes to express his sincere gratitude to Dr. N. Rajaratnam for his guidance, and advice throughout his studies.

The assistance of both Dr. A. Mercer and Dr. V Galay in reviewing of this study is greatly appreciated.

Thanks are due Mr. S Lovell in constructing and maintaining the test facilities.

The author wishes to acknowledge the contribution of oil supplied by Imperial Oil Ltd. for this study.

The author is grateful to Mrs. C Woolley Berry for her continued encouragement and support during his studies.



## TABLE OF CONTENTS

	PAGE
CHAPTER 1 INTRODUCTION	
1.1 General .....	1
1.2 General Behaviour of Oil Slicks	
Retained by a Boom .....	1
1.3 Scope of Study .....	5
CHAPTER 2 LITERATURE REVIEW	
2.1 General .....	7
2.2 Headwave .....	7
Von Karman (1940) .....	8
Benjamin (1968) .....	9
Wilkinson (1971) .....	12
Hale, Norton, and Rodenberger (1974) ..	15
Milgram and Van Houten (1978) .....	16
2.3 Viscous Zone .....	18
Cross and Hoult (1971) .....	19
Wicks (1969) .....	20
Wilkinson (1971,1973) .....	23
Lindenmuth, Miller and Hsu (1970) ....	26
Hale, Norton, and Rodenberger (1974) ..	29
Milgram and Van Houten (1978) .....	34
2.4 Interfacial Instability .....	38
Wicks (1969) .....	40
Lindenmuth, Miller and Hsu (1970) ....	41



## TABLE OF CONTENTS con't

	PAGE
Wilkinson (1973) .....	41
Hale, Norton, and Rodenberger (1974) .....	42
Kelvin - Helmholtz Instability .....	43
Jones (1972) .....	50
Leibovich (1976) .....	50
Milgram and Van Houten (1978) .....	59
2.5 Summary .....	62
CHAPTER 3 SCOPE OF LABORATORY STUDY	
3.1 General .....	65
3.2 Equipment .....	66
3.3 Measurements .....	70
3.4 Oil Supply .....	80
CHAPTER 4 ICE COVERED OIL SLICKS	
4.1 General .....	82
4.2 Velocity Distribution .....	82
4.3 Shear Stress .....	87
4.4 Interfacial Instability .....	91
CHAPTER 5 EXPERIMENTAL RESULTS	
5.1 General .....	97
5.2 Test Schedule .....	97
5.3 Series A Test Results .....	99
5.4 Series B Test Results .....	103
5.5 Series C Test Results .....	105



## TABLE OF CONTENTS con't

	PAGE
CHAPTER 6 DISCUSSION	
6.1 General .....	107
6.2 Headwave .....	108
6.3 Velocity Distribution .....	109
6.4 Interfacial Instability .....	111
CHAPTER 7 CONCLUSIONS AND RECOMMENDATIONS	
7.1 Conclusions .....	113
7.2 Recommendations .....	114
*****	
TABLES .....	115
FIGURES .....	120
BIBLIOGRAPHY .....	135
APPENDIX A OIL SLICK PROFILES .....	139
APPENDIX B OIL VELOCITY PROFILES .....	151



## LIST OF TABLES

TABLE	PAGE
3.1 OIL PROPERTIES .....	116
5.1 TEST SCHEDULE .....	117
5.2 INTERFACIAL VELOCITY DATA .....	119



## LIST OF FIGURES

FIGURE	PAGE
1.1 CHARACTERISTIC OIL SLICK PROFILE .....	121
2.1 DEFINITION SKETCH .....	122
2.2 VISCOUS ZONE CONTROL ELEMENT .....	123
2.3 MILGRAM AND VAN HOUTEN OIL SLICK .....	124
2.4 INSTABILITY DEFINITION SKETCH .....	125
3.1 SCHEMATIC FLUME CONFIGURATION .....	126
4.1 IDEALIZED VELOCITY DISTRIBUTIONS .....	127
4.2 FORCE BALANCE CONTROL ELEMENT .....	128
5.1 EFFECTIVE LENGTH .....	129
5.2 ICE FREE VELOCITY DISTRIBUTION .....	130
5.3 ICE COVERED VELOCITY DISTRIBUTION .....	131
5.4 CORRELATION OF INTERFACIAL VELOCITY WITH FREE STREAM VELOCITY .....	132
5.5 CORRELATION OF SHEAR STRESS WITH INTERFACIAL VELOCITY .....	133
5.6 CORRELATION OF FRICTION COEFFICIENT WITH REYNOLDS NUMBER .....	134



## LIST OF SYMBOLS

A	=	coefficient
a	=	interfacial wave amplitude
B	=	coefficient
C	=	wave velocity
C	=	shear stress coefficient
C	=	coefficient
D	=	approach water depth
d	=	water depth below oil
d	=	partial derivative
d	=	droplet diameter
F	=	dimensionless Froude Number
G	=	function used by Lindenmuth et al
g	=	gravity
H	=	dimensionless depth = h/D
h	=	depth of oil
$h_1$	=	head loss
i	=	$(-1)^{1/2}$
K	=	wave number
$K_s$	=	grain size roughness
L	=	dimensionless length
l	=	oil slick length
M	=	dimensionless thickness (Milgram and Van Houten)
$M_f$	=	calculated dimensionless thickness
m	=	depth of oil below orginal water surface
$P_*$	=	dimensionless pressure gradient



## LIST OF SYMBOLS. con't

P	=	pressure
q	=	unit discharge
$R_x, R_e$	=	Reynolds Number
S	=	functions of wave velocity
s	=	specific gravity
s	=	wave slope
T	=	surface tension
t	=	time
U	=	velocity
V	=	volume of oil
V	=	vertical velocity
W	=	third velocity component
$W_e$	=	Weber Number
X	=	dimensionless longitudinal distance
x	=	longitudinal distance
Y	=	dimensionless vertical distance
y	=	vertical distance

### Other Symbols

$\Delta$	=	del operator
$\eta$	=	interfacial wave
$\mu$	=	viscosity
$\phi$	=	velocity potential
$\phi'$	=	velocity potential perturbation



## LIST OF SYMBOLS . con't

$\rho$	=	density
$\sigma$	=	shear stress
$\sigma$	=	wave period
$\omega$	=	wave frequency

### Subscripts

a	=	air
av	=	average
b	=	bottom
cr	=	critcal
d	=	droplet
h	=	headwave
i	=	interface
m	=	maximun
o	=	oil
o/a	=	oil - air
o/w	=	oil - water
w	=	water
x	=	longitudinal distance
0,1,2,3,4	=	coefficients



## CHAPTER 1

### INTRODUCTION

#### 1.1 General

During the past decade, considerable investigative research has been directed towards establishing a basic understanding of the dynamic behaviour of oil slicks. The scope of these previous research studies has been limited to the occurrence of oil spills in open (ice free) waters. The frequency of oil spills within ice covered rivers will probably increase as the development of northern pipelines is accelerated. An oil spill, in all likelihood will flow under an ice cover once it enters a river. This trend dictates the necessity for expanding the research to encompass oil spill retention under ice covered water. The objective of this study is to examine particular characteristics of an oil slick retained by a boom under an ice cover in flowing water.

#### 1.2 General Behaviour of Oil Slicks Retained by a Boom

Development of a hypothesis concerning the characteristics of oil slicks under an ice cover requires prior appreciation of the basic behaviour of oil slicks in open flowing waters. For this study the term oil slick is restricted to a fixed volume of oil retained upstream of a boom within a fixed width of channel. The following paragraphs summarize these basic characteristics.

Oil, due to its buoyancy, floats on water and disperses to



form a continuously expanding film. The spreading of an oil slick is the result of two physical forces. First, the force of gravity induces the horizontal flow of oil due to the excess pressure inside the slick. Second, the net pull of surface tension forces at the air - water - oil interface acts in the outward radial direction. These two driving forces are opposed by inertial and viscous forces. This film can be less than a millimetre thick.

The convective movement of the oil slick in flowing water coupled with the extreme thinness of the oil slick dictates that, for economic removal, the oil must be ponded to a sufficient depth by means of a mechanical barrier termed boom. Any attempt to draft off the oil, without an increase in depth, results in the inclusion of large quantities of water, thus adding to the time, and consequently, the costs of removal.

The analysis of an oil slick formed by towing a boom in calm water is similar to the analysis of an oil slick retained by a stationary boom in flowing waters, since the ensuing relative current will pond the oil in front of the boom. Oil retained by a boom assumes a distinctive shape, influenced by the dynamic and viscous shear forces, as a result of the relative current between the flowing water and arrested oil. Figure 1.1 depicts the characteristic shape of the oil slick profile at three different phases induced by various current velocities.

The shape of the arrested oil slick has been divided into



three regions, (indicated in Figure 1.1.b) characterized by the relative magnitudes of viscous and dynamic forces acting longitudinally.

The first region is termed the headwave or frontal zone and portrays the shape of a half arrow-head. The headwave is a distinguishing trait of all two phase density stratified flows in which one fluid advances on the other. The leading edge of an oil slick is similar to those observed when salt water intrudes into fresh water, when a cold front encroaches on a warm front, and when submerged sediment laden water flows into reservoirs. The shape of the headwave is governed by the dynamic force exerted on the oil slick from the balance between horizontal momentum and hydrostatic force.

The second region is designated as the mid-region or viscous zone. The shape of the viscous zone is governed by the cumulative viscous shear forces which supercede the dynamic forces after a distance of about 10 - 20 thicknesses from the leading edge. The viscous shear force induces a "piling up" of the oil which when balanced by the increasing hydrostatic pressure in the oil, results in a gradual thickening of the slick from its minimum thickness immediately downstream of the headwave.

The third region is termed the near boom zone. The boom protrudes deeper than the oil slick forming a stagnation point as water flows beneath the boom, which induces a local thinning of the oil slick upstream of the boom.



The prediction of equilibrium oil slick thicknesses for diverse velocity ranges is derived from detailed analysis of the preceding regions. Typical profiles of oil slicks at three such velocity ranges are portrayed in Figure 1. The transition between these ranges are not clearly distinguishable and the limits vary with the properties of oils. Order of magnitude velocity boundaries are given in Figure 1.1 for the three states of oil slick profiles.

A comprehensive study of the oil slick phenomenon not only considers the equilibrium profile described above, but also includes an examination of oil slick behaviour beyond the range of equilibrium velocity limits. Failure of a boom to retain oil is the consequence of two independent mechanisms. The first, referred to as drainage, is simply the lack of sufficient boom draft to arrest the oil. The thickness of the slick at the boom is predominantly dictated by the relative velocity of the water resulting in an equilibrium thickness and length of slick for a given volume of oil and velocity. Therefore, if the boom draft is too shallow, the oil will flow under the boom sufficiently reducing its volume until a new equilibrium thickness, compatible with the existing boom draft, is established. Oil slick drainage due to insufficient boom draft occurs very quickly and can ultimately result in considerable loss of oil.

The second mode of failure, entitled entrainment, is independent of boom design and occurs at higher water velocities. Superimposed over the length of the oil slick are interfacial waves travelling longitudinally from the leading edge of the oil slick to



the boom. When two different liquids move, with different tangential velocities across their interface, the kinetic energy of motion will cause undulations on the interface to grow in amplitude. This phenomenon is called Kelvin - Helmholtz Instability.

As the water velocities exceed a certain critical value, these interfacial waves break, resulting in oil droplets being entrained into the flowing water. Owing to the buoyant properties of the oil, these droplets will rise to the oil-water interface and migrate towards the boom. Consequently, if the slick is of insufficient length so that the oil droplets do not have time to rise to the oil slick and coalesce before reaching the near boom region, they will be swept under the boom. It is the loss of oil which does not coalesce and is swept past the boom that constitutes entrainment loss. Even though the critical droplet formation velocity is sustained, there may be no actual loss of oil. The majority of the wave breaking and oil droplet entrainment occurs in the headwave region as indicated in Figure 1.1.c. Prevention of oil entrainment is not suppressed by a well adapted boom design but rather by the appropriate deployment of the boom.

### 1.3 Scope of Study

The previously mentioned description of the characteristic traits of oil slick behaviour in open waters are well documented in available literature (Wicks (1969), Lindenmuth, Miller, and Hsu (1970), Cross and Hoult (1971), Wilkinson (1971, 1973), Hale, Norton, and Rodenberger (1974), and Milgram and Van Houten (1978)). However,



the current state of knowledge regarding the effects of an ice cover is deficient. This thesis studies the differences in behaviour of ice covered oil slicks from ice free oil slicks.

The scope is restricted to the treatment of a solid ice cover as a boundary condition and does not consider deviations in dynamic behaviour as induced by changes in the physical properties of the oil resulting from interaction between oil and ice. The emphasis of the study addresses the basic characteristics of the oil slick profile and interfacial stability rather than the detailed design of booms or recovery methods. As indicated earlier, the oil slick under question is composed of a fixed volume of oil retained upstream of a rigid boom in a fixed width flowing channel.

The approach used in the remainder of this study is as follows. First, a presentation of a detailed literature review of ice free oil slicks is given in Chapter 2. Chapter 3 outlines the laboratory study of oil slicks both with and without an ice cover. Chapter 4 develops various mathematical relationships describing the expected differences between ice free and ice covered oil slicks. Chapter 5 presents the experimental results and Chapter 6 develops an interpretation of these results which leads to an explanation for the increased thickness of the oil slick profile under an ice cover and for the apparent stability of the oil-water interface. Finally, Chapter 7 summarizes the conclusions and suggests recommendation for further study.



## CHAPTER 2

### LITERATURE REVIEW

#### 2.1 General

The objective of this study, (as previously stated), is to examine specific characteristics of an oil slick retained by a boom under an ice cover in flowing water. As a preparatory phase, an extensive survey of existing literature was conducted. This survey encompassed the analytical and experimental studies pertaining to the headwave phenomena, the effects of currents on viscous zone development, oil entrainment and drainage failure, interfacial stability and other related subjects. The major emphasis of the reviewed studies was restricted, in scope, to ice free conditions, whereas the limited amount of literature addressing the problem of ice covers neglected the dynamic behaviour of oil, but rather investigated the physical properties of the oil and their interaction with ice.

This chapter presents a concise summary of the afore-mentioned oil slick studies through the examination of individual components involved in the oil slick phenomena.

#### 2.2 Headwave

The leading edge of all density stratified flows is customarily designated as the headwave (Figure 2.1.a). The characteristic shape, and subsequently the analysis, of an oil slick



headwave is analogous to that of submerged gravity currents investigated by several researchers as saltwater intrusions.

Dimensional analysis reveals that the details pertaining to stratified flow can be described by three basic non-dimensional parameters. These parameters are: the Reynolds Number (ratio of inertial to viscous forces), the Weber Number (ratio of inertial to interfacial tension forces), and the Densimetric Froude Number (ratio of inertial to buoyant forces). Wilkinson (1971) has demonstrated that flow in the vicinity of the headwave is dominated by the dynamic and buoyant forces. Consequently the effects of interfacial surface tension and viscosity are secondary, thus the headwave phenomena can be adequately characterized by the Densimetric Froude Number. Designating the approach velocity as  $U$ , the specific gravity of oil as  $s$ , with the headwave thickness as  $h$ , then the Densimetric Froude Number (hereafter termed the Froude Number) is defined as:

$$F_h = \frac{U}{[g (1-s) h]^{1/2}} \quad (2.2.1)$$

#### Von Karman (1940)

An ideal fluid model for steady propagation of gravity currents derived from the application of the steady state irrotational Bernoulli Theorem, applied between the stagnation point forward of the leading edge of the headwave, and points on the interface downstream was postulated by Von Karman. Assuming that the interface becomes horizontal, the resulting relationship between the propagation



velocity ( $U$ ) of the gravity current and current thickness ( $h$ ) is:

$$h = \frac{U^2}{2g(1-s)} \quad (2.2.2)$$

In comparison to Equation (2.2.1) this yields a Froude Number of  $\sqrt{2}$ .

### Benjamin (1968)

Benjamin presents a comprehensive treatment involving the application of inviscid fluid theory to steady gravity currents, in which he disputes Von Karman's assumption of energy conservation as unjustifiable. Rather, Benjamin states that a more fundamental condition is the overall balance of momentum flux against hydrostatic forces in the fluid.

The theoretical analysis of the headwave, regardless of whether the gravity current is the bottom fluid (as in the case of oil slicks) is similar. In this analysis, the gravitational constant  $g$  will appear multiplied by a similar factor of  $(1-s)$ . Expanding this concept, Benjamin argues that the upper fluid could be replaced by an air-filled cavity displacing liquid beneath a horizontal boundary. However, to establish continuity within this review, the following theoretical results extacted from Benjamin's paper include the factor  $(1-s)$ .

Equating the change in the momentum flux with the pressure forces between an approaching section of depth  $D$  and a downstream



section beneath the oil slick of depth  $d$ , coupled with the equation of continuity, the following relationship for the downstream depth  $d$  as a function of the approach velocity  $U$  is obtained.

$$\frac{U^2}{g(1-s)D} = \frac{d(D^2 - d^2)}{D^2(2D - d)} \quad (2.2.3)$$

Alternately, expressed in terms of the headwave thickness  $h = D-d$ , Equation (2.2.3) defines the Froude Number as:

$$F_h = \frac{(D-h)(2D-h)}{D(D+h)} \quad (2.2.4)$$

This definition of the Froude Number for the headwave is derived on the basis of momentum balance.

A second equation incorporating a headloss  $h_L$  can be obtained from the application of the Bernoulli energy equation between the same approaching section and receding downstream section. The momentum equation combined with this energy equation yields the following relationship for energy loss  $h_L$  in terms of the headwave thickness:

$$h_L = \frac{(D-2h)h^2}{2(D^2-h^2)} \quad (2.2.5)$$

If energy was conserved, (i.e.  $h_L=0$ ), as assumed by Von Karman, then the non-trivial solution of Equation (2.2.5) reveals that the headwave thickness  $h$  must occupy exactly one half the depth of flow in the approaching section. However, the headwave thickness, as reported by various investigators, assumes a range of values all of



which are considerably less than one half the approaching flow depth. Moreover, observed headwaves are characterized by the leading front possessing a wave like form (so called "head") whose peak obtains a thickness up to twice the downstream height. Observations reveal that the leeward side of this wave is a highly turbulent zone suggesting some form of wave breaking. This wave breaking process is indicative of an energy loss mechanism, and Equation (2.2.5) dictates the energy loss mechanism, and Equation (2.2.5) dictates the energy loss requirements, for various headwave thicknesses, necessary to satisfy the governing momentum Equation (2.2.4).

Specifying  $h_m$  as the maximum thickness of the leading wave trough, and using the concepts of irrotational flow beneath the receding oil slick (at thickness  $h$ ) is subcritical. This condition is satisfied when the range of downstream thicknesses exceeds  $h / D > 0.6527$ .

The headwave observed at the front of oil slicks is essential, not merely incidental, to the dissipative processes necessary to satisfy both the momentum and energy considerations. Utilizing an integral form of momentum balance and Bernoulli's theorem, Benjamin established that magnitude of the maximum headwave thickness  $h_m$  must adhere to the following relationship:

$$h_m / h > F_h^2 \quad (2.2.6)$$

⋮

For the limit of infinite depth, Equation (2.2.4) yields the value of



the Froude Number  $F_h$  as  $\sqrt{2}$ . Keulegan (1958) reports on his experiments involving saltwater wedges a ratio of  $h_m/h$  as 2.36 which complies with the theoretical condition of Equation (2.2.6).

### Wilkinson (1971)

The previous theoretical analysis and accompanying experimental studies were motivated by the need to investigate gravity currents other than the oil slick phenomena. A direct analysis of the oil slick headwave (which closely parallels the arguments employed by Benjamin) was conducted by Wilkinson. As previously disclosed, Wilkinson demonstrated the dominance of dynamic over viscous forces in the vicinity of the headwave. The momentum flux under the oil slick results in the slick experiencing a balancing pressure force of the order  $\rho_w U^2 h$ . The slick is simultaneously subjected to a viscous shear force, resulting from the cumulative interfacial shear stress of the order:

$$\sigma_i = C_i \rho_w \frac{1}{2} U^2 dx$$

The ratio of shear forces to dynamic pressure forces at any section from the front of the oil slick will be of the order:

$$\frac{C_i}{2} \times \frac{x}{h}$$

Extracting from the experimental work of Cross and Hoult (1971), the value of the interfacial shear coefficient of an oil slick  $C_i$  as



0.01, Wilkinson concludes that the dynamic forces exceed the viscous forces by a factor of 10 for approximately 20 slick thicknesses downstream from the front of the slick.

Equating the dynamic pressure forces with the momentum flux, Wilkinson's resulting momentum equation for the Froude Number in terms of a relative depth  $H = h/D$  is:

$$F_h = \left[ (2-H) \left( \frac{2H}{1-H} + \frac{1}{s} \right)^{-1} \right]^{1/2} \quad (2.2.7)$$

Examining the case of infinite depth, Equation (2.2.7) yields the value of the Froude Number  $F_h$  as  $(2s)^{1/2}$ . The resulting value for the headwave thickness  $h$  deviated from Benjamin's prediction by the factor  $1/s$ . This difference stems from the replacement of Benjamin's air cavity under a solid boundary with an oil slick at a free surface. Wilkinson's analysis accounts for the rise of the oil slick above the mean free surface of the approaching section. If Wilkinson's stagnation point was taken at the top of the oil surface, then Benjamin's results are obtained.

Experiments on peanut oil, conducted by Wilkinson, corroborate the theoretical relationship of Froude Number variation with relative depth. Comparison between various other experimental studies and the theoretical analysis presented by Benjamin and Wilkinson reveals a tentative verification of the ideal fluid theory but also exhibits deviations arising from real fluid properties. Keulegan reported a Froude number of  $F_h = 1.2$  for a saltwater wedge



with a relative depth ratio of  $h/D$  of 0.111. The corresponding theoretical Froude Number of  $F_h = 1.23$ , as predicted from Equation (2.1.4) is in close agreement. Oil slick studies performed by Lindenmuth, Miller, and Hsu (1970) describe values of the Froude Number  $F_h$  ranging from a low of 1.0 to a high of 1.3. Lindenmuth et al noted that the Froude Number decreased as the oil slick thickness (and consequently the relative depth) increased, which is a direct interpretation of the afore-mentioned theoretical analysis. However, consideration of the experimental facilities utilized indicates that there was insufficient variation in the relative depth to account for the range of observed Froude Numbers. Two real fluid properties were considered to be instrumental in producing the variations in Froude Numbers. It was remarked that increasing interfacial surface tension tends to reduce the thickness of the headwave at a given speed.

A second observed property is that an increase in viscosity apparently induces a greater thickness of the headwave at a given water current.

Benjamin resolved in his discussion of experiments by Zukoski (1966) involving the advance of an air bubble in a long water filled tube, that the reduction in observed propagation velocity, as noted by Zukoski, were smaller than predicted by theory due to the effects of surface tension. The surface tension influenced the propagation velocity by two distinct mechanisms. First, the neglect of surface tension would over estimate the balancing pressure in the headwave at



the stagnation point, and secondly, the downstream forces balancing the momentum flux should be lower due to the contribution of surface tension at the interface. Though Zukoski's experiments revealed that surface tension effects resulted in a reduction of the propagation velocity, an alternative interpretation, similar to that of the Lindenmuth et al study, is that the surface tension contributes to a reduction in the headwave thickness at a given water current.

Hale, Norton, Rodenberger (1974)

Realizing the role of real fluid properties, Hale et al, developed an equation for the headwave thickness in which the effects of surface tension ( $T$ ) and viscosity ( $\mu_w$ ) were incorporated. Correlating the Froude number with Reynolds and Weber numbers, by the utilization of a least squares fit to their experimental data, the following relationship for the maximum headwave thickness ( $h_m$ ) was developed;

$$h_m = \frac{7.535.U^{3.254} \mu_w^{0.0157}}{g (1-s)^{1.325} T^{0.325}} \quad (2.2.8)$$

This relationship indicates the magnitude of the influence the effects of real fluid properties exercise on the development of the headwave thickness. Similar to the observations of Lindenmuth et al, Equation (2.1.8) reveals that comparatively, as the viscosity increases, so does the headwave thickness, and that increases in surface tension result in a decrease in headwave thickness.



Milgram and Van Houten (1978)

In a recent study, Milgram and Van Houten dispute the hypothesis, as prescribed by Wilkinson and others, that the dynamic forces predominate the viscous forces in determining the headwave profile.

The afore-mentioned analysis by Benjamin and, again, by Wilkinson, indicated that an energy loss must occur to satisfy the momentum flux requirements. If viscous shear forces are neglected the only mechanism for dissipation of energy is the breaking of the leeward side of the headwave which results in the generation of rotational flow and a consumption of energy. However, Milgram and Van Houten advocate that the consideration of a free surface and shear stress at the oil water interface remove the theoretical necessity for breaking of the headwave.

Various experimental studies including Wicks (1968), Wilkinson and Lindenmuth et al all observed that the headwave would break only at the higher velocities tested. Their studies focused solely on the spatially constant shear stress in the viscous downstream zone, and as a result neglected to include the effects of shear stress in the vicinity of the headwave.

The major emphasis of the Milgram and Van Houten investigation was the disclosure of the relative importance of shear stress not only in the downstream viscous zone but, also, its role in



the development of the headwave profile. Evaluation of the oil slick profile and its dependence on shear stress was accomplished through the following analysis.

It was assumed that a potential flow approximation of the flowing water phase was accurate for predicting pressures in the water. Thus the pressure along the bottom of the oil layer was calculated for potential flow along the oil slick profile measured experimentally. This calculated pressure distribution and the measured oil thickness distribution were in turn implemented to determine the shear stress distribution utilizing an equation relating the interfacial shape, pressure and shear stress. Although the complete details of the development of the equation are contained in a following section dealing with the viscous zone, the basic rationale of the equation consists of a force balance for a differential element of the oil slick. In order to compare the relative effects of friction and pressure on the determination of the interfacial shape, a new oil slick thickness distribution in the absence of dynamic forces was calculated by the previous equation using the calculated shear stresses and setting the dynamic pressure and its horizontal derivatives to zero. Milgram and Van Houten present several plots of the experimentally measured profiles and calculated profiles based on shear stress for a complete range of experimental conditions. In the range of lower velocities, and consequently for oil slicks without the observed breaking headwave, the two profiles match satisfactorily. The most remarkable feature of the analysis was that the calculated friction coefficients in the vicinity of the headwave assumed a range



of values exceeding those previously reported in the literature by a factor of 10. As a result of the apparent matching of the calculated and measured oil slick profiles and large shear at the headwave Milgram and Van Houten concluded that the previously cited assumption that friction is unimportant in the headwave development is ill-founded. However, observation of the calculated profiles at the high velocities revealed that their analysis deteriorates to the point of inaccurately describing the development of a breaking headwave.

### 2.3 Viscous Zone

In the mid region of the oil slick between the headwave and the restraining boom the oil slick undergoes more gradual thickening than in the headwave. Contrary to the headwave zone where the dynamic pressure forces contribute to the development of the oil slick profile, the viscous shear stresses are predominantly responsible for the profile in the mid region. Hence, this region is entitled the viscous zone (Figure 2.1.b).

The viscous shear forces are cumulative along the length of the slick downstream from the leading edge of the oil, thus contributing to a gradual increase in the thickness of the oil slick. The cumulative shear forces are balanced by an increasing hydrostatic pressure gradient corresponding to the increasing thickness of oil.

Associated with the viscous shear forces are interfacial waves superimposed on the mean oil slick profile. These waves



originate at the leading edge of the oil slick and travel downstream through the viscous zone with a characteristic shape and velocity. Section 2.4 (Interfacial Instabilities) covers this phenomenon in detail. The remainder of this section is concerned strictly with the development of the mean oil slick profile in the viscous zone.

### Cross and Hoult (1971)

One of the original analysis of the viscous zone was presented by Cross and Hoult. Their experiments were conducted for a low range of water velocities at which no noticeable headwave was formed and thus their analysis did not distinguish between a headwave and a viscous zone.

Assuming the momentum flux within the oil to be an order of magnitude less than the momentum in water, Cross and Hoult equated the hydrostatic pressure gradient arising from the depth of oil  $h$ , to the interfacial shear stress  $\sigma_i$ . This force balance takes the form of;

$$\rho_w g(1-s) h \frac{dh}{dx} = \sigma_i = \frac{1}{2} \rho_w C_i U^2 \quad (2.3.1)$$

If the coefficient of friction  $C_i$  is assumed to be constant, as suggested by their experiments, then the integration of Equation (2.3.1) yields the following relationship for the oil slick profile;



$$h^2 = \frac{U^2}{g(1-s)} C_i x \quad (2.3.2)$$

The oil slick profile assumes a parabolic shape with the thickness growing to the one half power of the longitudinal distance. The experimental profiles revealed values for the coefficient of friction  $C_i$  to be 0.005 for No. 2 oil and 0.008 for soybean oil.

Cross and Hoult's argument for a spacial constant value of the coefficient of shear friction  $C_i$ , used to evaluate the interfacial shear as a function of the approach water velocity, were based on the following analogy employing a sand roughened flat plate. At low Reynolds Number  $R_x$  (Reynolds Number expressed with longitudinal distance  $x$  as a length scale), the plate appears smooth and  $C_i$  will decrease with increasing distance  $x$ . However, at higher values of  $R_x$  (supposedly after the headwave region) if the grain roughness  $K_s$  increases with distance such that the ratio  $K_s/x$  remains constant then  $C_i$  will attain a constant value. Cross and Hoult observed that the interfacial waves would grow in magnitude as they migrated downstream, and thus, they argued that the increasing wave amplitudes provided an increasing roughness height  $K_s$ , sufficient to yield a constant value for the coefficient of friction.

### Wicks (1969)

A considerably more complex analysis of the viscous zone was developed by Wicks in which he utilized experiments encompassing a broader range of flow conditions conducted on a much larger scale.



Wicks observed the headwave zone to be distinct from the viscous zone. Based on a concept of boundary layer separation and reattachment, Wicks defined the start of the viscous zone at a distance of  $25 h_m$  (maximum headwave thickness) from the leading edge of the oil slick. Wicks draws an analogy to Plate's (1964) investigation of abrupt surface roughness in a turbulent boundary layer, in which reattachment occurred about 50 disturbance heights downstream. Benjamin has shown that the maximum headwave thickness to be approximately twice the thickness of the downstream neck of the headwave. Wicks took the difference in thickness to be analogous to an abrupt surface roughness and consequently assumed that reattachment occurs at a distance of 25 times the maximum headwave thickness as given by Benjamin.

Reattachment of the boundary layer in flowing water induces a drag on the oil interface which in turn sets up a circulation within the oil layer. Wicks' analysis of the progressive thickening of the oil slick involves the simultaneous solution of the following three equations. First, the circulation in the oil phase is related to the interfacial drag by the application of the Navier-Stokes equation. Assuming a linear velocity distribution between the downstream oil-water interfacial velocity  $U_i$  and the upstream oil-air interfacial velocity  $U_t$ , will yield a relationship between the oil-water interfacial velocity  $U_i$  and the interfacial shear stress  $\sigma_i$  as follows;



$$U_i = \frac{\sigma_i h}{2 \mu_0} \quad (2.3.3)$$

Boundary layer theory is used to describe the local shear stress caused by the water flow as a function of the difference between the free stream velocity and interfacial velocity as;

$$\sigma_1 = 1/2 \rho_w C_i (U - U_i)^2 \quad (2.3.4)$$

Wicks adopts, from Schlichting, two relationships for the coefficient of friction as functions of the Reynolds Number  $R_x$ . Finally, a force balance in the horizontal direction shows that the slope of the interface must exactly balance the interfacial shear stress;

$$\sigma_i = \rho_o g h \frac{dh}{dx} \quad (2.3.5)$$

Numerical solution of these relationships yields a prediction of the slick thickness as a function of the longitudinal distance.

A literature review by Lau and Kirchefer (1974) outlines two criticisms of Wicks' analysis. First, the assumption of a linear velocity profile within the oil is inconsistent with other reported observations in which the oil-water interfacial velocity exceeds the oil surface velocity several times. Secondly, Wicks' force balance Equation (2.3.5) has neglected the component of the hydrostatic pressure in the direction of the sloping interface.



Wilkinson (1971, 1973)

A third method of analysis for the viscous zone was described by Wilkinson. The emphasis of his study focused on the endeavor to incorporate the boundary effects inherent in a finite depth of flow. Wilkinson's force analysis of the headwave zone (Section 2.1) indicated that after some 20 thicknesses downstream any further increase in thickness was due to viscous effects. Downstream of the headwave zone, Wilkinson utilized the following three assumptions to develop a viscous zone model:

- 1) The momentum flux due to circulation in the oil slick is small in comparison to the interfacial shear forces.
- 2) The flow beneath the oil slick is steady and uniform in distribution over the depth of flow.
- 3) The equilibrium of the retained oil slick dictates that any change in the longitudinal gradient of inertial and pressure forces must be balanced by the boundary shear stress.

This third premise equally applies to a control element composed of the oil slick and underlaying water flow, or a control element of the oil slick alone (Figure 2.2).

Wilkinson derived the following equation for an overall momentum balance in terms of unit discharge  $q$ ;

$$\frac{d}{dx} \left[ \frac{1}{2} \rho_w g s (d+h)^2 + \frac{1}{2} \rho_w g(1-s) d^2 + \frac{\rho_w q^2}{d} \right] = -\sigma_b \quad (2.3.6)$$



Consideration of the forces acting on a control element consisting of the oil slick alone yields;

$$\frac{d}{dx} \left[ \frac{1}{2} \rho_0 g s h^2 \right] = \sigma_i - \rho_0 g s h \frac{d(d)}{dx} \quad (2.3.7)$$

The boundary and interfacial shear stresses are defined respectively as;

$$\sigma_b = 1/2 C_b \rho_w U^2 \quad \text{and} \quad \sigma_i = 1/2 C_i \rho_w U^2$$

In terms of the densimetric Froude Number, Equations (2.3.6) and (2.3.7) can be combined non-dimensionally to form;

$$2H \frac{dH}{dX} [D_t - (H + (\frac{F}{D_t - H})^2)] = (\frac{F}{D_t - H})^2 [ \text{Term A} ] \quad (2.3.8)$$

$$\text{Term A} = \frac{C_i}{s} [D_t - (1-s)(H - (\frac{F}{D_t - H})^2)] + C_b H$$

$$\text{In which } H = \frac{h}{D}, D_t = \frac{d}{D}, X = \frac{x}{D} \text{ and } F = \frac{U}{[g(1-s)D]^{1/2}}$$

Equation (2.3.8) contains a singularity for the interfacial slope  $dH/dX$  when;

$$D_t = H + (\frac{F}{D_t - H})^2 \quad (2.3.9)$$

At lesser values of  $H$ , the interfacial slope  $dH/dX$  is positive, indicating a thickening of the oil slick. The interfacial slope becomes infinite for the singularity at the critical thickness.



Finally, for larger values of  $H$  the interfacial slope is negative.

A peculiar characteristic of the critical oil slick thickness, given by Equation (2.3.9), is its independence from viscous forces. However, the maximum length of a slick at which this critical thickness occurs depends totally on the magnitude of viscous stresses.

Numerical integration of Equation (2.3.9), between the oil slick thickness at the neck of the headwave and the critical thickness, indicates the maximum length and consequently the volume of the viscous zone is a function of the Froude Number and the magnitude of the interfacial ( $C_i$ ) and boundary ( $C_b$ ) coefficients of friction. This procedure reveals that the dimensionless depth  $D_T$  does not exceed unity by more than a few percent and, therefore, the maximum dimensionless slick thickness can be adequately expressed as;

$$H = 1 - F^{2/3} \quad (2.3.10)$$

Small scale experiments performed by Wilkinson indicate the interfacial shear stress coefficient  $C_i$  is not spatially constant as originally assumed, but rather, decreases with the longitudinal distance. This concept was observed as a more gradual thickening of the oil slick than that predicted by Equation (2.3.8). If Wilkinson had incorporated a spatially varying coefficient of friction into his analysis, the singularity of Equation (2.3.8) and resulting critical thickness would not have been affected, since the critical thickness criteria stems from a Froude Number instability.



Lindenmuth, Miller and Hsu (1970)

In an attempt to investigate the role of waves on the performance of various oil slick retention devices, a series of large scale oil slick tests were conducted by Lindenmuth et al. A preliminary set of experiments were performed in the absence of waves to establish a set of control data.

In an effort to support the experimental findings, a simplified analysis of the viscous zone was derived by the consideration of a differential control volume of oil. The net hydrostatic forces acting on the control were equated with the shear stress at the interface to yield the following

$$\frac{h}{dx} \frac{dh}{\rho_0 g(1-s)} = \text{sum } \sigma_i \quad (2.3.11)$$

This force balance of the control volume differs from that given by Cross and Hoult in Equation (2.3.1) by the factor  $\rho_0 / \rho_w$ . The difference is due to the allowance for the oil slick to float above the water free surface. The slick thickness  $h$  is related to the depth of oil below the water surface  $m$  by;

$$m = \frac{\rho_0}{\rho_w} h$$

Lindenmuth et al realized that the major difficulty in applying this theory lay in the complexity of evaluating the shear



forces. Available boundary layer theories are inadequate to account for the effects of interfacial waves, flow separation at the headwave, oil viscosity, and circulation within the oil layer. However, it is suggested that for engineering estimates, adequate oil slick geometries could be calculated on the assumption of a constant shear force along the slick. Integration of Equation (2.3.11) coupled with a constant shear assumption yields a parabolic shape of the oil slick thickness distribution in the following form;

$$h(x)^2 = G(x) + h_N^2 \quad (2.3.12)$$

in which  $G = \frac{C_j U^2}{\rho_0 g(1-s)}$  and  $h_N$  = thickness at the neck of the headwave.

Application of Equation (2.3.12) to the experimental data reveals a range of interfacial shear coefficients from 0.002 for diesel fuel to 0.013 for freshwater over saltwater. Engineering estimates of the volume of oil retained by a boom is given by the integration of Equation (2.3.12);

$$V(x) = V_h + 2/3G (h_N^2 + G(x))^{2/3} - h_N^3 \quad (2.3.13)$$

Based on experimental data for the headwave geometries the volume of oil in the headwave is given by;

$$V_h = 15.6 h_N^2 (\text{ft}^2/\text{ft})$$



Lindenmuth et al proposed that utilization of Equations (2.3.12) and (2.3.13) would provide sufficient estimation for the required boom draft to prevent drainage failure of a given quantity of oil, in the absence of waves.

Although this study is not directly concerned with the effects of approaching waves on oil slicks, the following comments on the development of the viscous zone, influenced by waves, as noted by Lindenmuth et al, are briefly discussed. The purpose of their presentation here is to provide a comparative background for the brief discussion of the detailed study of wave interaction on interfacial velocities and shear stresses outlined in the next section.

The range of tests conducted indicated that under certain conditions a significant increase in the oil slick thickness could occur due to waves. Typically the slick would thicken at the wave crests and decrease in the waves troughs. The development of the viscous zone appeared to be a complex function of the wave heights, wave period, and boom response to waves. Lindenmuth et al were unable to provide a quantitative theory as to their relative roles but several trends were noted. The wave steepness, defined as the ratio of wave height to wave length, was found to be the predominant parameter influencing the oil slick thickness. The ratio of mean slick thickness in waves to mean slick thickness in calm water was found to be non-linearly proportional to wave steepness. The maximum increase in slick thickness occurred when the incident waves were breaking.



The headwave was strongly disturbed under certain conditions, suggesting that the phenomena does not result from a simple superimposition of velocities. Furthermore, it was noted that the large increase in slick thickness occurred for the full range of frequencies tested, indicating that a simple resonance phenomenon was not the responsible mechanism. It was discerned that when the wave frequency was sufficiently high, such that wave lengths were less than 3 times the boom draft, these waves were completely reflected by the boom with no resulting increase in slick thickness.

In conclusion, Lindenmuth et al suggest that due to the complex nature of waves effects on the viscous zone, any boom draft requirements dictated by a "current only" analysis may have to be increased by a factor of 2 or more.

#### Hale, Norton, and Rodenberger (1974)

A most comprehensive investigation of the effects of currents and waves on an oil slick was conducted by Hale, Norton and Rodenberger. The major emphasis of their study was directed towards the development of a mathematical oil droplet entrainment model, and towards the evaluation of various oil slick recovery devices. However, extensive preliminary study of the interface within the viscous zone was conducted to establish a complete understanding of the oil slick phenomenon. This study consisted primarily of the collection of a comprehensive set of velocity data; the resulting implications are presented briefly in the following section. Details



concerning the precise magnitude for the data are presented later in this study to complement velocity data acquired by author during the course of the experimental phase of the investigation.

Using a pitot tube, at several different sections along the oil slick, velocity profiles in the water below the oil slick were established. A non-linear least squares regression was employed to match the observed velocities to the following distribution;

$$U = A_1 - A_2 \exp^{-A_3 y} \quad (2.3.14)$$

Where  $y$  is the distance below the free surface and  $A_1$ ,  $A_2$  and  $A_3$  are the computed coefficients.

This form of velocity distribution was in agreement with the observed velocities. Although the velocity data was applied to a one-seventh power law velocity distribution, it was unable to duplicate the same degree of correlation as in the previous distribution.

Defining the shear stress at the interface as;

$$\sigma_i = \mu_w \left( \frac{dU}{dy} \right)_i$$

Hale et al evaluated the shear stress by the differentiating Equation (2.3.14). This process lead to an interesting observation concerning the magnitude of shear stress at various sections along the



slick. Hale et al reported that the interfacial shear coefficients in the vicinity of the headwave were 1/100 of those in the mid-region as reported by Cross and Hoult. This led Hale et al to the conclusion that Wilkinson's assumption of the insignificance of shear stresses in the frontal zone is valid.

Expanding on the concept of Cross and Hoult that the interfacial shear stress is balanced by the horizontal hydrostatic pressure gradient corresponding to the increase in the thickness of oil (Equation (2.3.1)), Hale et al developed the following relationship between the average interfacial shear coefficient  $C_i$ , the average thickness  $h_{av}$  and the slick length  $l$ ;

$$C_i = \frac{9 g(1-s) h_{av}^2}{4 l U^2} \quad (2.3.15)$$

Substitution of the experimental data into Equation (2.3.15) reveals relatively the same shear coefficients as previously reported by Cross and Hoult.

In addition to the water velocity measurements, an attempt was made to develop a model for the velocities within the oil slick itself. The velocity gradient in the oil at the interface was derived by equating the shear stress in the water to that in the oil. Thus, the oil velocity gradient at the interface is;



$$\frac{dU}{dy} \Big|_{\text{i oil}} = \frac{\mu_w}{\mu_o} \frac{dU}{dy} \Big|_{\text{i water}}$$

An additional boundary condition was established by timing the velocities of chips on the oil-air surface. These two measurements coupled with the known zero shear on the surface and the requirement of mass continuity within the circulating oil layer lead to the development of a velocity profile in the oil layer. The coefficients of the following relationship were evaluated for these considerations;

$$U = B_1 + B_2 Y^{B_3-1} \exp^{-B_4 Y^{B_3}} \quad (2.3.16)$$

Where  $Y$  is the dimensionless depth (ie. 0.0 at the free surface, and 1.0 at the interface)

However, due to the random nature of interfacial velocities and gradients arising from the complication introduced by interfacial waves, the results of this analysis were considered to be questionable by Hale et al.

A dimensionless interfacial velocity ( $U_i/U_0$ ) relationship was developed by equating the velocities to the Reynold Number  $R_e$ , viscosity ratio ( $\mu_o / \mu_w$ ) and the dimensionless slick position ( $x/t$ ). Using a least square procedure, the following equation was derived;



$$\frac{U_i}{U} = 6.20 \left( \frac{\mu_o}{\mu_w} \right)^{-0.0397} \left( \frac{x}{t} \right)^{-0.133} R_e^{-0.214} \quad (2.3.17)$$

Though the scatter in data was considerable, Equation (2.3.17) indicates a strong trend for a decrease in  $U_i$ , with increasing  $x$  (the downstream distance).

A major emphasis of the investigation by Hale et al was directed towards the study of the combined effects of currents and waves. Although the details of their study are beyond the scope of this study, some of the basic conclusions regarding the interfacial shear stresses and velocities, as affected by waves, have been extracted and are presented briefly in the following paragraphs.

The oil slick set-up induced by waves is mainly an effect of the mass transport in waves and energy transfer from waves to the oil slick. The most simple analysis is accomplished by the superimposition of a progressing wave system velocity field on the velocities of the current alone. Hale et al have demonstrated that if the phase shift between the motions in oil and water is zero, then the interfacial shear will be independent of the waves. However, if a phase shift occurs, the shear stress takes the following form;

$$\sigma_i = 1/2 C_i \rho_w (U^2 + q^2 \omega^2 (1 - \cos \phi)) \quad (2.3.18)$$

Their analysis is insufficient to predict the magnitude of phase shift, but it does provide a mechanism by which waves can alter



the interfacial shear and consequently the oil slick length.

A model test utilizing a compliant barrier (wave reflects less than 10 percent of incident wave) were conducted over a complete range of velocities and wave climates. At low current velocities, waves tended to increase the slick length with the exception of steep waves. At higher current velocities all waves induced a decrease of the oil slick. The periodic water velocities caused local variation in slick thickness in a manner similar to that observed by Lindemuth et al. Hale et al were unable to describe the effects of waves in any systematic manner. The only conclusion postulated is that waves could significantly alter slick lengths but their simple analysis of the interfacial shear was inadequate to fully describe this complex process.

#### Milgram and Van Houten (1978)

An ingenious analysis of the oil slick problem is presented in a recent paper by Milgram and Van Houten. The prime objective of their analysis was to evaluate the relative importance of interfacial shear stress and dynamic pressure in determining the thickness distribution of an oil slick. As mentioned in the previous section dealing with headwaves, Milgram and Van Houten argue that if shear stresses in the frontal zone are sufficiently high then the theoretical necessity for a breaking headwave, as suggested by Benjamin, is removed. Milgram and Van Houten cite as preliminary evidence, that the concept that dynamic forces are not dominant in the



headwave region, one of the basic observations derived during experimental work with oil slicks. More explicitly, the leading edge of the slick, as observed by all authors, is an order of magnitude less than 60 degrees to the horizontal, as predicted by the dynamic analysis of Von Karman.

Their analysis and subsequent arguments supporting the postulation of equal dominance of shear stresses and dynamic forces stems from the following combination of theory and experiment. In theory, it was assumed that potential flow approximates the flow within the water phase to a sufficient degree of accuracy. Thus, utilizing experimental measurements of the oil slick thickness as a boundary condition, numerical analysis could calculate the flow and corresponding pressure distribution. A theoretical model equating the pressures, oil thickness shape, and shear stresses was then utilized to evaluate the shear stress distribution from the measured oil shape and calculated pressure distribution.

Numerical integration of the water velocity potential provided the tangential velocity  $V_t$  along the measured oil slick shape. The dynamic pressure  $P$  along the interface was then given by the Bernoulli equation, in a non-dimensional form as;

$$P = 1 [1 - \left( \frac{U_t}{U} \right)^2] \quad (2.3.19)$$



Arguing that measurements by Hale et al indicate that the velocity in the oil are sufficiently smaller than those in the water, Milgram and Van Houten assumed that dynamic pressure and momentum fluxes within the oil can be neglected. The remaining mean forces are shown in Figure 2.3.a. These are, pressure forces on the vertical faces, steady and dynamic pressure forces along the lower interface, and the combined viscous shear and Reynolds stresses along the interface. The interfacial stresses can be expressed in terms of the approach velocity  $U$  and a spacial variant coefficient of friction  $C_i$ . Pressure continuity relates the mean thickness of oil  $h$  to the oil thickness  $h$  as measured below the original free surface in the following form;

$$h = \frac{\rho_w g m + P}{\rho_o g} \quad (2.3.20)$$

The measured slick profile  $m$  and the horizontal length scale  $x$  can be described non-dimensionally by the factor  $g/U^2$ .

$$\text{Such that } M = \frac{m g}{U^2} \text{ and } L = \frac{x g}{U^2}$$

A balance of the horizontal forces on the differential element of oil, coupled with the afore-mentioned factors, yield the following basic equation relating the shape of the oil to the dynamic pressure and shear forces at the interface.

$$(M + P)[(1-s)\frac{dM}{dL} + \frac{dP}{dL}] = \frac{1}{2} s C_i \quad (2.3.21)$$



The experimental portion of Milgram and Van Houten's study encompassed a broad range of water velocities and oil properties. They have presented several plots of these various experiments which consisted of the measured interface shape  $m$ , the calculated pressure distribution  $P$  and the calculated shear stress distribution  $C_i$ . In order to evaluate the relative effects of friction and pressure in determining the interfacial shape, Milgram and Van Houten developed a relationship to predict the oil thickness distribution in the absence of dynamic pressures. This relationship consisted of setting the dynamic pressure and its horizontal derivative to zero in Equation (2.3.21) and solving for  $M$ . This solution was defined as  $M_f$ ;

$$M_f(x) = \left( \frac{s}{1-s} \int C_i(x) dx \right)^{1/2} \quad (2.3.22)$$

This frictional oil thickness distribution was plotted with the above mentioned distributions. Figure 2.3.b and 2.3.c show two typical plots as traced from Milgram and Van Houten. These two plots reveal the two distinct shapes of the calculated interfacial friction distributions. The Type I distribution (Figure 2.3.b) was observed to have a maximum shear in the vicinity of maximum headwave thickness. The magnitude of the maximum friction coefficient ranged from 0.013 to 0.073 which is an order of magnitude greater than the friction coefficients previously reported by other investigators. The friction distribution decreases to a range between 0.004 to 0.012 behind the headwave. Type I distributions were observed when the interfacial waves were diminutive. However, when the interfacial waves exceeded a specific value the shear distribution took another shape as indicated



in Figure 2.3.c. The Type II distribution were characterized by more than one peak in the maximum value of friction coefficients. The first peak occurred upstream of the maximum oil thickness in the headwave with a second peak immediately downstream of the headwave. The magnitude of the coefficients for Type II distributions ranged up to 0.33.

The calculated oil thickness  $M_f$  was observed to positively match the measured oil thickness  $M$  for Type I distributions. The two plots were practically identical in the viscous zone. Based on their calculations Milgram and Van Houten state the assumption that the friction was instrumental in determining the geometry of the rear portion of the oil layer propounded by several previous investigators, is justified. However, due to the apparent match of the two oil thicknesses in the vicinity of the headwave, Milgram and Van Houten conclude that the previous assumption, specifically that the friction is unimportant for the forward portion of the layer, is ill-founded.

## 2.4 Interfacial Instability

The preceding two sections have dealt with the equilibrium characteristics of an arrested oil slick. However, the successful containment of an oil slick must include consideration of the various aspects of boom failure. Aside from the obvious failure resulting from insufficient boom draft, termed oil drainage, a complex failure mechanism entitled entrainment failure must, also, be taken into consideration. Entrainment failure stems from the interfacial shear



instabilities and the resultant formation of interfacial waves. In the vicinity of the headwave, the interfacial waves break and oil droplets are entrained in the water. The actual magnitude of oil loss by this mechanism is dependent on the ability of the oil droplets, once entrained into the flowing water, to rise back to the slick interface and coalesce before being swept under the boom. This entrainment failure, which occurs at current velocities of approximately 0.4 meters per second, is invariant to the actual design of the boom and, thus becomes a fundamentally limiting factor in oil spill retention and recovery.

The development of numerous models for predicting the oil droplet entrainment losses have resulted from the various studies of oil slick entrainment failure. These models, though different in degree of complexity, consist primarily of an evaluation of the rates of droplet formation at velocities exceeding the critical formation velocity, examination of the droplet characteristics, trajectories and terminal velocities, and an investigation of the reattachment phenomena. The details of these entrainment loss models is beyond the scope of the experimental portion of this study. Thus, the remainder of this section will briefly examine various failure criteria and then addressed the development of interfacial waves resulting from K-H instability. This treatment shall consist of an examination of the basic problem and method of analysis of K-H instability waves with emphasis on its application to oil slick interfaces.



Wicks (1969)

Since the oil droplet entrainment phenomena was first reported by Wicks (1969), several theoretical and empirical correlations for the critical velocity  $U_{cr}$ , of entrainment initiation, and various models of entrainment losses have been evolved.

Wicks suggested that droplet entrainment is inevitable as a result of the unstable headwave predicted by Benjamin's analysis. Wicks observed interfacial waves formed at the leading edge of the oil slick, which grew in magnitude as they migrated downstream toward the headwave. Droplets were torn from the rear of the headwave and entrained in the flow. Based on experimental observations, Wicks stated that the velocity at which the oil droplets are torn from the headwave appears to be in agreement with the predictions of a critical Weber Number, as suggested by Hinze, for gradual acceleration of the dispersed phase. In terms of the critical velocity  $U_{cr}$ , the average droplet diameter  $d$ , and the interfacial surface tension  $T$ , the Weber Number is defined as;

$$(W_e) = \frac{\rho_w U_{cr}^2}{T} d = 14.0 \quad (2.4.1)$$

Wicks further stated that the formation of waves at the oil-water interface, within the viscous zone, corresponded well with the predictions of Kelvin - Helmholtz instability phenomena (hereafter termed K-H instability).



Lindenmuth, Miller, and Hsu (1970)

Lindenmuth et al proposed that droplet formation behind the headwave is due to form drag. As water flows under the headwave, a low pressure region develops aft of the headwave. Then, as the velocity of the current increases, the low pressure eventually becomes sufficient to tear oil away from the rear of the headwave, with the resulting formation of oil droplets. Experimentally, the critical velocity at which oil droplet formation commences was observed to be primarily a function of interfacial surface tension.

Wilkinson (1973)

Wilkinson indicated that the development of interfacial waves was in some respects similar to the growth of wind induced waves on a free surface. The occurrence of interfacial waves suggested that energy was being transferred from the main flow into the oil slick, possibly satisfying the energy dissipation requirements of Benjamin's headwave theory. However, Wilkinson's experimental observations of the interfacial wave characteristics revealed that only five percent of the available energy was consumed by the flux of wave energy.

Wilkinson had realized that the K-H instability was responsible for the production of interfacial waves, but he made no reference to its role as a mechanism for the entrainment phenomena.



Hale, Norton, and Rodenberger (1974)

The extensive investigation conducted by Hale et al suggested that the use of a critical Weber Number is an adequate means to evaluate the critical velocity for oil droplet formation. Their experimental work confirmed that droplet formation occurs strictly at the aft of the headwave but that actual entrainment of the oil droplets exists throughout the entire length of the slick.

Kelvin - Helmholtz Instability

The basic principle behind investigations of the stability of fluid flow is that given an initial flow, the superimposition of small perturbations upon the flow are examined to determine whether the amplitude of the disturbances increase or decrease with time, thus determining whether a given flow is stable or unstable.

K-H type of instability is that which occurs when two different liquids move with different tangential velocities across their interface. The momentum exchange induces any wave disturbance on the interface to grow in amplitude to the verge of mixing the two liquids. Interfacial surface tension tends to reduce the unstable growth, as does viscosity, but to a secondary degree.

Alternately, K-H instability can be interpreted as the resulting action of the pressure distribution in phase with the interface elevation, attempting to overcome the "stiffness" (due to



the restoring force of gravity and surface tension) of the interface. This type of interpretation is typically followed by an examination of the instability of a vortex sheet at the oil-water interface.

Though rigid mathematical analysis of vortex sheets at liquid interfaces has been studied in some detail, it will be the former description of the K-H instability phenomena that will be addressed in the remaining paragraphs.

The basic mathematical analysis of K-H instability is well documented in existing literature. The succeeding analysis follows closely that presented by Lamb, (Art 232).

A simple case of instability occurs when two fluids, homogenous within themselves, of densities  $\rho_w$  and  $\rho_o$ , one beneath the other ( $\rho_w > \rho_o$ ), move in a parallel direction with uniform velocities  $U_w$  and  $U_o$ . The definition sketch of Figure 2.4 is developed for three phase flow (addressed later in this section) but, also, serves as a definition sketch for two phase flow. If the flow in the upper and lower layers is assumed to be irrotational, then the velocity potentials of  $\phi_o$  and  $\phi_w$  which satisfy the Laplace Equation exist.

$$\Delta^2 \phi_o = 0 \quad \text{and} \quad \Delta_2 \phi_w = 0 \quad (2.4.2)$$

If the velocity potentials are disturbed by infinitesimally small perturbation  $\phi_o'$  and  $\phi_w'$  so that ;



$$\phi_o = U_o x + \phi_o' \text{ and } \phi_w = U_w x + \phi_w' \quad (2.4.3)$$

It follows that the perturbations themselves must, also, adhere to the Laplace equations.

$$\Delta^2 \phi_o' = 0 \quad \text{and} \quad \Delta^2 \phi_w' = 0 \quad (2.4.4)$$

Considering the interface between the two liquids to be the y origin and assuming the liquids infinite in both directions, then the dynamic boundary condition (B.C.) for the perturbation is;

$$\lim_{y \rightarrow \infty} \phi_o' = 0 \quad \text{and} \quad (2.4.5)$$

$$\lim_{y \rightarrow -\infty} \phi_w' = 0$$

Utilizing these two B.C.s the solution to Equation (2.4.4) can take the following form;

$$\phi_o' = A_o \exp(-Ky + i(Kx - \sigma t)) \quad (2.4.6)$$

$$\phi_w' = A_w \exp(Ky + i(Kx - \sigma t)) \quad (2.4.7)$$

In which  $\sigma = KC$  and  $K$  = wave number (positive and real)

$C$  = wave velocity (complex)

The interface between the two liquids is a streamline of both fluids and the path of a particle on the interface is described as  $y = n(x, t)$ .



The total derivative

$$\frac{D}{Dt} (y - \eta(x, t)) = 0 \quad (2.4.8)$$

is a kinematic boundary condition which indicates that once a particle is on the interface, it stays on the interface. Expanding the total derivative (Equation (2.4.8)) and realizing that vertical velocity  $V$  can be expressed in terms of the velocity potential results in two additional kinematic B.C.'s.

For the top fluid;

$$\frac{d\eta}{dt} + U_0 \frac{d\eta}{dt} = -\frac{d\phi'_0}{dy} \quad \text{at } y = \eta \quad * \quad (2.4.9)$$

and for the bottom fluid;

$$\frac{d\eta}{dt} + U_w \frac{d\eta}{dt} = -\frac{d\phi'_w}{dy} \quad \text{at } y = \eta \quad (2.4.10)$$

If the amplitude of  $\eta$  is assumed to be small, then utilization of Taylor's Expansion allows the previous two B.C. to be evaluated at  $y = 0$ .

An additional dynamic boundary condition results from consideration of the continuity of pressure at the interface. (In this case surface tension is neglected.) Recalling that the interface is a streamline, the Bernoulli Equation for the top fluid is;

\* The symbol  $d$  represents the partial derivative



$$\frac{d\phi'}{dt} + \frac{1}{2} (U_0^2 + V_0^2) + \frac{P}{\rho_0} + gn = C(\text{constant})$$

or to a first order approximation,

$$\frac{P_0}{\rho_0} = -\frac{d\phi'_0}{dt} - U_0 \frac{d\phi'_0}{dx} - gn + C \quad (2.4.11)$$

Similarly the Bernoulli Equation for the bottom fluid is;

$$\frac{P_w}{\rho_w} = -\frac{d\phi'_w}{dt} - U_w \frac{d\phi'_w}{dx} - gn + C \quad (2.4.12)$$

The two fluids share a common streamline at the interface and the pressure  $P$  is constant on both sides of this streamline (in the absence of surface tension.) Thus, equating equation (2.4.11) and (2.4.12) yields;

$$\rho_0 \left( \frac{d\phi'_0}{dt} + U_0 \frac{d\phi'_0}{dx} + gn \right) = \rho_w \left( \frac{d\phi'_w}{dt} + U_w \frac{d\phi'_w}{dx} + gn \right) \quad (2.4.13)$$

Defining the form of the interface  $n$  as;

$$n = a \exp[i(Kx - \sigma t)] \quad (2.4.14)$$

Utilizing the general solutions for the perturbations  $\phi'_0$  and  $\phi'_w$  (ie. Equations (2.4.6) and (2.4.7)), the dynamic boundary condition based on continuity of pressure at the interface (equation (2.4.13)) becomes;

$$\rho_0 (iA_0 \sigma + U_0 iKA_0 + ga) = \rho_w (-iA_w \sigma + U_w iKA_w + ga) \quad (2.4.15)$$

The kinematic boundary conditions at the interface (Equation (2.4.9) and (2.4.10)) can be reduced in a similar manner by



substituting Equation (2.4.6), (2.4.7), and (2.4.14) to form;

For the top fluid;

$$ia(U_0K - \sigma) = A_0K \quad (2.4.16)$$

and for the bottom fluid;

$$ia(U_wK - \sigma) = -A_wK \quad (2.4.17)$$

The simultaneous solution of Equations (2.4.15), (2.4.16), and (2.4.17) for the three unknowns  $A_0$ ,  $A_w$ , and  $\sigma$  yield;

$$\rho_0(KU_0 - \sigma)^2 + \rho_w(KU_w - \sigma)^2 = gK(\rho_w - \rho_0) \quad (2.4.18)$$

The quadratic solution of Equation (2.4.18) for the phase velocity  $C = \sigma/K$ , of an interfacial disturbance is;

$$\frac{\sigma}{K} = \frac{\rho_0 U_0 + \rho_w U_w}{\rho_0 + \rho_w} \pm \left[ \frac{g}{K} \frac{\rho_w - \rho_0}{\rho_w + \rho_0} - \frac{\rho_0 \rho_w}{(\rho_w + \rho_0)^2} (U_0 - U_w)^2 \right]^{1/2} \quad (2.4.19)$$

The first term is referred to as the weighted (by density) mean velocity of the two fluid streams. Relative to this velocity, interfacial waves travel with a wave velocity  $\pm C$  as given by;

$$C^2 = C_0^2 - \frac{\rho_0 \rho_w}{(\rho_0 + \rho_w)^2} (U_0 - U_w)^2 \quad (2.4.20)$$



$$\text{Where } C_0^2 = \frac{g \rho_w - \rho_o}{K \frac{\rho_w + \rho_o}{\rho_o \rho_w}}$$

$C_0$  is the wave velocity of disturbances in the absence of currents. These waves would subside with time and result in a stable flow. However, the interfacial waves would be unstable if  $C$  is imaginary. That is, if;

$$(U_o - U_w)^2 > \frac{g \frac{\rho_w^2 - \rho_o^2}{\rho_o \rho_w}}{K} \quad (2.4.21)$$

The results of this form of analysis reveal that in the absence of any stabilizing forces, such as surface tension, the interface will be unstable for any small disturbance.

The neglect of interfacial surface tension between oil and water, is totally unjustified for the evaluation of K-H instabilities of oil slicks. Incorporating the effects of surface tension into the above analysis will only alter the dynamic boundary condition of pressure continuity at the interface. The previous analysis assumed that pressure at the interface of the two fluids were equal. However, the inclusion of surface tension dictates that the surface tension  $\sigma$ , must be balanced by the pressure difference at the interface: ie.

$$\rho_w - \rho_o = -T \left( \frac{d^2 n}{dx^2} + \frac{d^2 n}{dy^2} \right) \approx -T \frac{d^2 n}{dx^2} \quad \text{at } y = 0 \quad (2.4.22)$$

Applying the two linearized Bernoulli Equations (2.4.11) and (2.4.12) to Equation (2.4.22) at  $y = 0$  yields;



$$\rho_0 \left( \frac{d\phi'_0}{dt} + U_0 \frac{d\phi'_0}{dx} + g_n \right) - \rho_w \left( \frac{d\phi'_w}{dt} + U_w \frac{d\phi'_w}{dx} + g_n \right) = -T \frac{d^2 n}{dx^2} \quad (2.4.23)$$

Pursuing the similar solution of the previous example, the resulting second order polynomial for wave velocity C and the following roots;

$$C = \frac{\rho_w U_w + \rho_0 U_0}{\rho_w + \rho_0} \pm [C_0^2 - \rho_0 \rho_w \left( \frac{U_0 - U_w}{\rho_0 + \rho_w} \right)^2]^{1/2} \quad (2.4.24)$$

$$\text{In which } C_0^2 \text{ is now } C = g \frac{\rho_w - \rho_0}{K \frac{\rho_w + \rho_0}{\rho_w + \rho_0}} + \frac{T K}{\rho_w + \rho_0} \quad (2.4.25)$$

As previously indicated the first term of Equation (2.4.24) is the weighted mean velocity and  $C_0$  is the interfacial velocity of disturbance waves in the absence of currents. Thus as before if C is positive and imaginary, instability will occur, ie. if;

$$\rho_0 \rho_w \left( \frac{U_0 - U_w}{\rho_0 + \rho_w} \right)^2 > C_0^2 > C_{0 \min}^2 \quad (2.4.26)$$

$C_0$  is a function of the disturbance wave number K , and has a minimum value of;

$$C_{0 \ min} = \left[ 2Tg \frac{(\rho_w - \rho_0)}{(\rho_0 + \rho_w)^2} \right]^{1/2} \quad (2.4.27)$$

at a critical wave number K of;

$$K_{cr}^2 = g \frac{(\rho_w - \rho_0)}{T} \quad (2.4.28)$$



Therefore, surface tension will suppress the K-H instability below a critical velocity difference of;

$$(U_o - U_w)^2 < \frac{2Tg (\rho_w - \rho_o)}{\rho_o \rho_w} \quad (2.4.29)$$

Jones (1972)

The previous K-H instability analysis deals with two semi-infinite inviscid fluids of different density, each moving at a given uniform velocity. However, the critical velocities sustained from this form of analysis appears to be only of the order of magnitude of those reported in the literature for critical velocities at the onset of droplet formation. In reality, the oil slick layer has a finite thickness in which the free surface of the oil slick does not necessarily adhere to the previously used boundary condition of infinite depth. Jones (1972) addressed this problem by conducting a linear K-H instability analysis for a slick of arbitrary but finite, thickness. Jones concluded that a thin slick would be unstable at a velocity lower than the critical velocity for a thick slick.

Leibovich (1976)

Leibovich has conducted a linear K-H instability analysis which leads to the opposite conclusion from Jones' prediction that a thick slick is more stable than a thin one. Leibovich states that Jones omitted the effects of the air-oil surface tension and air



density, thus imposing a constant pressure boundary condition at the air-oil interface. Leibovich argues that the justification was not valid and he indicates that Jones conclusions regarding the destabilizing effects of decreasing the slick thickness was, also, invalid. A brief description of Leibovich's analysis follows.

Considering the configuration of Figure 2.4, the stability analysis consists of three fluid layers. The three velocities can be perturbed by  $\phi_w'$ ,  $\phi_o'$ , and  $\phi_a'$  which must satisfy the Laplace Equations

$$\Delta^2 \phi_w' = 0 \quad \Delta^2 \phi_o' = 0 \quad \Delta^2 \phi_a' = 0 \quad (2.4.30)$$

The air phase and water phase are still assumed to be infinite, so that the dynamic boundary conditions of;

$$\lim_{y \rightarrow \infty} \phi_a' = 0 \quad \text{and}$$

$$\lim_{y \rightarrow -\infty} \phi_w' = 0$$

This leads to the following solution to Equations(2.4.30);

$$\phi_a' = A_a \exp[-Ky + i(Kx - \sigma t)] \quad (2.4.31.a)$$

$$\phi_w' = A_w \exp[ Ky + i(Kx - \sigma t)] \quad (2.4.31.b)$$

However, the finite thickness of oil depth  $h$  requires a more general solution to the Laplace Equation;



$$\phi'_0 = (A_0 \cosh Ky + B_0 \sinh Ky) [\exp i(Kx - \sigma t)] \quad (2.4.32)$$

There exists two interfaces which serve as streamlines between the three liquids. Following a similar argument that led to the kinematic boundary condition of Equation (2.4.8), the total derivative of a particle path can be applied to the oil-air interface  $y = n_2$  and to the oil-water interface  $y = n_1$ :

$$\frac{Dn_1}{Dt} = 0 \quad \text{and} \quad \frac{Dn_2}{Dt} = 0$$

Expanding these derivatives in terms of the partial derivatives and applying them to both sides of the streamline interface results in the following four kinematic boundary conditions;

$$\frac{dn_1'}{dt} + U_a \frac{dn_1'}{dx} = -d\phi_a' \quad \text{at } y = h \quad (2.4.33.a)$$

$$\frac{dn_1'}{dt} + U_o \frac{dn_1'}{dx} = -d\phi_o' \quad \text{at } y = h \quad (2.4.33.b)$$

$$\frac{dn_2'}{dt} + U_o \frac{dn_2'}{dx} = -d\phi_o' \quad \text{at } y = 0 \quad (2.4.33.c)$$

$$\frac{dn_2'}{dt} + U_w \frac{dn_2'}{dx} = -d\phi_w' \quad \text{at } y = 0 \quad (2.4.33.d)$$

Two additional dynamic boundary conditions arise from the pressure force balance at the interfaces. Defining the oil-air surface tension as  $T_{o/a}$  and the oil-water surface tension as  $T_{o/w}$ , the two force balance equations are;



$$\rho_o - \rho_a = -T_{o/a} \frac{d^2 \eta_1}{dx^2} \quad \text{at } y = \eta_1 \quad (2.4.34.a)$$

$$\rho_w - \rho_o = -T_{o/w} \frac{d^2 \eta_2}{dx^2} \quad \text{at } y = \eta_2 \quad (2.4.34.b)$$

Since the interfaces are streamlines, the pressure forces can be evaluated by a linearized Bernoulli Equation, thus, reducing the force balance Equation (2.4.34.a and .b);

$$\rho_o \left( \frac{d\phi'_o}{dt} + U_o \frac{d\phi'_o}{dx} + g\eta_1 \right) - \rho_a \left( \frac{d\phi'_a}{dt} + U_a \frac{d\phi'_a}{dx} + g\eta_1 \right) = -T_{o/a} \frac{d^2 \eta_1}{dx^2} \quad (2.4.35.a)$$

$$\rho_w \left( \frac{d\phi'_w}{dt} + U_w \frac{d\phi'_w}{dx} + g\eta_2 \right) - \rho_o \left( \frac{d\phi'_o}{dt} + U_o \frac{d\phi'_o}{dx} + g\eta_2 \right) = -T_{o/w} \frac{d^2 \eta_2}{dx^2} \quad (2.4.35.b)$$

The interfacial displacements can be defined in a general form as;

$$\eta_1 = a_1 \exp[i(Kx - \sigma t)] \quad (2.4.36.a)$$

$$\eta_2 = a_2 \exp[i(Kx - \sigma t)] \quad (2.4.36.b)$$

Substituting the defined interfacial displacements, Equations (2.4.36.a and .b), the general solutions of the perturbations Equations (2.4.31.a and .b) and (2.4.32) into the six boundary conditions (Equations (2.4.33.a , .b , .c , and .d) and (2.4.35.a and .b) and performing the required differentiation yields;

$$i a_1 (U_a K - \sigma) = A_a K \exp(-Kh) \quad (2.4.37.a)$$

$$i a_1 (U_o K - \sigma) = -K(A_0 \sinh Kh + B_0 \cosh Kh) \quad (2.4.37.b)$$



$$i a_2 (U_0 K - \sigma) = -KB_0 \quad (2.4.37.c)$$

$$i a_2 (U_w K - \sigma) = -A_w K_0 \quad (2.4.37.d)$$

$$\rho_0 [(A_0 \sinh Kh + B_0 \cosh Kh)(U_0 K - \sigma) i + g a_1] \quad (2.4.37.e)$$

$$- \rho_a [A_a i (U_a K - \sigma) + g a_1] = T_{0/a} a K^2$$

$$\rho_w [A_w i (U_w K - \sigma) + g a_2] \quad (2.4.37.f)$$

$$- \rho_0 [A_0 i (U_0 K - \sigma) + g a_2] = T_{a/w} a K^2$$

These six equations with the six unknowns  $A_a$ ,  $A_0$ ,  $A_w$ ,  $B_0$ ,  $a_1$ , and  $a_2$  have a solution only if the determinant of the coefficients vanishes. This leads to the eigen value equation for the wave speed  $C$  as;

$$\rho_0 (U_0 - C)^2 [\rho_0 (U_0 - C)^2 \tanh Kh + S_2(C)] \quad (2.4.38.a)$$

$$+ S_1(C) [\rho_0 (U_0 - C)^2 + S_2(C) \tanh Kh] = 0$$

$$\text{Where } S_1(C) = \rho_w (U_w - C)^2 - (\rho_w - \rho_0) g / K - K T_{0/w}$$

$$\text{and } S_2(C) = \rho_a (U_a - C)^2 - (\rho_0 - \rho_a) g / K - K T_{0/a}$$

K-H instability occurs when the solution for the wave speed  $C$  becomes imaginary. By examining the limits of the oil thickness  $h$ , as it tends to zero and as  $h$  tends to infinity, a comparison between the relative stability of thin and thick oil slicks can be drawn.

In the limits of  $h$  tends to zero ( $h \rightarrow 0$ ), Equation (2.4.38) reduces to;



$$S_1(C) + S_2(C) = 0 \text{ or}$$

$$\rho_w(U_w - C)^2 + \rho_a(U_a - C)^2 - (\rho_w - \rho_a) \frac{g}{K} - K(T_{o/a} + T_{o/w}) = 0$$

in which the solution of the wave speed  $C$  is (2.4.39);

$$C = \frac{\rho_a U_a + \rho_w U_w}{\rho_a + \rho_w} \pm \left[ \frac{1}{\rho_a + \rho_w} \frac{g (\rho_w - \rho_a) + K(T_{o/a} + T_{o/w})}{K} - \rho_a \rho_w \left( \frac{U_w - U_a}{\rho_a + \rho_w} \right)^2 \right]^{1/2}$$

Equation (2.4.39) is the same solution for air flow over water but the surface tension  $T_{a/w}$  is replaced by  $T_{o/a} + T_{o/w}$ . The form of the equation is similar to that derived for an infinite thickness of oil (Equation (2.4.24)). In the limit of the oil thickness  $h$  tending to zero, the oil velocity and density play no part in the stability of waves. Instability will occur when;

$$(U_w - U_a)^2 > \frac{\rho_a + \rho_w}{\rho_a \rho_w} \frac{g (\rho_w - \rho_a) + K(T_{o/a} + T_{o/w})}{K} \quad (2.4.40)$$

The stabilizing influence of a thin film on water as derived from the elastic properties of very thin films (Lamb Art 351) has been neglected in the K-H analysis.

Examination of the limit of thick oil slicks, when  $h$  tends to infinity, reduces Equation (2.4.38) to;

$$\rho_0 [(U_0 - C)^2 + S_1(C)] [\rho_0 (U_0 - C)^2 + S_2(C)] = 0 \quad (2.4.41)$$



When the first bracket of Equation (2.4.41) is equal to zero, the K-H instability corresponding to the oil-water interface occurs if;

$$(U_w - U_o)^2 > \frac{\rho_o + \rho_w}{\rho_o \rho_w} \left[ g (\rho_w - \rho_o) + K T_{o/w} \right] \quad (2.4.42)$$

The minimum critical speed  $U_{cr} = [U_w - U_o]$  at which instability will occur is given for a minimum value for the critical wave number  $K_{cr}$ .

$$U_{cr}^2 = 2 \frac{(\rho_o + \rho_w)}{\rho_o \rho_w} \left[ T_{o/w} g (\rho_w - \rho_o) \right]^{1/2} \quad (2.4.43)$$

with a corresponding critical wave number of;

$$K_{cr}^2 = \frac{(\rho_w - \rho_o) g}{T_{o/w}} \quad (2.4.44)$$

The critical speed for the thin oil slick can be expressed as;

$$U_{cr}^2 = 2 \left[ \frac{T_{o/a} + T_{o/w}}{\rho_a} g \frac{\rho_w}{\rho_a} \right]^{1/2} \quad (2.4.45)$$

A comparison between Equation (2.4.43) and (2.4.45) indicates, that in the limits, a thin oil slick is considerably more stable than a thick oil slick under similar conditions. This result is contingent upon the fact that the oil-air surface tension has a stabilizing influence when the layer is thin, but has less influence when the layer is thicker.



It has been consistently observed in various studies that the initiation of oil droplet formation occurs at velocities in excess of those predicted by K-H analysis. Citing the work of Drazin (1970), in which it was shown that unstable waves may be stabilized by the non-linear terms ignored in the linear stability analysis, Liebovich argues that wave breaking should occur at some velocity exceeding  $U_{cr}$  by the previous linearized K-H instability analysis. According to Drazin's non-linear analysis, infinitesimal amplitude waves grow until they achieve a finite amplitude. The wave length remains unchanged during amplification and corresponds to the critical wave number  $K_{cr}$  given by linear stability analysis as the fastest growing waves. A time independent equilibrium amplitude  $A_c$  for the critical wave number  $K_{cr}$  is described as;

$$U_w - U_0 = U_{cr}(1 + 5/32 K_{cr}^2 A_{cr}^2) \quad (2.4.46)$$

where  $K_{cr} A_{cr} = s$  = wave slope

Liebovich concludes that waves along the oil-water interface break and lead to droplet formation when the equilibrium, most stable, waves achieve a maximum wave slope. Thus if the critical breaking wave slope  $s$  is constant then droplet formation should occur at a velocity  $U_d$ , as a constant multiple of  $U_{cr}$ , ie.  $U_d = kU_{cr}$ .

Interfacial waves breaking with a wave slope near unity would account for the experimental droplet formation velocities reported by Hydronautics. Their droplet formation velocity  $U_d$  can be expressed as;



$$U_d = 2.2 U_{cr} \quad (2.4.47)$$

The literature has repeatedly reported that oil droplet formation is basically restricted to the headwave zone. As previously mentioned, Wicks has suggested that the headwave dominance stems from the instability of the headwave at the point of maximum thickness discussed by Benjamin. Hydronautics argue the droplet formation on the lee of the headwave results from an adverse pressure gradient. Leibovich postulates a more simplistic cause. The local current speed is greatest at the maximum thickness point. This locally higher current speed implies that droplets can be split off from the headwave by breaking of the K-H waves prior to oil droplet formation elsewhere. A range of  $U_w - U_0$  thus exists where droplets form only at the headwave. At higher speeds the droplet shedding rate will continue to be greatest at the headwave but shedding would be expected everywhere along the oil slick. Leibovich derives the maximum current velocity from the recognition of Benjamin's headwave Froude Number as  $U_{max} = 2U_d$ . The previous section has shown that the current velocity for droplet formation is  $U_d = 2.2 U_{cr}$ , thus the actual velocity at which the droplets are torn from the oil slick is given as;

$$U_{max} = 2.2 (2)^{1/2} U_{cr} = 3.1 U_{cr} \quad (2.4.48)$$

Leibovich concludes that since droplets will not be shed from the downstream portion of the oil slick until the local current velocity exceeds  $U_{max}$ , there is a range of currents velocities  $U_d$ ;

$$2.2 U_{cr} < U_d < 3.1 U_{cr}$$



for which droplet formation must be confined to the headwave.

Milgram and Van Houten (1978)

Milgram and Van Houten have reported several experimental observations that reinforce the hypothesis that droplets are generated by the breaking of Kelvin - Holmholtz waves. Initially, they were concerned that the observed interfacial waves were results of the Tollmien-Schlichting instability phenomena. Tollmien-Schlichting instability occurs during the transition from laminar to turbulent boundary layer flow along the interface when the viscous forces, which have been restraining the small disturbances, are overwhelmed by the inertial dynamic forces. Milgram and Van Houten present the following three reasons to indicate that the observed interfacial waves were in fact, Kelvin-Helmholtz waves and not the results of fluctuations in Tollmien-Schlichting waves.

1) The characteristics of Kelvin-Helmholtz waves depend on fluid densities, interfacial tensions, and flow speed, but not on downstream location. For a given oil type and flow speed, the waves we observed had constant phase speed and wavelength as they moved downstream, thus behaving as Kelvin-Helmholtz waves. On the other hand, Tollmien-Schlichting waves would be expected to become longer and move more slowly as they move downstream as a result of the increasing Reynolds Number and boundary layer thickness with downstream position.

2) As the flow speed was slowly increased, the waves first appeared near the leading edge of the oil slick, as would be expected for Kelvin-Helmholtz waves because the shear layer in the water is stronger there than it is further downstream. Tollmein-Schlichting waves would be expected to appear downstream first owing to the larger Reynolds Number based on slick length for downstream regions than for upstream regions.



3) At the higher flow speeds when the interface is quite rough, starting a short distance downstream from the region where the waves begin, the boundary layer must become turbulent and cease to support Tollmien-Schlichting waves having any regularity. However, we observed interfacial waves possessing some regularities over almost the entire slick, although their amplitudes were substantially diminished far downstream. This indicates that they were not Tollmien-Schlichting waves.

Milgram and Van Houten observed that the waves did not appear at the leading edge, but rather appeared a short distance aft of the leading edge. They attribute this to the stabilizing effect of a thin slick as indicated by Leibovich, since the leading edge of the oil slick is very thin in comparison to the headwave maximum thickness. The amplitude of the interfacial waves was largest in the vicinity of the headwave corresponding to the region of maximum shear coefficients (section 2.2.) and both shear and wave amplitude was found to increase with increasing water velocity.

Droplet formation always occurred on the leeward side of the headwave where the local water velocity was highest. However, under certain conditions some of the oil slicks had a geometry with the highest local velocity occurring in the viscous zone of the oil slick although K-H waves did not break within the viscous zone. From this observation, Milgram and Van Houten suggest that the droplet generation phenomena is more complex than postulated by Leibovich, who determined that entrainment occurs with any specific oil wherever a certain critical speed is exceeded in the flow beneath the oil, independent of the portion of the slick at which the required velocity occurs. Milgram and Van Houten speculate that the amplitude of the



interfacial waves depends not only on the water speed below the boundary layer in the water, but also on the boundary layer thickness itself. When the layer is thick, changes in interfacial shape lead to smaller pressure changes than when the boundary layer is thin. Droplet formation was observed only in the headwave where the local water velocity was high and the boundary layer was thin (as indicated by high friction coefficients). Downstream, though the local velocity was high, the boundary layer was considerably thicker and no droplet formation was observed. The wave slope of breaking interfacial waves was reported to be close to unity as required by Leibovich's theory, but increased boundary layer thickness reduces the amplitude growth more than was suggested by Leibovich.

Another aspect of K-H instability reported by Milgram and Van Houten was the apparent inconsistency between the most unstable wave length of classical K-H waves and those observed during the course of their experiments. They cite observing wave lengths in the range of 10 to 25 centimeters for a heavy mineral oil, whereas, the critical wave length given by Equation (2.4.43) indicates the waves should have been 4.3 centimeters in length. Evidently the relatively large damping of the very short waves prevented them from growing large enough to break. Considerable shorter waves were observed in diesel oil, in which Equation (2.4.43) yielded a critical wave length of 2.4 centimeters. Since the kinematic viscosity of the diesel oil is less than 3 percent of that for the heavy mineral oil, the shorter K-H waves undergo less damping and as a result waves of the order of  $K_{cr}$  were observed. Milgram and Van Houten concluded that the viscosity of



the oil plays a role in determining the critical speed of droplet formation by suppressing the growth of the most unstable K-H waves when the viscosity is sufficiently high.

## 2.5 Summary

In summary, the following conclusions pertaining to the headwave zone can be drawn. The theoretical analysis by Benjamin appears to describe the asymptotic thickness of the neck, downstream of the maximum thickness of the headwave, with a fair degree of accuracy. This analysis, based on the concept of momentum balance, allows for the prediction of the headwave with a simple Froude number model. Benjamin's analysis further describes the magnitude of the energy loss which is required for this momentum balance. However, the neglect of shear stresses results in the breaking of the headwave to achieve this desired energy dissipation. In order for the headwave to break, the oil thickens to roughly twice the downstream depth causing the water to become super-critical locally. The results of Milgram and Van Houten's testing strongly suggests that the shear stresses predominate in the energy loss mechanism and, thus, at the lower velocities, and consequently lower energy loss levels, the oil slick is observed without a breaking headwave. However, at the larger velocities when the energy loss requirements are maximum, the shear stresses are insufficient to consume all the energy and the headwave must break in the manner previously described.



There is total agreement, between the various investigators, concerning the governing forces which come into play within the viscous zone. There are several models developed which describe the growth of the viscous zone by various methods of accumulating the interfacial shear stresses. It is only magnitude of shear stress and the method of utilizing the shear stresses that differs.

The simplest models employing constant shear were proposed by Cross and Hoult, by Lindenmuth, Miller, and Hsu, and by Hale, Norton, and Rodenberger. This last study included several empirical relationships to describe the various aspects of the viscous zone.

There are two main attributes which stem from Wicks' analysis. The evaluation of interfacial shear stress is not limited to a spacial constant coefficient of friction. Furthermore, the shear stress is evaluated from the difference between the interfacial velocity  $U_i$  and the free stream velocity  $U$ . The major contribution of Wicks' analysis has been the attempt to include the mechanics of flow within the oil slick in evaluation of the oil slick thickness in the viscous zone.

The principal contribution of Wilkinson's viscous zone model is the employment of the boundary shear for the flow of finite depth. The major practical application of this concept should be in the extrapolation of model to prototype oil slick geometries.



Milgram and Van Houten's detailed analysis of the viscous zone demonstrated conclusively the importance of the interfacial shear stress in the development of the viscous zone. They suggested that the friction distributions fall into two distinct types but were unable to formulate boundary limits.

The onset of entrainment failure is the result of Kelvin - Helmholtz instability at the oil-water interface. The most comprehensive analysis of linear K-H instability is given by Leibovich. Linear K-H instability analysis under predicts the critical velocity for interfacial breakup. Citing the work of Drazin (non-linear K-H instabilities), Leibovich demonstrates the interfacial breakup occurs at a finite value higher than predicted by linear K-H analysis. Milgram and Van Houten further argue that the development of a interfacial boundary layer retards the critical breakup velocity by suppressing the growth of the shortest (most unstable) waves.

This literature review documents the basic oil slick phenomenon for the ice free oil slick. The subsequent chapters will examine various components of the oil slick as they are affected by the addition of a solid ice cover.



## CHAPTER 3

### SCOPE OF LABORATORY STUDY

#### 3.1 Introduction

The experimental phase of this study was directed to the investigation of the characteristic behaviour of ice covered oil slicks. The experiments were designed to address the following objectives:

- 1) Initially, to determine insight into the basic characteristics of oil slicks, control experiments were conducted under a varying range of flow conditions in order to observe and document the behaviour of ice free oil slicks.
- 2) A primary objective was to identify the fundamental characteristics of oil slicks as influenced by the presence of an ice cover. Under a similar set of flow conditions utilized in the control experiments, the addition of a model ice cover permitted the observation and documentation of the basic differences in behaviour of ice covered oil slicks.
- 3) In order to determine the mechanisms by which the differences in behaviour evolved, detailed velocity profiles within the oil slick and water phase were measured in both the control and ice covered experiments. This provided the basis for an evaluation of the shear stress at the interface



and examination of its changes as influenced by an ice cover.

4) The formation of interfacial waves has been demonstrated to be responsible for the initiation of entrainment failure of oil slicks. An objective in this study was to indentify the role of a solid boundary (ice cover) as it affects growth of interfacial waves.

In order to pursue these objectives, several measurements were conducted to establish the various properties of oil slick behaviour relating to the slick thickness profile, velocity profile, and the interfacial wave characteristics. Both the control and ice covered experiments encompassed a complete range of Froude Numbers in which the primary variable was the water current.

The remainder of the chapter describes the various aspect of the testing arrangement and outlines the experimental procedures utilized in this study.

### 3.2 Equipment

The experimental tests were conducted at the T Blench Hydraulics Laboratory, located at the University of Alberta.

The model basin utilized for all the oil slick tests consisted of a self contained re-circulating flume. The useable test section measures 5.0 m in length, 0.46 m inside width, and 0.9 m in



depth. Both of the flume walls were constructed of plexiglass, 12 mm in thickness, which facilitated both ease of observation and photography. The bed of the flume consisted of aluminum plate constructed in a fixed position of zero slope. A schematic diagram of the general flume configuration is depicted in Figure 3.1.

Located at the upstream end of the test section was a headbox measuring approximately 1.8 m in length, 1.0 m in depth and 0.5 m in width. Water was introduced from a pipe, over the full width of the bottom, at the upstream portion of the headbox. Inside the headbox was a baffle system consisting of a full depth coarse metal screen covered with a rubberized porous material similar to a furnace air filter. This baffle system coupled with a floating plywood board was required to minimize the severe turbulent fluctuation of the water surface induced by the water discharging into the headbox.

The sufficiently narrow width of the headbox removed the need for a lateral transition. Between the headbox and the upstream of the test section, the flume was fitted with an entrance gate. During the course of testing, this gate was raised above the water surface and consequently had no effect on the control of the flow. Water levels in the flume were maintained by the adjustment of the variable position undershot gate, located downstream of the test section. Water discharging from the undershot gate was conveyed down a short free flowing chute into the sump.

The steel sump, isolated solely to the flume, provided a



storage capacity of 4.5 m<sup>3</sup>. The self contained re-circulating flume was furnished with a pump and appropriate piping between the sump and headbox. The pump, in its current piping configuration was capable of delivering a maximum discharge of 0.061 m<sup>3</sup>/s. The flow was regulated by a gate valve downstream of the pump adjacent to the headbox. The regulated discharge was monitored with an inline magnetic flowmeter located between the pump and the gate valve.

The afore-mentioned flume configuration had been constructed several years prior to the initiation of this study. This flume was selected for use in this study, primarily because its isolated sump removed the danger of lost oil contaminating the rest of the hydraulics laboratory. However, in order to conduct the oil spill tests, two additional features were incorporated into the flume configuration.

The first modification consisted of constructing an auxiliary undershot gate within the test section. Located 1.0 m upstream of the water level control gate, this second gate provided an oil slick boom of variable boom draft. A plywood sheet was mounted on a rack and pinion thus allowing adjustment in the boom draft. Since the boom was free to move in the vertical direction, rubber strips 3 cm wide, were mounted at the side of the boom on the upstream face forming a concave seal against the wall of the flume.

The water flow in a flume has an inherent lateral velocity distribution resulting from the boundary layer effects of the flume



walls. This velocity pattern yields a stagnation pressure distribution at the boom associated with a lateral vortex formation at the walls of the flume immediately upstream of the boom. If unarrested, these vortices quickly drain the oil slick beneath the boom, regardless of the boom draft. Suppression of these vortices was accomplished by the installation of a 0.1 m thick strip of rubberized porous mat on the upstream face of the boom. This mat reduced the higher water velocities over the central portion of the boom and suppressed the resulting differential pressure gradient to a level incapable of driving the vortices. A secondary function of the porous mat was to absorb wave energy and minimize the reflection of waves (characteristic of a rigid boom) in the oil.

The second addition to the flume was the incorporation of a removable ice cover. The model ice cover consisted of a single 0.2 m x 0.012 m thick strip of plexiglass and two strips of plywood 0.13 m x 0.012 m thick fastened on either side of the plexiglass to form a solid smooth cover 0.46 m wide x 0.012 m thick. The central transparent section of the ice cover permitted both the observation and the overhead lighting of the oil slick. The model cover was 3.5 m long and was floated on the surface of the oil and water upstream of the boom.

The model cover was narrower than the flume to facilitate ease of removal, thus the ice cover was propelled upstream by the shear forces exerted by the oil slick as the upper layer of oil flowed upstream. The ice cover was wedged in place to prevent this problem.



Since the model ice cover consisted of only a smooth solid sheet it did not attempt to model all aspects of a real ice cover. Only those characteristics determined by a solid boundary on the surface of the oil were investigated and no consideration was given to behavioural changes induced by the interaction of the oil and ice with respect to their thermal and or chemical properties.

### 3.3 Measurements

To achieve the experimental objectives outlined at the begining of this chapter, three distinct characteristics of the oil-slick were monitored. The principal measurement consisted of determining the chartacteristic length and thickness profile over a complete range of flow conditions.

A major emphasis of this study addressed the measurement of velocity profiles both in and below the oil slick. This type of measurement was fundamental in establishing the interfacial shear stresses and in developing an understanding of the internal flow mechanisms of an oil slick.

The last series of measurements consisted of defining the interfacial wave characteristics as functions of both time and space.

The remainder of the section addresses the specific details involved in the three forms of measurements.



The characteristic length scales of the oil slick were successfully determined by two independant methods. The most obvious of these was to measure the oil slick profile outlined on the plexiglass flume walls. The oil slick was in continuous motion as interfacial waves travelled down its entire length. Thus, the thickness profile was recorded by visual integration (with time) of the interfacial position every 0.05 m along its length. Although the oil slick shape at the flume walls appeared to be adequately representative of the oil thickness for the full width at a given section, the leading edge of the slick was not spacial invariant. The recorded slick length was derived from the visual averaging the positon of the leading edge of the oil slick over the flume width.

As second set of oil slick profiles was determined, indirectly by recording the oil slick phenomena on super 8 mm film. To facilitate accurate measurements, the flume wall was outlined with thin black tape to form a grid network composed of 0.05 m squares. Viewing of the film enabled a frame by frame analysis of the oil slick profiles, and facilitated describing the instantaneous interfacial wave forms.

A third method employed to measure the oil slick profile was somewhat unproductive. This procedure consisted of utilizing a water surface probe to indicate the oil-water interface. The probe consisted of a thin steel rod in which the resistance of water at varying depths of penetration provided input for a feed-back circuit which in turn positioned the probe mechanically to maintain a constant



depth of penetration. Since oil is a relative insulator, the electronic controls could be adjusted to have the probe penetrate the oil and detect the oil-water interface. This type of apparatus could ideally produce a continuous plot of the oil-water interface in the middle of the flume away from any wall effects. However, with the passage of an interfacial wave, the probe would follow the water surface down as the oil thickened but it failed to return as the wave passed. The apparent reason for the probe's failure was that a thin layer of oil would adhere to the probe and fail to rise at the same rate as the general oil-water surface owing to the oil's high viscosity. Thus with a coating of oil on the probe, the probe constantly stayed at the maximum oil depth with successive passage of interfacial waves

One of the principal objectives of this study was to examine the interfacial shear stresses as influenced by the addition of an ice cover to the oil slick. Earlier investigators have evaluated the interfacial shear stress indirectly from an overall force balance of the oil slick. Wicks (1968) considered the effects of a velocity distribution by assuming a linear distribution throughout the oil slick. Wicks' velocity profile consisted of identical velocities and quantities of flow above and below the midpoint of the oil slick. Further researchers have shown the velocity distribution to deviate drastically from Wicks' simplified model, but their velocity measurements have consisted only of crude estimates of the top surface and interfacial surface velocities. Therefore the major emphasis of this study is to delineate the internal velocity distribution of an oil



slick and evaluate its role on the interfacial shear stress.

In this investigation, three independent techniques were employed to describe the velocity field within the oil slick. Briefly they were:

- 1) The timing of particles on both the top surface and interfacial surface was utilized to determine each of the velocities respectfully.
- 2) A pitot tube coupled with a differential pressure transducer was used to establish the velocity field below the oil-water interface.
- 3) A laser anemometer was used to accurately establish velocity profiles in the water phase and within the oil slick itself.

These first two methods are similar to those utilized by the previous researchers. However, due to the major drawbacks inherent in their usage they are limited to the crude estimation of the velocity distribution. The timing of particles has the obvious limitation of establishing only two points on a velocity distribution. The major handicap associated with the use of a pitot tube is that the size of the instrument is so large, compared to the flow, that the instrument invariably interacts with and induces changes in the velocity field.

On the other hand, a laser anemometer does not disturb the flow and can be used to accurately define the velocity of a point. It



was perceived that the use of a laser anemometer would be unique to this oil slick study and it would provide considerable data on the velocity profile in the oil slick.

A brief description of each of these three methods follows.

The first method of measuring the travel time of particles was utilized in most oil slick tests, including those not directed solely to velocity measurements. This method, though somewhat crude, provided a quick and easy verification of the velocities determined by the other two methods.

Each velocity measurement at a given point consisted of the average of a minimum of three separate trials. An individual trial involved the release of a small paper flag upstream to the point of interest and timing its travel over a distance of at least 30 cm. The corresponding velocity was assigned to the midpoint for the test reach.

The small paper flag would float on the water at the oil-water interface. However, in some cases, the paper flags released at the interface would assume an orientation deviating from parallel with the interface. This behaviour would result in an observed velocity slightly lower than the true interfacial velocity. This problem was not evident with the top surface and it was considered that the surface flags accurately represented the surface velocity.

This method was subsequently used to estimate point



velocities for both the interface and top surface at intervals approximately 60 cm. apart.

The pitot tube measurements were originally used as an independent check of the laser anemometer velocity measurements conducted below the oil in the water phase. However, an attempt to measure the velocities using a pitot tube, within the oil slick was conducted with some degree of success.

The pitot tube was connected to a differential pressure transducer with a full scale range of  $\pm 1.0$  inches of water. The analog output from the transducer was input to a strip chart recorder. Individual point velocities were derived from averaging the strip chart recording of a two or three minute continuous sample.

There were two major problems associated with the utilization of the pitot tube measurements in this study. First, the extension of the pitot tube into the water from the top surface required that the tube penetrate through the oil slick into the water phase. The portion of the tube penetrating onto the water below the oil experienced a form drag associated with the water velocity. This form drag would result in a reduction in pressure within the immediate vicinity of the pitot tube. Consequently some of the oil from the slick would be "sucked" into the water phase. However, this problem was restricted to a finite layer below the oil slick. Below this layer the intrusion of oil was insignificant, compared to the depth of velocity measurement, so the oil failed to adversely influence the



reading. Above this finite layer, in close proximity to the interface, the pitot tube had insufficient penetration resulting in a minimum form drag and no noticeable disturbance in the oil-water interface.

The second major drawback concerning the usage of pitot tube occurred during the measurements of the interfacial velocities. The interface exists in a continuously changing form in the presence of interfacial waves, travelling the entire length of the oil slick. With time this results in a change in the fluid medium at a given fixed depth of penetration in the vicinity of the interface. A problem resulted with the passage of interfacial waves as the static and dynamic ports of the pitot tube were exposed to either oil or water. The oil and water phases would transmit pressure fluctuations as different rates resulting in some erroneous readings at the interface.

Even with these major obstacles inherent with the usage of a pitot tube at the interface, the measurements proved to confirm the measurements obtained by the laser anemometer.

The laser doppler anemometer (LDA) is a sophisticated and accurate technique of measuring fluid velocities. Even though it is a complex and extremely expensive method, it offers the primary advantage of non-disturbance within the flow, since only the laser beam is in direct contact with the flow. The flow in an oil slick is confined to a small layer and any conventional probe induces changes



in the velocity field as it attempts to measure it. It is the non-disturbance property of laser anemometry that makes it attractive for this type of study.

A second advantage to usage of this technique is its possible utilization when the condition of a solid ice cover exists on top.

The equipment used in laser anemometry consists of a laser, transmitting optics, receiving optics, and a signal processor. A simple model, termed the fringe model, describes the basic physics utilized in laser anemometry.

First the laser beam is split with a prism into two parallel beams. These beams are focused with a diverging lens characterized by a short focal length, to form an intersection point within the velocity field. If a projection of the intersection were conducted, the image formed would be a pattern of vertical lines of light and dark. These are the interference fringes caused by the intersection between the two monochromatic laser beams. The fringe spacing is a function of the intersection angle and the wave length of the laser light. As a particle within the velocity field passes through the intersection point it reflects scattered light as it moves from the dark to light fringes. This "signal" is received by an electro-optical device and is converted to an analog electrical signal. The signal takes the form of a sine wave with an amplitude proportional to the amount of light scattered in a period equal to the time taken by the particle to cross a single fringe of light and



dark. Since the fringe spacing is constant with a given intersection angle, the instantaneous velocity can be calculated from the signal period.

There are several methods of utilizing the laser anemometry technique. The first, termed forward scatter, exists when the transmitting and receiving optics are on opposite sides of the flume. The second method, termed back scatter, exists when both the transmitting and receiving optics reside on the same side of the flume. The forward scatter method is preferable since the resulting signal is much stronger and easier to track. However, physical space limitation on the flume dictated the use of the back scatter method. As a result of using back scatter, and the resulting weaker signal, the maximum penetration of the intersection point was limited to approximately 5 cm inside of the flume wall. This could have been easily increased with the use of a stronger laser had one been available. One advantage gained with the back scatter method is that it is fairly simple to mount both the transmitting and receiving optics on the same transversing base.

In addition to the limitation of only 5 cm penetration of the oil slick for the velocity measurements, a second handicap was encountered when measuring zero velocity in the oil slick layer. Interfacial waves travelling the length of the oil slick induce a superimposition of small orbital velocities over the shear velocities of the oil slick in its steady state. Therefore, in certain regions the instantaneous velocity at a given point could be either upstream



or downstream. In the laser anemometer configuration utilized during this study, the instrumentation was unable to detect the direction of velocity. Rather the calculations determined were limited to the absolute magnitude of velocity. This was of minor consequence when the oil velocity direction was obvious but in regions of near zero velocity, when the instantaneous velocity alternated direction, the time average velocity at a given point consisted of a summation of the magnitude of instantaneous velocities. Thus, under certain conditions when the time average velocity was zero resulting from the cancellation of the upstream and downstream component velocities, the LDA recorded erroneous velocity magnitude.

A method exists to overcome this handicap but the required instrumentation was unavailable for the study. Briefly, it consists of the measurement of velocity deviations from an artificial velocity base greater than any encountered in the velocity field.

Though some problems were encountered in the utilization of the laser anemometer, the final results proved to meet expectations. The use of a LDA system allows for the definition of the time average velocity gradient encountered in the internal flow of oil. This technique was, also, implemented when an ice cover extended the oil slick. Chapter 4 presents the experimental velocity profiles depicting the difference in oil slick circulation as influenced by the addition of an ice cover.

The investigation of interfacial waves on the oil slick was



composed of two forms of measurements. First, wave speeds were estimated from the timing of wave crests passing fixed points. A deficiency in these measurements stemmed from the continuously changing form of the waves. The interfacial waves expanded and diminished in amplitude as they migrated downstream. Only the largest waves would maintain a recognizable shape for a continuous distance, and thus only the largest waves could be monitored.

A second and more detailed analysis of the interfacial waves was possible with the use of super 8 mm film. The side of the flume was marked out into a grid pattern. Knowledge of the filming speed thus allowed for a detailed frame by frame examination of the film footage. These measurements resulted in both definition of wave velocity and characteristic shape.

### 3.4 Oil Supply

The basic characteristics of oil slick behaviour vary according to properties of the particular oil involved. Three distinct types of oil were utilized in the experimental phase of this study. The physical properties of these oil, as analyzed by the Standards Laboratory associated with the Chemical Engineering Department at the University of Alberta, are presented on Table 3.1. The reported properties result from tests performed on each of the oil, prior to their use in the flume. Extended use in the experimental study resulted in slight changes in the physical properties but these changes were ignored in the following analysis.



The first oil studied was a common rapeseed vegetable oil available from any retail outlet. This oil would emulsify rapidly during the tests turning the water into a milky color that hindered the observation of the oil slick. In addition, this oil was unsuitable for the laser anemometer velocity measurements.

The second oil was labeled CWO base and was supplied by the Strathcona refinery of Imperial Oil Company Limited. During the testing period this oil remained fairly clear and as a result it was utilized exclusively in the velocity measurements.

The last oil was a dark heavy machine oil acquired from dead storage at the University of Alberta Hydraulics Laboratory. Owing to its high viscosity, this oil was utilized in the investigation of the extreme characteristics of viscosity.

An elaborate oil recovery system was unwarranted as the amount of oil (less than  $0.05\text{ m}^3$ ) employed during individual tests was diminutive. Oil was introduced into the flow by simply pouring pre-measured amounts of oil upstream of the slick. The oil was allowed to flow freely from a bucket onto the water surface in an attempt to minimize the droplet formation and entrainment.

After testing was completed, the oil was recovered with the use of an ordinary wet-dry shop vacuum cleaner and stored in large plastic containers where the oil and water mixture from the vacuum cleaner would separate.



## CHAPTER 4

### ICE COVERED OIL SLICKS

#### 4.1 General

Previous experimental and analytical studies, documented in the literature, have systematically characterized the ice free oil slick phenomena. The purpose of this chapter is to examine, analytically, the changes induced by an ice cover in the behaviour of oil slicks retained upstream of a rigid boom in flowing water. This treatment will be limited to two major areas. First, the addition of a ice cover will alter the internal velocity distribution of the oil. This will, subsequently, affect the force balance of the oil slick. The second major effect of the ice cover will be its influence on the instability of the oil-water interface. These two areas will be examined in detail in the remainder of this chapter.

#### 4.2 Velocity Distribution

Previous investigators, with the exception of Wicks, have ignored the role of internal oil velocity distributions. The momentum within the oil phase is an order of magnitude less than the underlying water phase, consequently the analysis of ice free oil slicks have not been adversely hampered by neglecting the momentum within the oil. However, as indicated in the following section, the oil velocity distributions within the ice free and ice covered oil slicks are shown to be markedly different.



This difference stems from the balance of mass and momentum in the oil slick. The shear force, exerted by the flowing water, on an ice free oil slick induces a forward (downstream) flow of oil towards the boom. However, since the oil is arrested at the boom, a return flow of oil occurs in the upper layer of the slick. The conservation of mass dictates that this mass flux of the return flow must equal the mass flux of oil in the downstream direction. The resulting idealized velocity distribution in an ice free oil slick is shown in Figure 4.1.a as a typical case.

The addition of an ice cover over an oil slick restricts the velocity on the upper surface of the oil to zero, in order to satisfy the condition of no slip at a (rigid) boundary. The reduction of the velocity profile in the upper layer of oil to zero at the oil-ice-interface retards the return momentum flux. However, since the shear forces on the oil-water interface induces relatively the same downstream flow of oil, (a similar momentum flux), the oil slick must thicken to compensate for the momentum deficit resulting from the retarded upper layer return flow. A typical idealized velocity profile in an ice covered oil slick is shown in Figure 4.1.b.

The idealized velocity distributions can be developed by solving the one dimensional Navier-Stokes Equations. It will be assumed that the velocities within the oil are laminar in magnitude and the flow steady. The superimposed orbital velocities induced by the passage of interfacial waves will be ignored.



Referring to the idealized velocity distributions depicted in Figures 4.1.a and 4.1.b , one dimensional flow is defined when the vertical velocity V and lateral velocity W are zero, and the longitudinal velocity U is a function of longitudinal distance x and vertical distance y (ie.  $U = u(x,y)$ ). In addition, the pressure P is also a function of x and y such that  $P = p(x,y)$ . These conditions limit the general form of the Navier-Stokes (N-S) equations to;

N-S Eqn. x direction

$$0 = \frac{-1}{\rho} \frac{dp}{dx} + v \frac{d^2U}{dy^2} \Rightarrow \frac{d^2U}{dy^2} = \frac{1}{\mu} \frac{dp}{dx} \quad (4.2.1)$$

N-S Eqn. y direction

$$0 \approx \frac{dp}{dy}$$

N-S eqn. z direction

$$0 \approx \frac{dp}{dz} \Rightarrow P = p(x) \quad (4.2.2)$$

Continuity Eqn.

$$\frac{du}{dx} = 0 \Rightarrow U = u(y) \quad (4.2.3)$$

Equations (4.2.2) and (4.2.3) indicate that the piezometric pressure is a function of x only and velocity is solely of y, therefore Equation (4.2.1) can only be satisfied if the left hand side and the right hand side are equal to a constant  $C_0$ .



$$\frac{d^2u}{dy^2} = \frac{1}{\mu} \frac{dp}{dx} = C_0 \quad (4.2.4)$$

The general solution to Equation (4.2.4) takes the following form;

$$U = \frac{1}{2\mu} \frac{dp}{dx} y^2 + C_1 y + C_2 \quad (4.2.5)$$

The specific solution for an ice covered oil slick is similar to Couette flow between two parallel flat walls. Referring to Figure 4.1.b the following boundary conditions are evident.

$$\text{At } y = 0 \ U = 0 \rightarrow C_2 = 0$$

$$\text{At } y = h \ U = U_i \text{ interfacial velocity}$$

$$U = \frac{U_i}{h} - \frac{1}{2\mu} \frac{dp}{dx} \frac{h^2}{h}$$

The resulting specific solution for the velocity  $U$  is;

$$U = \frac{y}{h} U_i \frac{-h^2}{2\mu} \frac{dp}{dx} \frac{y}{h} \left( 1 - \frac{y}{h} \right) \quad (4.2.6)$$

Schlichting defines a dimensionless pressure gradient as;

$$P_* = \frac{h^2}{2\mu U_i} \frac{-dp}{dx} \quad (4.2.7)$$

Substituting the dimensionless pressure gradient  $P_*$  into equation (4.2.6), leads to the following dimensionless velocity distribution for Couette flow.



$$\frac{U}{U_i} = \frac{y}{h} [1 + P_* (\frac{1+y}{h})] \quad (4.2.8)$$

An additional boundary condition can be derived from continuity of mass. It was stated earlier that the downstream flow of oil equals the return flow of oil resulting in no net flow of oil past a given section.

$$q = \int_0^h U dy = 0 \quad (4.2.9)$$

Performing this integration yields a dimensionless pressure gradient of  $P_* = -3$ . Thus, Equation (4.2.8) becomes;

$$\frac{U}{U_i} = \frac{y}{h} [1 - 3 (\frac{1-y}{h})] \quad (4.2.10)$$

The maximum upstream velocity of  $U = -0.33 U_i$  occurs at  $y/h = 0.33$  from the top. At  $y/h = 0.67$  the velocity is zero.

The idealized distribution shown in Figure 4.1.b represents Equation (4.2.10).

The case of the ice free oil slick velocity distribution follows the preceding solution but with a different boundary condition on the free surface. Although the velocity on the surface has a finite value, the shear stress is zero. This can be represented by the first derivative of the velocity distribution being set to zero at the free surface.



$$\text{At } y = 0 \quad \frac{dU}{dy} = 0 \Rightarrow C_1 = 0$$

$$\text{At } y = h \quad U_i = U \Rightarrow C_2 = U_i - \frac{1}{2\mu} \frac{dP}{dx} h^2$$

Utilizing the dimensionless pressure gradient of Equation (4.2.7) the specific solution of Equation (4.2.5) in a dimensionless form is;

$$\frac{U}{U_i} = 1 - P_* \left( 1 - \frac{y}{h} \right) \quad (4.2.11)$$

The boundary condition of zero net flow past a given section yields a dimensionless pressure gradient of  $P_* = -3/2$ . Thus Equation (4.2.11) becomes;

$$\frac{U}{U_i} = 1 - \frac{3}{2} \left( 1 - \left( \frac{y}{h} \right)^2 \right) \quad (4.2.12)$$

The maximum upstream velocity of  $U = -0.5 U_i$  now occurs at the top  $y/h = 0$  and at  $y/h = 0.577$  the velocity is zero. The idealized velocity distribution presented in Figure 4.1.a is derived from Equation (4.2.12).

### 4.3 Shear Stress

Development of interfacial shear stress relationships readily follows the preceding laminar flow velocity distribution analysis. Laminar shear stress is proportional to the first derivative of the velocity distribution at the interface.



Differentiating Equations (4.2.10) and (4.2.12) yields the following shear stress relationships;

$$\begin{array}{ll} \text{Ice free} & \text{top } y = 0 \sigma_t = 0 \\ & \text{interface } y = h \sigma_i = \mu \frac{3U_i}{h} \end{array} \quad (4.3.1)$$

$$\begin{array}{ll} \text{Ice covered} & \text{top } y = 0 \sigma_t = -\mu \frac{2U_i}{h} \\ & \text{interface } y = h \sigma_i = \mu \frac{4U_i}{h} \end{array} \quad (4.3.2)$$

$$\quad (4.3.3)$$

A comparison can be made concerning the relative oil slick thickness between the ice free and ice covered conditions. Assuming that for similar approach velocities the interfacial velocities at a given distance from the leading edge of the slick will be basically the same for ice free and ice covered oil slicks, the interfacial shear stresses should be similar. Equating Equations (4.3.2) and (4.3.3) with similar interfacial velocities and shear stress results in the thickness of an ice covered oil slick 4/3 times the thickness of an ice free oil slick.

The utilization of shear stress estimates can be employed in the development of force balance relationships of the oil slick.

Consider the ice free oil slick control volume presented in Figure 4.2.a, the sum of horizontal force states;

$$P_1 + P_3 + \sigma_i \Delta x = P_2 \quad (4.3.4)$$



or

$$\frac{1}{2}\rho_0 gh^2 + \rho_0 g \frac{\rho_w}{\rho_0} (h + \frac{\Delta h}{2}) \Delta h + \sigma_i \Delta x = \frac{1}{2}\rho_0 gh^2 + \rho_0 g (h + \frac{\Delta h}{2}) \Delta h \quad (4.3.5)$$

Assuming  $\Delta h/2 \ll h$  and rearranging Equation (4.3.5) yields;

$$\sigma_i \Delta x = \rho_0 g \left(1 - \frac{\rho_0}{\rho_w}\right) h \Delta h \quad (4.3.6.a)$$

In terms of the interfacial slope  $\Delta m$  this is

$$\sigma_i \Delta x = \rho_w g \left(1 - \frac{\rho_0}{\rho_w}\right) h \Delta m \quad (4.3.6.b)$$

Referring to Figure 4.2.b the force balance for a control volume of oil under an ice covered oil slick leads to a similar solution in which;

$$(\sigma_i - \sigma_t) \Delta x = \rho_w g \left(1 - \frac{\rho_0}{\rho_w}\right) h \Delta h \quad (4.3.7)$$

Equation (4.3.7) applies equally to the increase in oil thickness and the interfacial slope.

Utilization of the previously developed shear stress relationships introduces a unique relationship.

For the ice free case, substituting Equation (4.3.1) for the interfacial shear stress of Equation (4.3.6) yields;



$$\frac{3 \mu U_i}{h} \Delta x = \rho_0 g \left(1 - \frac{\rho_0}{\rho_w}\right) h \Delta x \quad (4.3.9)$$

or rearranging

$$\frac{-3}{2} = \frac{-h^2}{2 \mu U_i} \left[ \rho_0 g \left(1 - \frac{\rho_0}{\rho_w}\right) \frac{\Delta h}{\Delta x} \right] \quad (4.3.10)$$

This corresponds directly to Schlichting dimensionless pressure gradient equation (4.2.7) in which,

$$\frac{dP}{dx} = \rho_0 g \left(1 - \frac{\rho_0}{\rho_w}\right) \frac{\Delta h}{\Delta x} \quad (4.3.11)$$

and results in the same Dimensionless pressure gradient  $P = -3/2$  as given by velocity solution of N.S. Equations.

In a similiar manner substitution of Equation (4.3.2) and (4.3.3) for the interfacial and top shear stress into Equation (4.3.8) yields;

$$\frac{-6 \mu U_i}{h} = \rho_w g \left(1 - \frac{\rho_0}{\rho_w}\right) h \Delta h \quad (4.3.12)$$

or

$$\frac{-3}{2} = \frac{-h^2}{2 \mu U_i} \rho_0 g \left(1 - \frac{\rho_0}{\rho_w}\right) \frac{\Delta h}{\Delta x} \quad (4.3.13)$$

As earlier presented the Dimensionless pressure gradient is now  $P = -3$ .



The direct consequence of these pressure gradients can be shown by the comparison of the interfacial slopes on ice covered and ice free oil slicks. The two slopes are related as;

$$\frac{\Delta h}{\Delta x} \text{ ice covered} = 2.0 \frac{\rho_o}{\rho_w} \frac{\Delta h}{\Delta x} \text{ ice free} \quad (4.3.14)$$

In conclusion, the difference between the velocity distributions and related force balance of ice covered and ice free oil slicks plays a dominant role in describing the influence of an ice cover on an oil slick

#### 4.4 Interfacial Instability

It has been noted by various researchers that the limiting factor to successful containment of oil slicks is the onset of breaking interfacial waves at water velocities of the order of 0.4 m/s. Section 2.4 on interfacial instabilities indicates that the development and eventual breakup of interfacial wave forms can be described by Kelvin - Helmholtz (K-H) instability analysis. Even though the solutions to linear K-H analysis do not predict the exact magnitude of wave breakup K-H analysis is sufficiently capable of indicating trends and order of magnitude on interfacial wave instability.

One of the earlier stated objectives was to document the development of interfacial waves as influenced by an ice cover. The following section outlines the development of K-H instability analysis



as governed by the addition of a solid cover.

Assuming the flow in the water and oil phases is irrotational, the velocity potentials and small perturbations must satisfy the Laplace Equations. Denoting the interface between the oil and water as  $y = 0$ , the following two boundary conditions (B.C.) exist;

B.C. 1) At the ice cover,  $y = h$ , the velocity normal to the ice is zero. Thus  $V_0' = 0 = \frac{d\phi_0'}{dy}$

B.C. 2) If the bottom of the water is sufficiently far, no perturbations exist. Thus  $\phi_w' = 0$  at  $y = -\infty$

The general solutions to the Laplace Equations with the preceding boundary conditions are;

$$\phi_0' = A_0 \cosh K(y-h) \exp [i(kx-\sigma t)] \quad (4.4.1)$$

$$\phi_w' = A_w \exp Ky \exp [i(kx-\sigma t)] \quad (4.4.2)$$

In which,  $A_0$ ,  $A_w$  are constants

$K$  = Wave number =  $2\pi/l$

$\sigma$  = wave period =  $2\pi/\tau$

The interfacial wave form of amplitude  $a$ , can be described as;



$$\eta = a \exp [i(Kx - \sigma t)] \quad (4.4.3)$$

The total derivative

$$\frac{D}{Dt} (\eta(x,t)) = 0 \quad (4.4.4)$$

states that a particle on the interface remains on the interfacial streamline. Expanding Equation (4.4.4) and evaluating at the interface  $y = 0$  (Taylors expansion) yields the following two kinematic boundary conditions;

$$\text{B.C. 3)} \frac{d\eta}{dt} + U_0 \frac{d\eta}{dx} = -\frac{\phi'_0}{dy} \quad \text{at } y = 0 \quad (4.4.5)$$

$$\text{B.C. 3)} \frac{d\eta}{dt} + U_w \frac{d\eta}{dx} = -\frac{\phi'_w}{dy} \quad \text{at } y = 0 \quad (4.4.6)$$

An additional dynamic boundary condition is derived from the balance of pressures at the interface with surface tension such that;

$$\text{B.C. 5)} P_w - P_0 = -T \frac{d^2\eta}{dx^2} \quad \text{at } y = 0$$

The interface is a common streamline between the two fluids, and thus the pressure can be evaluated with a linearized form of the Bernoulli Equation and Boundary Condition 5 becomes;

$$\rho_w \left( \frac{d\phi'_w}{dt} + U_w \frac{d\phi'_w}{dx} + g\eta \right) - \rho_0 \left( \frac{d\phi'_0}{dt} + U_0 \frac{d\phi'_0}{dx} + g\eta \right) = -T \frac{d^2\eta}{dx^2} \quad (4.4.7)$$



Substituting the general solution to the Laplace Equations (4.4.1) and (4.4.2) and the assumed interfacial shape, Equation (4.4.3) into the Boundary Conditions 3, 4, and 5 (Equations (4.4.5), (4.4.6), and (4.4.7)) results in the following three equations;

$$a i(U_0 K - \sigma) = K A_0 \sinh(Kh) \quad (4.4.8)$$

$$a i(U_w K - \sigma) = -K A_w \quad (4.4.9)$$

$$\rho_w [A_w i(U_w K - \sigma) + g a] - \rho_0 [A_0 i \cosh(Kh) (U_0 K - \sigma) + g a] = T a K^2 \quad (4.4.10)$$

The simultaneous solution for the three unknowns  $a$ ,  $A_0$ , and  $A_w$  yields the following

$$\rho_w (U_w - C)^2 + \rho_0 (U_0 - C)^2 \coth(Kh) - T K - \frac{g}{K} (\rho_w - \rho_0) = 0 \quad (4.4.11)$$

Solving for the interfacial wave speed  $C$  yields;

$$C = \frac{\rho_w U_w + U_0 D}{\rho_w + D} \pm \left[ \frac{g(\rho_w - \rho_0) + T K^2}{K \rho_w + D} - \frac{\rho_w D (U_w - U_0)^2}{(\rho_w + D)^2} \right]^{1/2} \quad (4.4.12)$$

In which  $D = \rho_0 \coth(Kh)$

The first term of Equation (4.4.12) is the weighted mean velocity of flow and the terms within the square root indicate the interfacial wave velocities. Instability of the interface will occur when  $C$  becomes imaginary. Denoting the critical flow velocity

$U_{cr} = U_w - U_0$ , instability is defined as;



$$U_{cr}^2 = \frac{(\rho_w) \rho_0 \coth Kh}{\rho_w + \rho_0 \coth Kh} \left[ \frac{g}{K} (\rho_w - \rho_0) + TK \right] \quad (4.4.13)$$

The density of water in the S.I. system is 1 g/cm<sup>3</sup>, thus for convenience Equation (4.4.13) reduces to;

$$U_{cr}^2 = 1 + \frac{\tanh Kh}{\rho_0} \left[ \frac{g}{K} (1 - \rho_0) + TK \right] \quad (4.4.14)$$

It is evident from Equation (4.4.14) that for a given wave Number K the critical velocity  $U_{cr}$  increases with the depth of oil h.

Reduced to a similar form, the analysis of ice free interfacial waves presented by Leibovich (Section 2.4 and Equations (2.4.40) and (2.4.42)) becomes;

For thin slicks as  $h \rightarrow 0$

$$U_{cr}^2 = g/K + K (T_{o/a} + T_{o/w}) \quad (4.4.15)$$

and for thick slicks as  $h \rightarrow \infty$

$$U_{cr}^2 = (1 + 1/\rho_0) [g/K (1 - \rho_0) + KT_{o/w}] \quad (4.4.16)$$

As previously stated Equations (4.4.15) and (4.4.16) show that ice free oil slicks are destabilized by increasing thickness. Initially it would appear that since Equation (4.4.14) indicates the converse for an ice covered oil slick that this alone should suffice in describing the stability of ice covered oil slicks. However, close examination reveals that for thick slicks, Equation (4.4.14) equals



Equation (4.4.16) and both ice free and ice covered thick slicks have similar instability. The conclusion drawn from a comparison of all three equations would be that ice free slicks should be as stable, if not more, than ice covered oil slicks.



## CHAPTER 5

### EXPERIMENTAL RESULTS

#### 5.1 General

The intent of this chapter is to present the results of the experimental phase of the study. As indicated earlier, the objectives of this investigation, aside from the initial familiarization with the behaviour of an ice free oil slick, were three-fold. First, a series of tests was conducted in conjunction with the control runs to identify the basic behavioural differences resulting from the addition of an ice cover. Secondly, the distribution of internal oil velocities was investigated both with and without an ice cover. Finally, the formation of interfacial waves as influenced by the addition of an ice cover was examined.

#### 5.2 Test Schedule

The afore-mentioned objectives were realized through three series of tests. The three series are broadly defined in the following paragraphs. It should be noted at this point that observations, documentation and objectives of several tests overlapped the series boundaries.



### Series A Preliminary Testing.

This series served to produce control tests of ice free oil slick behaviour and to develop an intial understanding of the influence of a solid ice cover. Series A was conducted exclusively with the rapeseed oil. A total of 15 tests consisted of longitudinal profile measurements were performed.

### Series B Velocity Distributions.

This series was restricted to defining the internal oil slick velocity distributions in both ice covered and ice free oil slicks. A total of 9 runs were conducted of which 8 utilized the CWO base oil, and 1 used rapeseed oil. In addition to the velocity data, longitudinal profiles were recorded.

### Series C Interfacial Waves.

This series of testing consisted of filming 20 individual tests. Stop action analysis of the films facilitated documentation of interfacial waves, longitudinal profiles, and observation of the headwave developments. Series C involved testing of all three oils.



Table 5.1 summarizes the complete range of test conditions utilized in the 44 tests.

The synopsis of test results are subsequently presented as a general discussion preceding the individual interpretation.

### 5.3 Series A Test Results

A brief description of the overall oil slick behaviour with and without an ice cover is a preliminary requisite for the appreciation of the experimental results. Information contained in this section is primarily a capsule summary of the observations concluded during the course of Series A testing. However, some of the general observations pertaining to different oils (ie.Series B and C) are included in this section. Subsequent sections will present the detailed experimental results of Series B and C.

Basically, a rigid boom of sufficient draft was deployed into the flume to arrest and pond a fixed volume of oil in order to form an oil slick of some deterministic shape. The longitudinal profiles corresponding to the 44 tests are recorded in Appendix A. The resulting shape, the oil slick assumed, can be characterized by three velocity ranges. The transition of the shape between these ranges was not clearly distinguishable and the range limits vary with the properties of the three oils tested.



Typically, at low water velocities of the order of less than 0.2 m/s, the oil slick assumed a smooth parabolic shape with little or no evidence of either a headwave or interfacial waves.

As the water velocities were increased to somewhere between 0.2 and 0.4 m/s, the oil slick profile obtained a more distinct shape, characterized by the formation of a headwave at the leading edge of the slick and the development of interfacial waves along the entire length of slick. For a given volume of oil, the oil slick length shortened as the velocity was incremented.

Finally, the last stage was obtained as the water velocities were further increased to exceed approximately 0.4 m/s. The oil slick continued to thicken and decrease in length until the interfacial waves started to break in the vicinity of the headwave. Oil droplets were entrained into the flow and when water velocities were sufficiently high, the oil droplets did not rise back and coalesce with the slick but rather swept past the boom. The breakup of interfacial waves resulted in a rapid loss of oil past the boom. Consequently, oil profiles and measurements in this study were restricted to velocities below this range.

The preceding description applies equally to the ice free and ice covered oil slicks, although the range limits varies between the three distinguishable stages.



It was observed that ice covered oil slicks exhibit two major deviations from their ice free counter-parts. The most obvious difference is that for similar relative velocities, ice covered oil slicks are thicker and shorter than ice free oil slicks. In addition the headwave itself appears to be thicker but less pronounced at the downstream contraction than at similar velocities in the ice free case. The second dissimilarity is the apparent stability of the interfacial waves and the associated diminished entrainment failure at comparable approach velocities to those of the ice free oil slicks.

As indicated above, ice covered oil slicks are shorter than their ice free counter-parts at similar approach velocities. The ice covered oil slick exhibit an analogous behaviour to ice free oil slick in their tendency to shorten with increasing approach velocity.

In order to represent the various oil slick lengths as a function of approach velocity a normalized "effective length" is defined. The effective length directly incorporates the relative influence of headwave thickness, near boom region, volume of oil, and the flume width.

The first factor to be considered in defining an effective length is the initial thickness of the headwave. The relative headwave thickness of two different oils should be related by the ratio of their specific weights (Equation 2.2.1). Drawing upon the difference between Benjamin and Wilkinson's definition of the Headwave Froude Number, the ice covered headwaves exceeds the thickness of ice free



headwaves by the inverse of specific weights. The definition of effective Length uses the specific gravity of rapeseed oil to normalize all 44 tests.

A second factor in the definition of the effective length pertains to the influence of the near boom region. In the immediate vicinity of the boom the thickness of oil is primarily governed by the stagnation pressure induced by the protruding boom draft. In this case it was assumed that this influence occurs for a reach length upstream of the boom equal to 5.0 times the boom draft. Consequently 5.0 boom drafts are subtracted from the measured oil slick length.

Finally the length of an oil slick is governed by the volume of oil tested and the width of the flume. In this case the width of the flume is constant for all tests and is not included in the effective length.

Coupling the preceeding factors together, the effective length of the oil slick is defined as;

Ice free;

$$\text{El.} = \frac{\frac{s_{\text{rape}}}{s_{\text{oil}}} \text{ length} - 5.0 \text{ boom draft}}{\text{volume}}$$

Ice covered;

$$\text{El.} = \frac{\frac{s_{\text{rape}}}{s_{\text{oil}}} \times \frac{1}{s_{\text{oil}}} \times \text{length} - 5.0 \text{ boom draft}}{\text{volume}}$$



Utilizing these relationships, all 44 test have been plotted as Effective length ( $E_l$ ) vs Approach Velocity and are presented in Figure 5.1 .

#### 5.4 Series B Test Results

Table 5.1 reveals that 9 runs were conducted to investigate velocity distributions. A total of 10 velocity profiles were recorded of which 4 were under an ice cover. These 10 velocity profiles are plotted in Appendix B

In order to validate the theoretical velocity distributions developed in Chapter 4 ,Equation (4.2.10) (ice covered) and Equation (4.2.12) (ice free), it is neccesary to reduce these profiles into a non-dimensional form.

As evident in Appendix B the interfacial velocities were not directly measured by the laser anemometry system. The interface oscillated vertically with each passage of an interfacial wave and since the laser was aimed at a fixed vertical location, the readings were conducted in a continuously changing medium between water and oil. The coefficients utilized with the laser system in calculating velocity differ with oil and water, and, thus, any attempt to directly calculate the interfacial velocity was impractical.



Estimates of the interfacial velocities were derived from the internally measured velocities and with the aid of the preceding theoretical relationships. In the case of ice free conditions, the surface velocity was first established by extrapolating the measured velocities immediately below the surface. This velocity was in turn assumed to be -0.5 times the interfacial velocity as suggested by Equation (4.4.12). For the ice covered condition, the interfacial velocity was calculated as -3.0 times the maximum upstream velocity. Both the surface and interfacial velocities developed in this manner are indicated in Appendix B.

Utilizing the estimates of interfacial velocity, dimensionless velocity profiles composed of  $U(\text{measured})/U_i(\text{calculated})$  vs  $y/h$  were established. The profile for the ice free and ice covered oil slicks are presented in Figures 5.2 and 5.3 respectively.

The development of the internal velocity distributions in Chapter 4 leads to an examination of shear stress and a comparison of the relative slick thickness between ice covered and ice free oil slicks. It was demonstrated that for similar shear stresses and interfacial velocities the ice covered oil slick should be  $4/3$  times as thick as their ice free counterpart. Visual comparison of the oil profiles contained in Appendix A for similar approach velocities reveal that this trend is reasonable. Specific comparison is not possible as the thickness of oil slicks varies with the longitudinal position and the length of ice free, in addition, ice covered oil



slicks also vary.

Support of the assumption of a similar interfacial velocity and shear stress is provided by the following analysis. Figure 5.4 represents the interfacial velocity as a function of approach velocity for both ice free and ice covered oil slicks. The general trend indicates both ice free and ice covered interfacial velocities are similar. Figure 5.5 reveals the shear stress  $\sigma_i$  vs.  $U_i$ ; as calculated by Equation (4.3.1), for the ice free case, and (4.3.3) for the ice covered example. Here again, the ice free and ice covered represent similar shear stress at comparable velcoities. The preceding two plots do not distinguish as to the longitudinal location of the recorded velocity data. However, Figure 5.6 reveals the shear stress coefficient as a funciton of longitidinal Reynolds Number. The coefficient is calculated as;

$$C_i = \frac{2 \sigma_i}{\rho_w U^2}$$

Table 5.2 reveals the primary data used to compile the preceding Figures 5.4, 5.5, and 5.6 .

### 5.5 Series C Test Results

It was observed in ice free oil slicks that intially short waves, at the leading edge, of the order of 5 cm. would grow as they migrated along the slick to become larger waves of the order 15 - 30



cm. within the viscous zone. These waves would travel downstream with the following speed;

Rapeseed oil      15 - 25 cm/s.

CWO base oil      10 - 20 cm/s.

Heavy gear oil      3 - 6 cm/s.

Since a complete range of superimposed waves existed along the slick, encompassing various wave lengths and periods, it was extremely difficult to pin point specific characteristics or develop relationships for the waves as functions of either the different oils or approach velocities in the various runs.

However, the major observation noted, though not quantified, was the addition of an ice cover markedly reduced the interfacial wave activity. Interfacial waves under an ice cover tend to travel slower and are composed of only a few waves with small amplitudes. It was noted that the waves consisted of a longer wave length than those in the ice free oil slick. The overall basic observation during the study indicated that ice covered oil slicks exhibit decreased wave activity, a stable interface, and are less susceptible to entrainment failure at comparable velocities to ice free oil slicks.



## CHAPTER 6

### DISCUSSION

#### 6.1 General

The observations of ice free oil slicks made during this study did not deviate to any significant degree from those reported in the literature reviewed. This chapter primarily addresses the observed behaviour of oil slicks as influenced by an ice cover.

The general characteristics of ice covered oil slicks simulate those of ice free oil slicks. For example, both types of oil slicks exhibit a decrease in oil slick length with an increase in velocity as indicated in the effective length plot of figure 5.1 . With the exception of the heavy oil (in which the viscosity greatly exceeds the other oils), this type of dimensional length/volume adequately describes the general length relationship as a function of approach velocity for both ice free and ice covered oil slicks. Deviations from a single line arise from experimental error, viscosity effects, and error in definition of an effective length (ie. boom draft factor).

The three major differences in behaviour of ice covered oil slicks are the altered headwave activity, a general increased oil slick thickness, and the apparent stability of the oil-water interface. These variations will compose the leading theme of the following sections.



## 6.2 Headwave

The development of the headwave is the one of the most dominant features of oil slicks retained by a boom. A simple Headwave Froude Number states that the thickness of the headwave is twice the thickness of the slick in the lee of the headwave. More specifically, the thickness is a function of Froude Number and relative depth. Benjamin argued that for conservation of energy and momentum the formation of the headwave is imperative. On the other hand, Milgram and Van Houten contradicted this premise by arguing that the shear stresses are all important in the formation of the oil slick profile. They further demonstrate (at low velocities) that in the absence of dynamic considerations the shear stress can adequately describe the oil slick shape. However, at higher velocities, when the headwave is visually obvious its existence can not be described from shear stresses alone. It was observed during the course of this study that with increasing velocity the headwave was more evident.

It is reasonable to consider that both of these arguments are valid to a degree. At lower velocities, the shear stresses are capable of consuming the energy necessary to satisfy Benjamin's momentum requirements, thus explaining the absence of any headwaves in the low velocity ranges. At velocities exceeding about 0.2 m/s, the headwave must form to meet the deficiency in energy consumption not supplied by shear stresses. Observations within this study indicate that the headwave only approached 2 times the thickness at the higher end of the velocities tested.



It was, also, observed that the ice covered oil slick exhibits a thicker headwave but it is less pronounced than in the ice free state at the downstream contraction. This could be caused by two factors. First, the velocity field approaching the oil slick is somewhat reduced in the boundary layer induced by the presence of an ice cover, possibly explaining the less pronounced headwave formation.

The second possible factor describing the increased thickness can be explained by comparing the analysis of headwaves by Benjamin and Wilkinson. Wilkinson allows the oil slick to rise above the water and assumes the stagnation point at the water surface. However, Benjamin's analysis of air cavities assumes the stagnation point is adjacent the cavity roof. This corresponds directly to an oil slick under an ice cover. Close examination of the two headwave thickness relationships reveals that Benjamin's thickness exceeds that of Wilkinson by the factor  $1/s$  (this factor was utilized in the definition of the effective length). Thus, as observed, it is valid that the headwave is thicker under an ice cover.

### 6.3 Velocity Distribution

The dimensionless velocity profiles presented in Chapter 5 (Figures 5.2 and 5.3) appear to be in reasonable agreement with the analytical velocity distributions developed in Chapter 4.

Examination of the velocity profiles contained in Appendix B reveal that the magnitude of velocity is such that the flow is



basically laminar. This supports the use of the simple 1-d solution of the Navier - Stokes Equations for the velocity distributions.

Visual comparison of the two distributions suggests that the deviations from the theoretical relationship are greater for the ice free case. This deviation from the theory probably stems from two sources. First, since the interfacial waves migrate downstream and induce the oil slick to oscillate vertically, the fixed position laser anemometry measurements are actually averaging the velocities from several different oil depths. The interfacial waves were most active in the ice free oil slick since the addition of an ice cover suppressed wave activity. The second source of error is from the neglect of the orbital velocities induced by the passage of interfacial waves. This error would be significant near the interface and of even more importance in the ice free state with its increased wave activity. Evidence of this error is indicated by the slower interfacial velocities measured by floating particles as shown in Appendix B. The particle velocities at the interface were considerably slower than the measured surface velocities and therefore demonstrated the trend for greater error close to the interface. In summary, even though some deviations from theory is evident, the general agreement between the measured and theoretical velocities appears to be acceptable.

In conclusion, the difference between the velocity distributions of ice covered and ice free oil slicks plays a dominate role in describing the influence of an ice cover on an oil slick.



#### 6.4 Interfacial Instability

The second major deviation in the oil slick behaviour, induced by the presence of an ice cover, is the apparent suppression of interfacial wave growth.

There are several possible reasons as to why the preceding conclusions are in direct contradiction to the linear K-H instability analysis. First, it has been suggested that interfacial wave growth is suppressed by the presence of a thick boundary layer. In the case of an ice covered oil slick the boundary layer already present from the ice cover itself should suppress interfacial waves at the interface. This is supported by the observation of waves of greater length on an ice covered oil slick which are less critical than the shorter waves that lead to breakup in K-H instability analysis.

Secondly, viscosity dampens the growth of interfacial waves. The increased thickness of the oil slick as previously demonstrated allows a greater internal dissipation of kinetic energy. This mechanism for viscous energy dissipation appears to suppress the K-H instability at the oil-water interface.

Finally, the preceding analysis has been simplified in several other areas. The K-H solution is based on the assumption of irrotational flow. The analytical and measured velocity distributions indicate that this is not valid for either the ice free and ice covered cases. Liebovich shown that neglect of the non-linear terms



in the solution of K-H instability analysis lead to lower critical velocities than those which exist before the onset of interfacial wave break-up.

In conclusion, although K-H instability analysis indicates that ice free oil slicks should be stable in comparison to ice covered oil slicks, the observations during this study support the preceding arguments that ice covered oil slicks are less subject to instability failure than their ice free counterparts.



## CHAPTER 7

### CONCLUSIONS AND RECOMMENDATIONS

#### 7.1 CONCLUSIONS

The general behaviour of ice free oil slicks is well documented in the available literature. This study serves as an initial evaluation of the effects a solid ice cover causes on the development of an oil slick retained by a boom. The major conclusions arising from this study are as follows:

1. There were no deviations in the behaviour of ice free oil slicks which were contrary to the literature.
2. The headwave under an ice cover was observed to be thicker than those of ice free oil slicks
3. Unique relationships for the internal oil velocities were introduced. The differences between the ice covered and ice free oil slick velocities play a dominate role in describing the influence of an ice cover.
4. As a result of the differences in velocity disrtibutions, the ice covered oil slicks are thicker and shorter.



5. A linear Kelvin - Helmholtz instability analysis indicate the stability of ice covered oil slicks increases with increasing oil slick thickness. However, K-H instability analysis shows that ice free oil slicks should always be more stable than ice covered oil slicks. The observations conducted in this study lead to a direct contradiction to the K-H instability analysis as ice covered oil slicks are more stable than their ice free counterparts.

## 7.2 RECOMMENDATIONS

Prior to the establishment of a comprehensive analytical model of ice covered oil slicks, several critical areas should be examined;

1. In order to facilitate the use of shear stress in a force balance, a more detailed velocity survey should be conducted along the entire oil slick length.
2. The question of interfacial instability shoud be addressed. Emphasis on the establishment of a relationship for the critical breakup velocity should be pursued.
3. The ice cover utilized in this study served only as a solid boundary condition. The effects of a real ice cover should be explored.



## TABLES



TABLE 3.1  
OIL PROPERTIES

OIL I Rapeseed oil

Viscosity	= 67.33	centipoise at 21.1° C
Surface Tension	= 14.71	dyne/cm
Density	= 0.915	gm/cm <sup>3</sup>

OIL II CWO Base

Viscosity	= 22.75	centipoise at 21.1° C
Surface Tension	= 28.24	dyne/cm
Density	= 0.862	gm/cm <sup>3</sup>

OIL II Heavy Oil

Viscosity	= 3794.	centipoise at 21.1° C
Surface Tension	= 32.33	dyne/cm
Density	= 0.910	gm/cm <sup>3</sup>

All oils were properties determined prior to use in the flume.



TABLE 5.1  
TEST SCHEDULE

RUN NUMBER	ICE	OIL	VOLUME liter	VELOCITY cm./s	WATER DEPTH cm.	BOOM DRAFT cm.	LENGTH cm.
<b>Series A</b>							
1	no	I	14	24.1	44	9	104
2	no	I	28	24.1	44	9	168
3	no	I	28	25.5	44	9	152
4	no	I	28	27.0	44	10	145
5	no	I	28	28.3	44	10	137
6	no	I	28	29.7	44	12	130
7	no	I	28	27.6	47	10	154
8	no	I	42	24.1	44	9	236
9	no	I	42	25.5	44	10	221
10	no	I	42	27.0	44	12	198
11	yes	I	42	27.0	44	15	191
12	yes	I	42	25.5	44	15	213
13	yes	I	42	23.6	46	15	251
14	no	I	42	23.6	46	12	267
15	no	I	28	27.8	47	12	152
<b>Series B</b>							
16	no	I	21	24.1	44	10	150
17	no	II	21	22.2	47	8	235
18	yes	II	21	22.0	47	8	213
19	no	II	21	28.6	44	9	190
20	yes	II	21	28.6	44	9	167
21	no	II	21	26.1	44	10	218
22	no	II	21	24.1	44	10	187
23	yes	II	21	28.3	44	10	169
24	yes	II	21	28.3	44	10	152



TABLE 5.1 con't

RUN NUMBER	ICE	OIL	VOLUME liter	VELOCITY cm./s	WATER DEPTH cm.	BOOM DRAFT cm.	LENGTH cm.
<b>Series C</b>							
25	no	II	21	25.3	44	9	213
26	no	II	21	26.8	44	9	179
27	no	II	28	28.2	44	9	213
28	no	II	28	29.2	44	9	192
29	no	II	28	30.6	44	9	178
30	no	II	28	26.2	44	9	229
31	yes	II	28	26.2	44	9	206
32	yes	II	28	27.5	44	9	190
33	no	II	28	27.5	44	9	210
25	no	II	21	25.3	44	9	213
26	no	II	21	26.8	44	9	179
27	no	II	28	28.2	44	9	213
28	no	II	28	29.2	44	9	192
29	no	II	28	30.6	44	9	178
30	no	II	28	26.2	44	9	229
31	yes	II	28	26.2	44	9	206
32	yes	II	28	27.5	44	9	190
33	no	II	28	27.5	44	9	210
34	no	II	28	28.5	44	9	201
35	yes	II	28	28.5	43	9	182
36	no	II	28	30.4	43	9	165
37	no	I	21	24.9	45	9	137
38	yes	I	21	24.9	45	9	122
39	yes	I	21	26.1	45	9	114
40	no	I	21	26.1	45	9	122
41	no	III	14	23.4	45	9	91
42	yes	III	14	23.4	45	9	84
43	yes	III	14	22.0	45	9	91
44	no	III	14	22.0	45	9	99



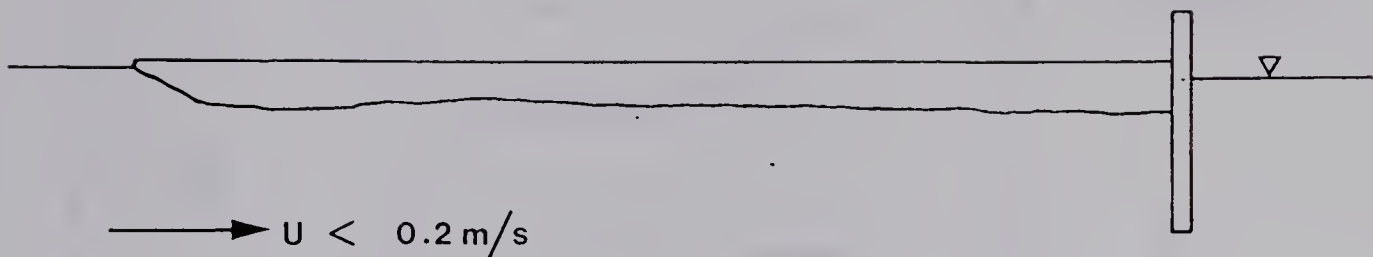
TABLE 5.2  
INTERFACIAL VELOCITY DATA

RUN NUMBER	ICE	$U_0$ cm s	$U_i$ cm s	h cm	$\sigma_i$ dyne cm <sup>2</sup>	$C_i$ $\times 10^4$	X cm	$R_x$ $\times 10^5$
16	no	24.1	12.0	4.5	1.76	6	83	2.00
17	no	22.2	9.0	2.5	2.38	9	160	3.55
18	yes	22.0	10.0	3.0	2.93	12	138	3.04
19	no	27.3	18.0	2.9	4.10	11	115	3.14
20	yes	27.5	17.0	3.4	4.40	12	92	2.51
21	no	22.5	16.0	2.6	4.06	13	138	3.52
21	no	25.5	16.0	2.4	4.40	13	83	2.12
22	no	28.3	15.5	3.0	3.41	8	132	3.74
23	yes	28.3	14.0	3.8	3.23	8	114	3.22
24	yes	29.3	20.0	3.7	4.75	11	77	2.26

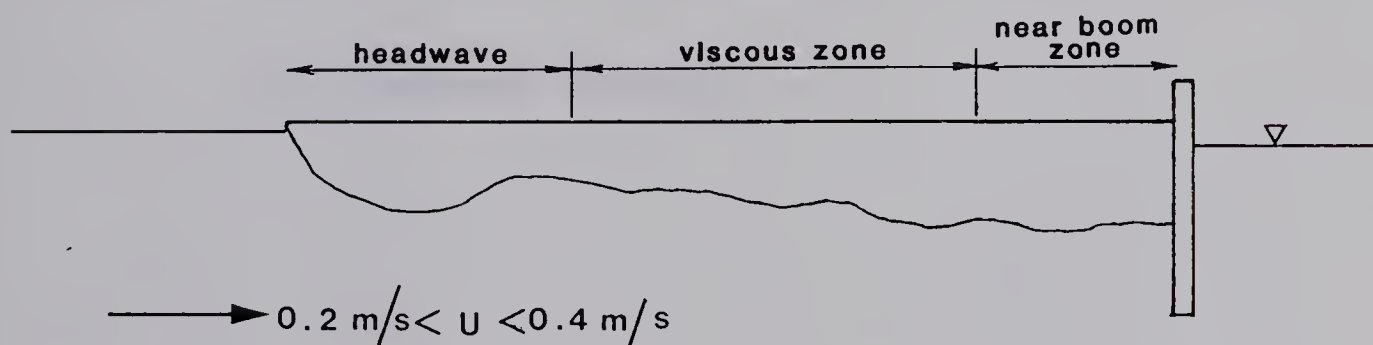


## FIGURES

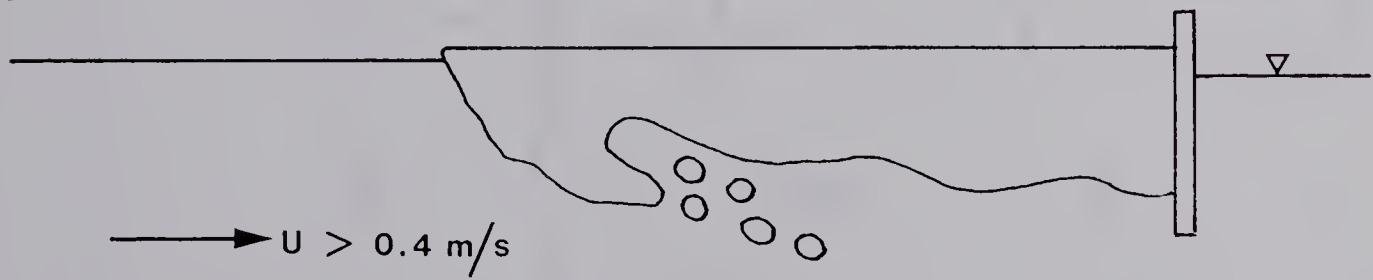




a) LOW VELOCITY



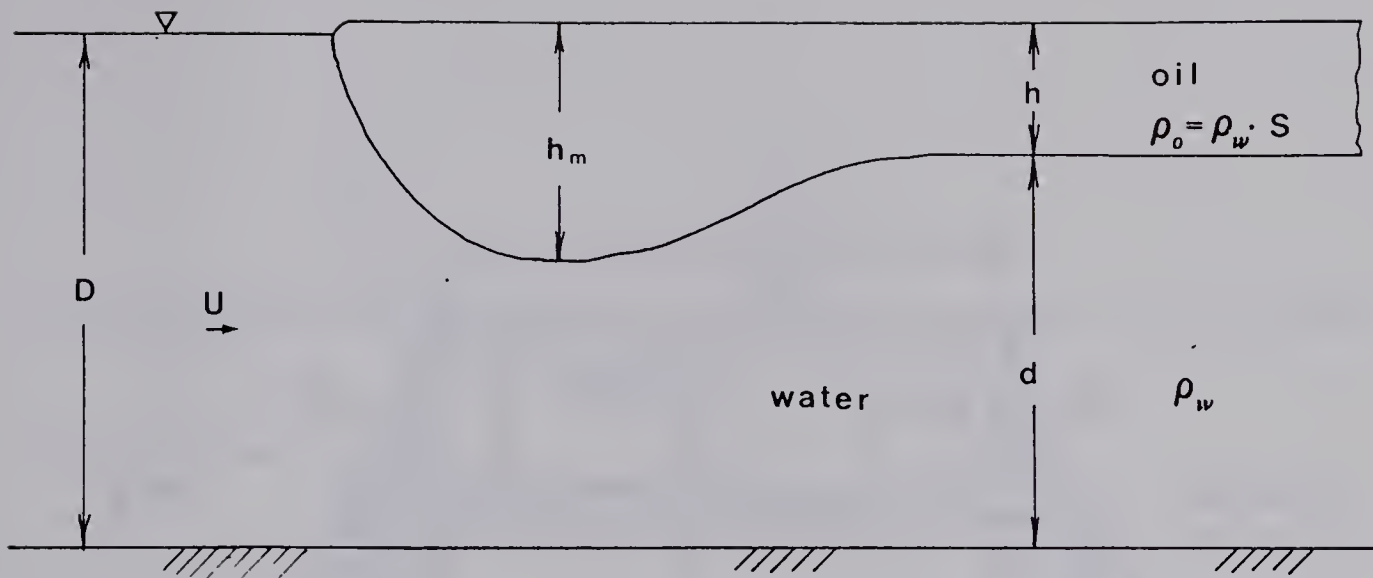
b) MEDIUM VELOCITY



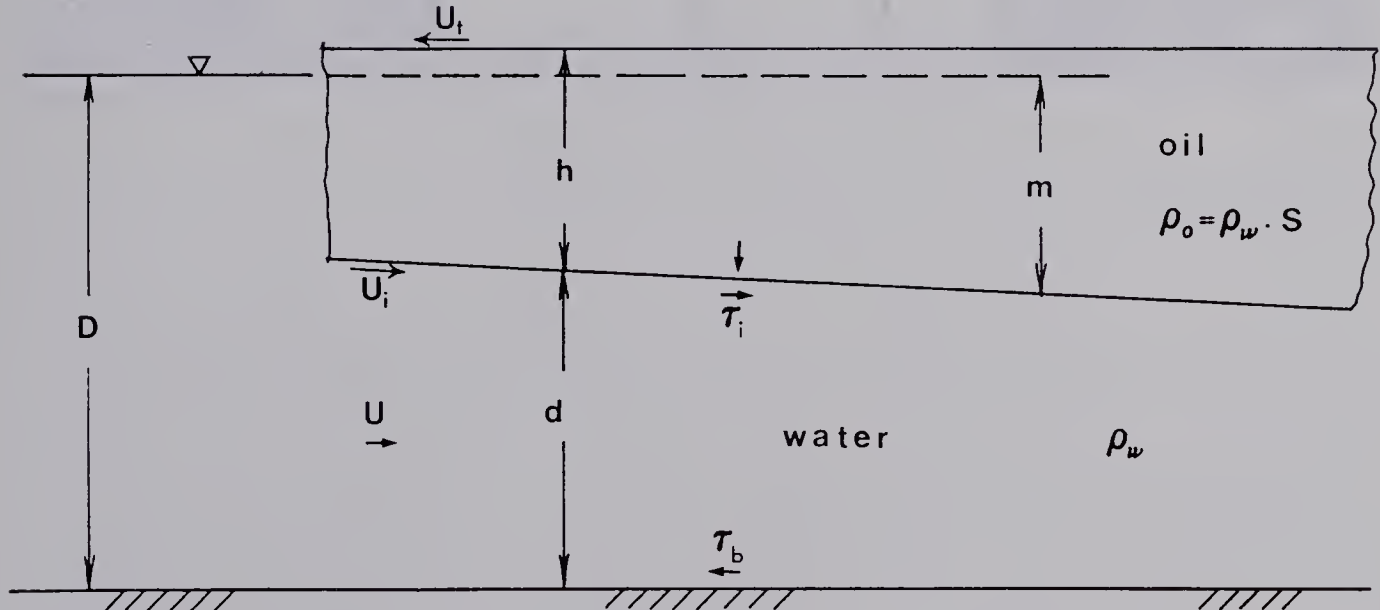
c) HIGH VELOCITY

FIGURE 1.1 CHARACTERISTIC OIL SLICK PROFILES





a) Headwave Definition



b) Viscous Zone Definition



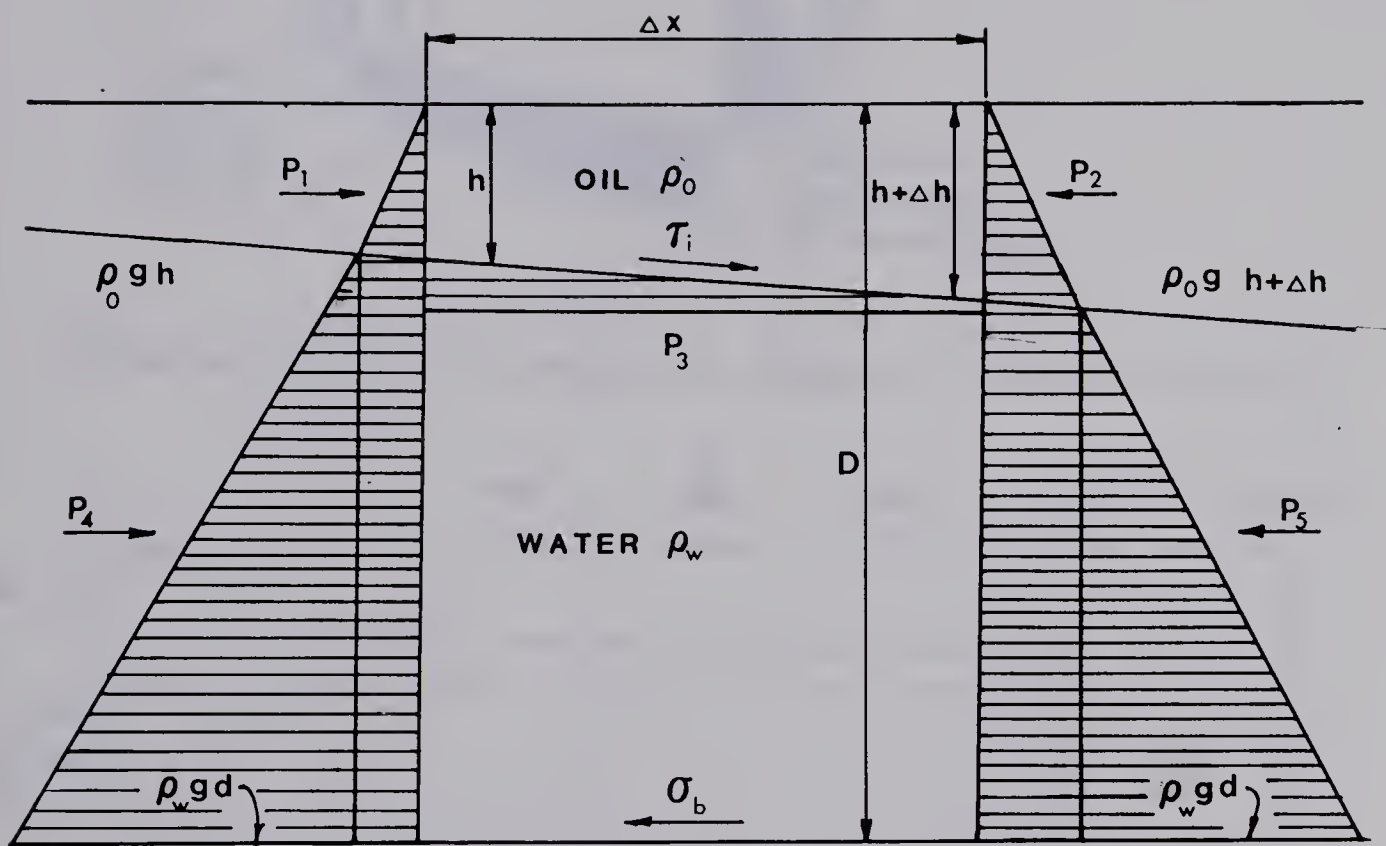
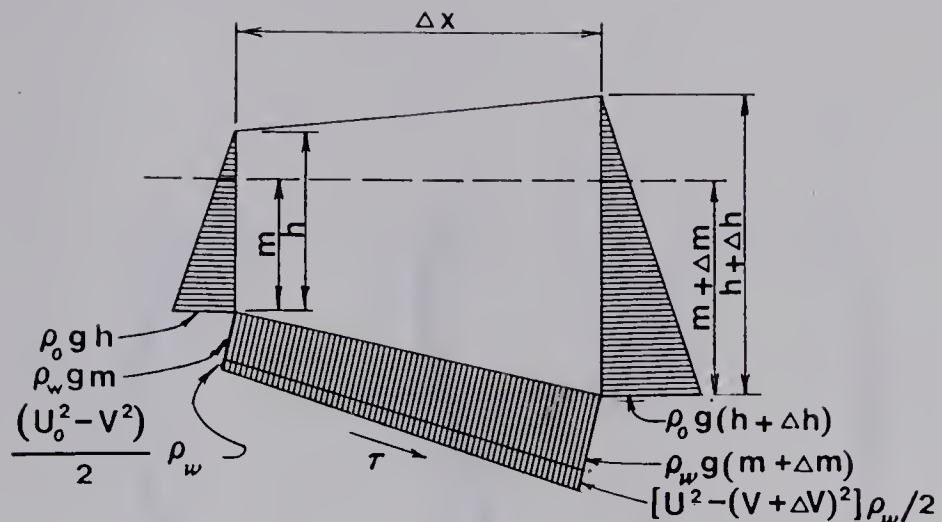


FIGURE 2.2

VISCOUS ZONE CONTROL ELEMENT





a) Forces acting on a differential element of length of the oil

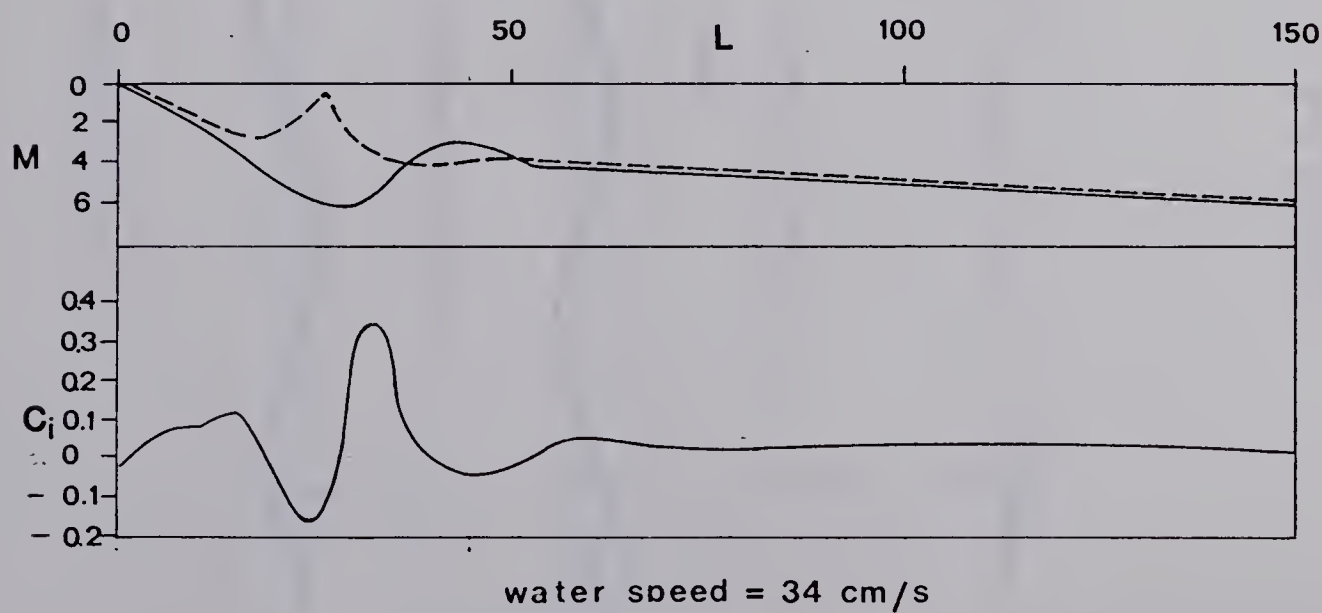
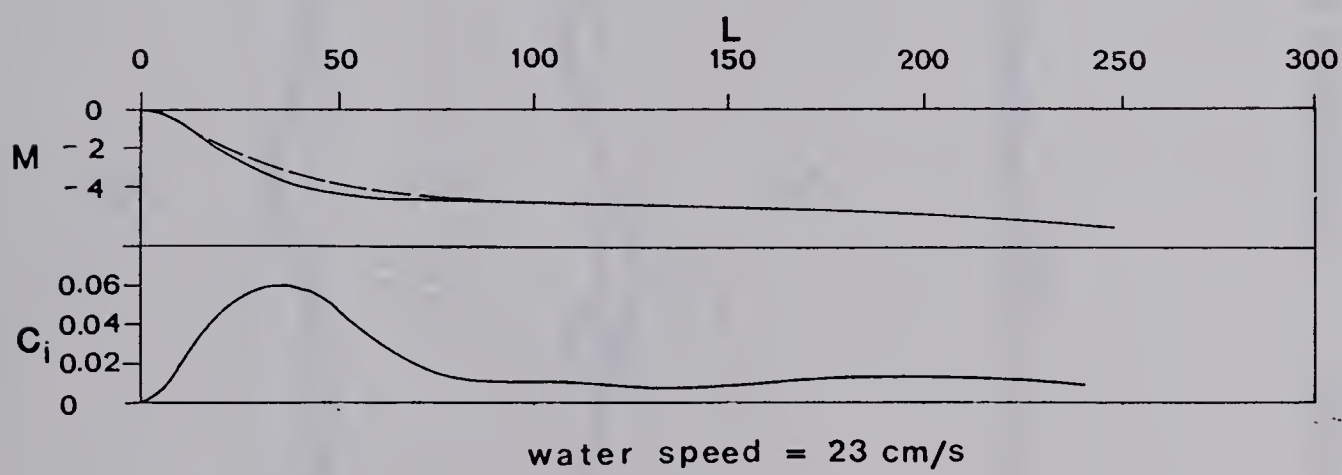


FIGURE 2.3

MILGRAM AND VAN HOULTEN OIL SLICK



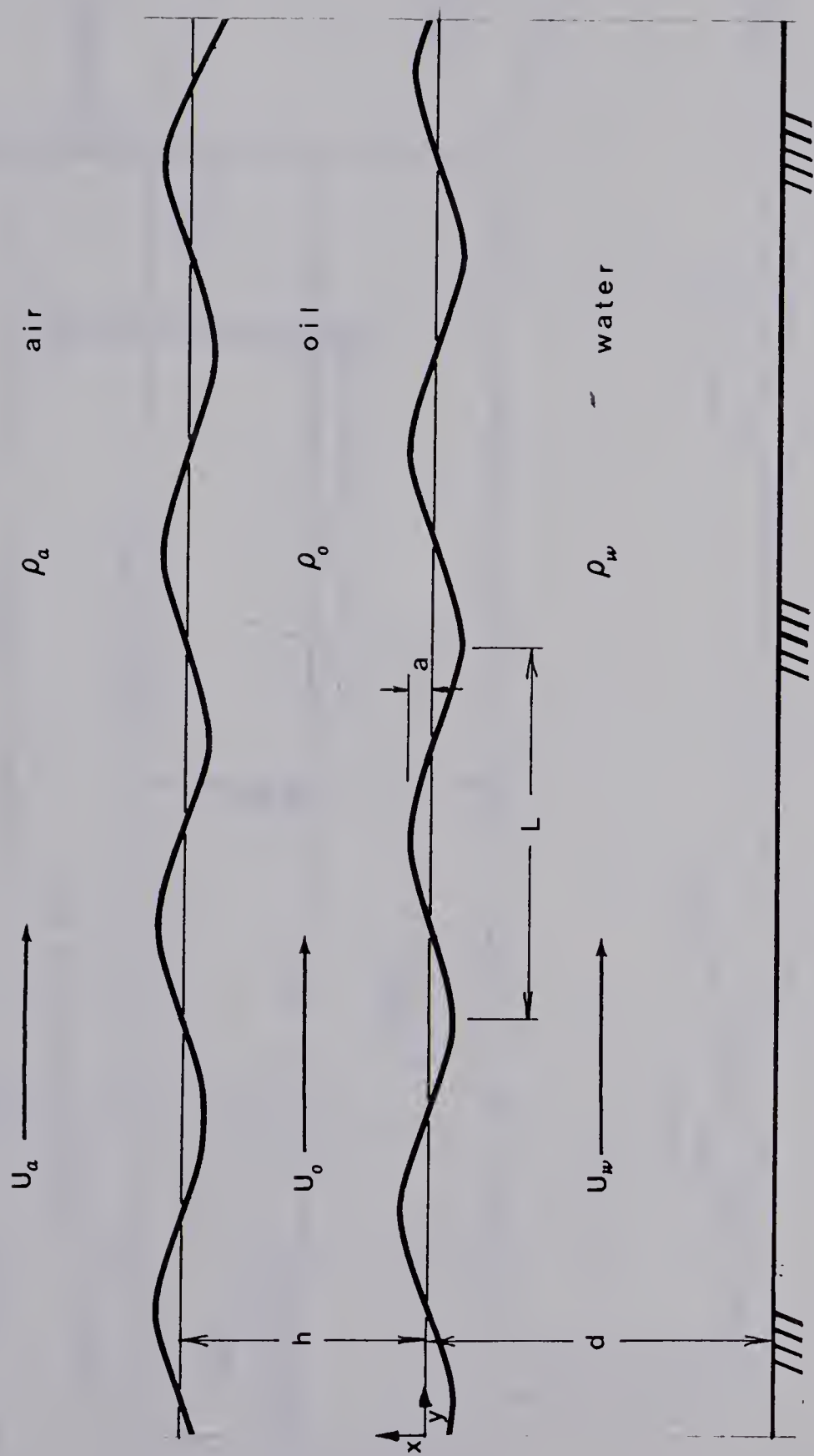


FIGURE 2.4 INSTABILITY DEFINITION SKETCH



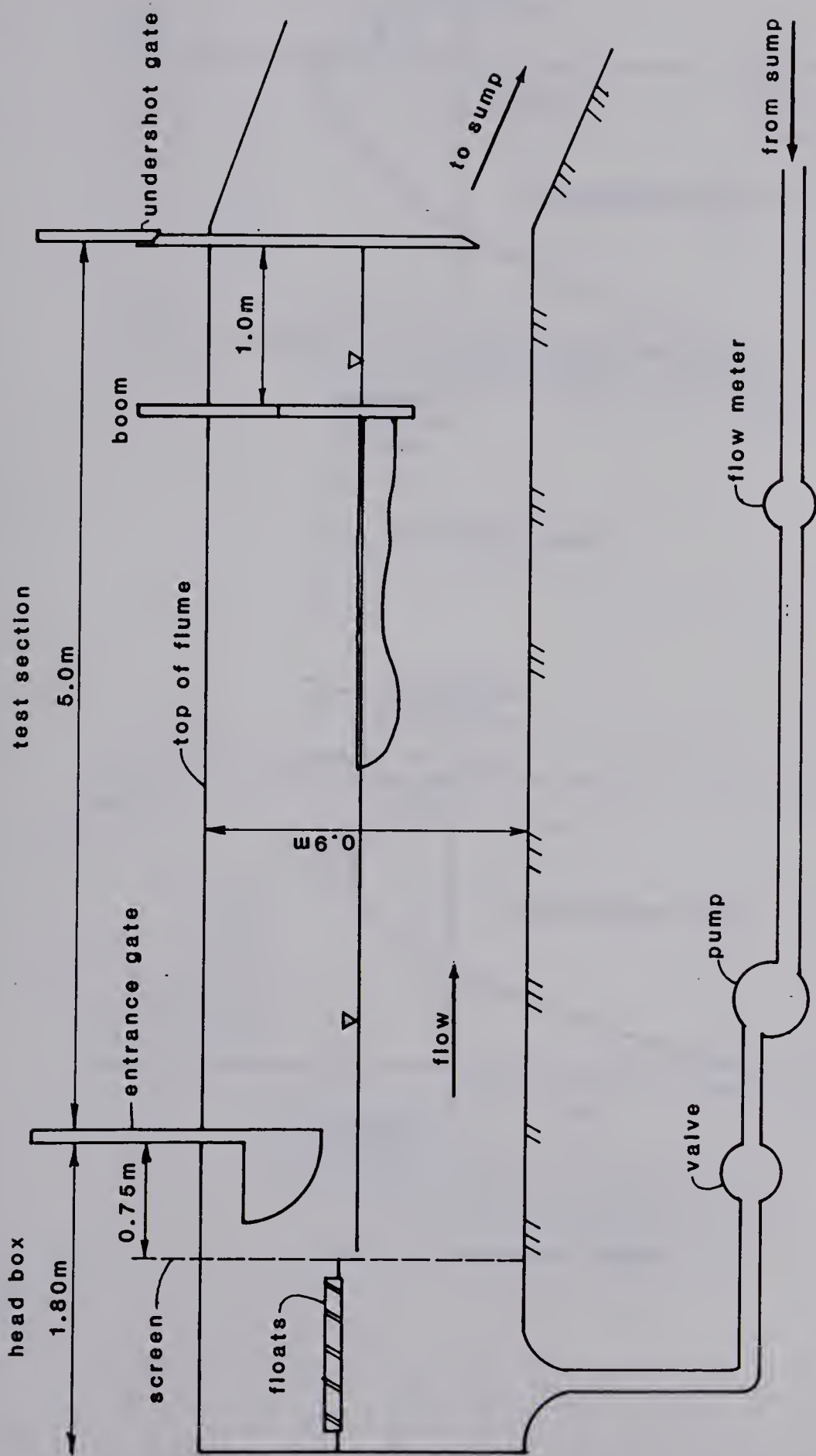
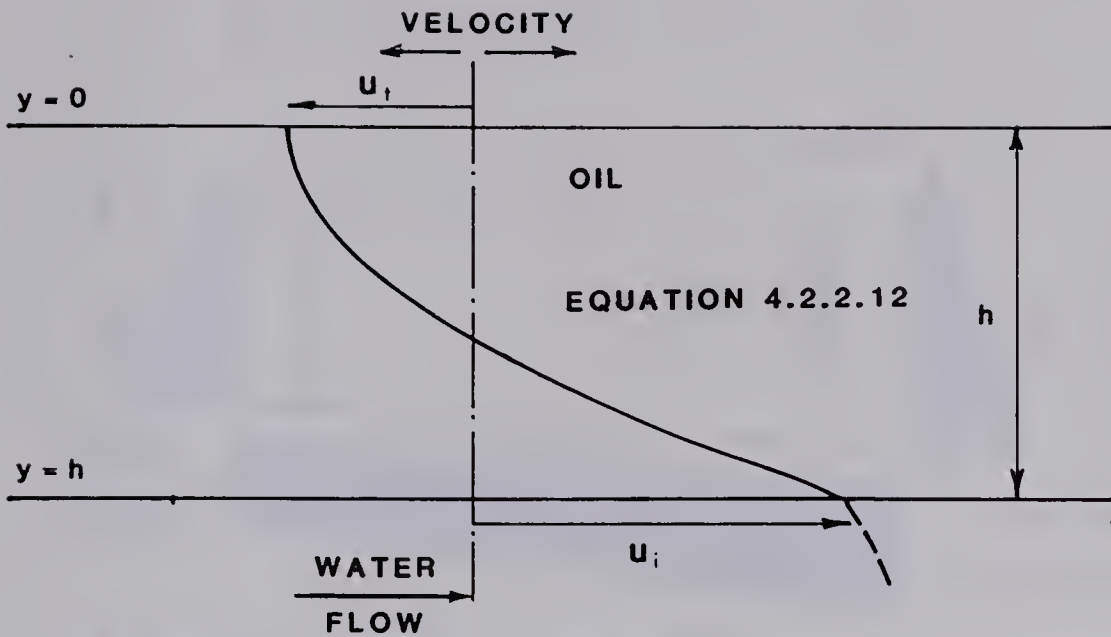
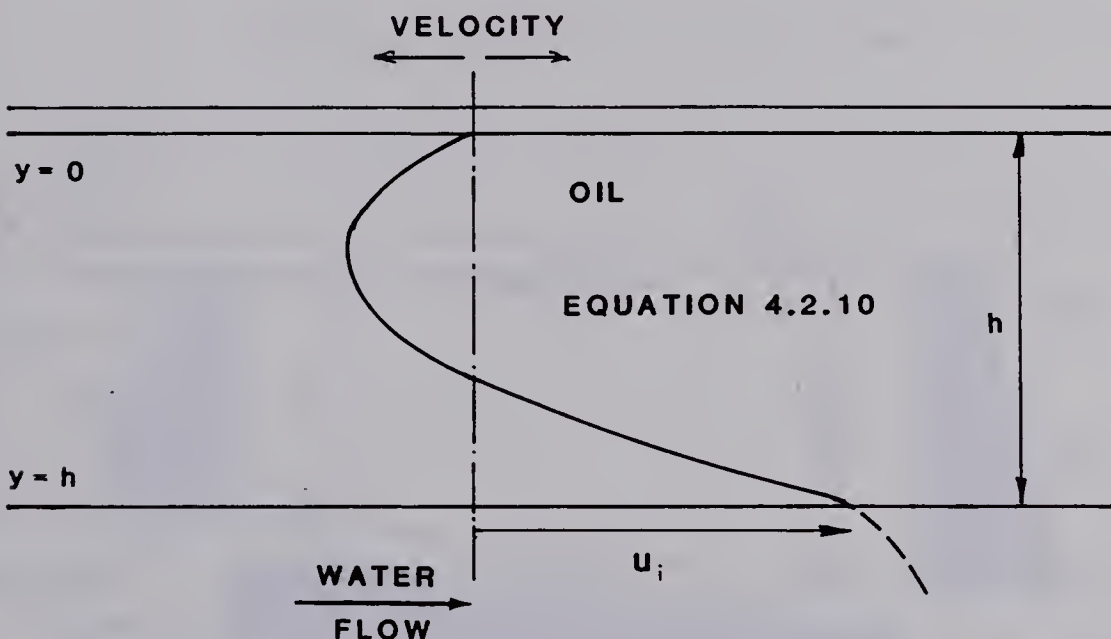


FIGURE 3.1 SCHEMATIC FLUME CONFIGURATION



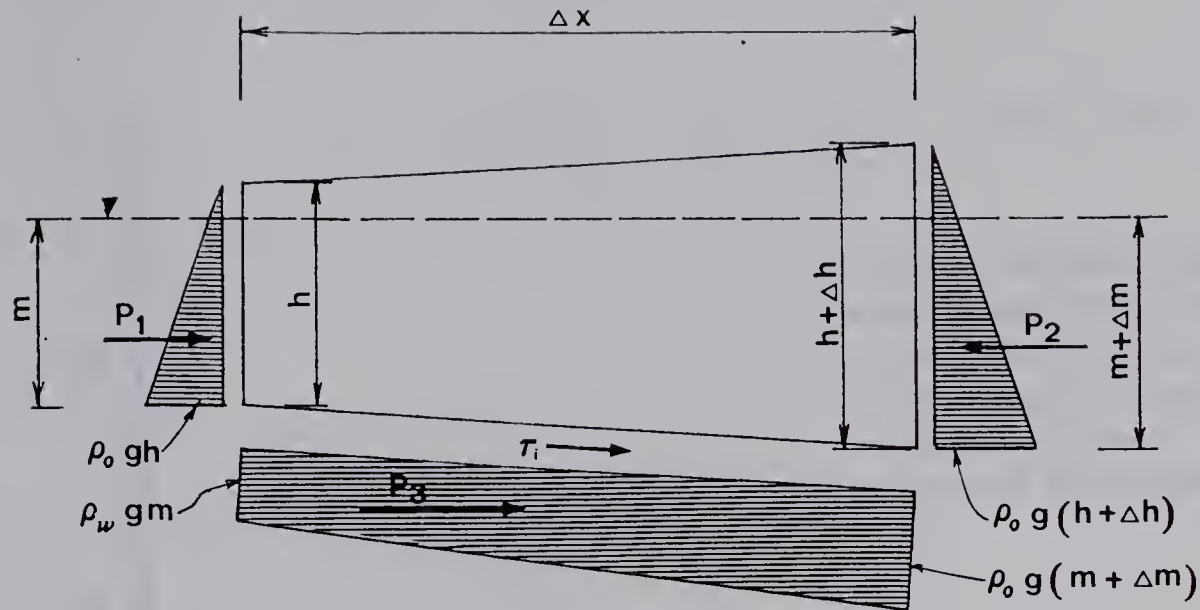


a) ICE FREE CASE



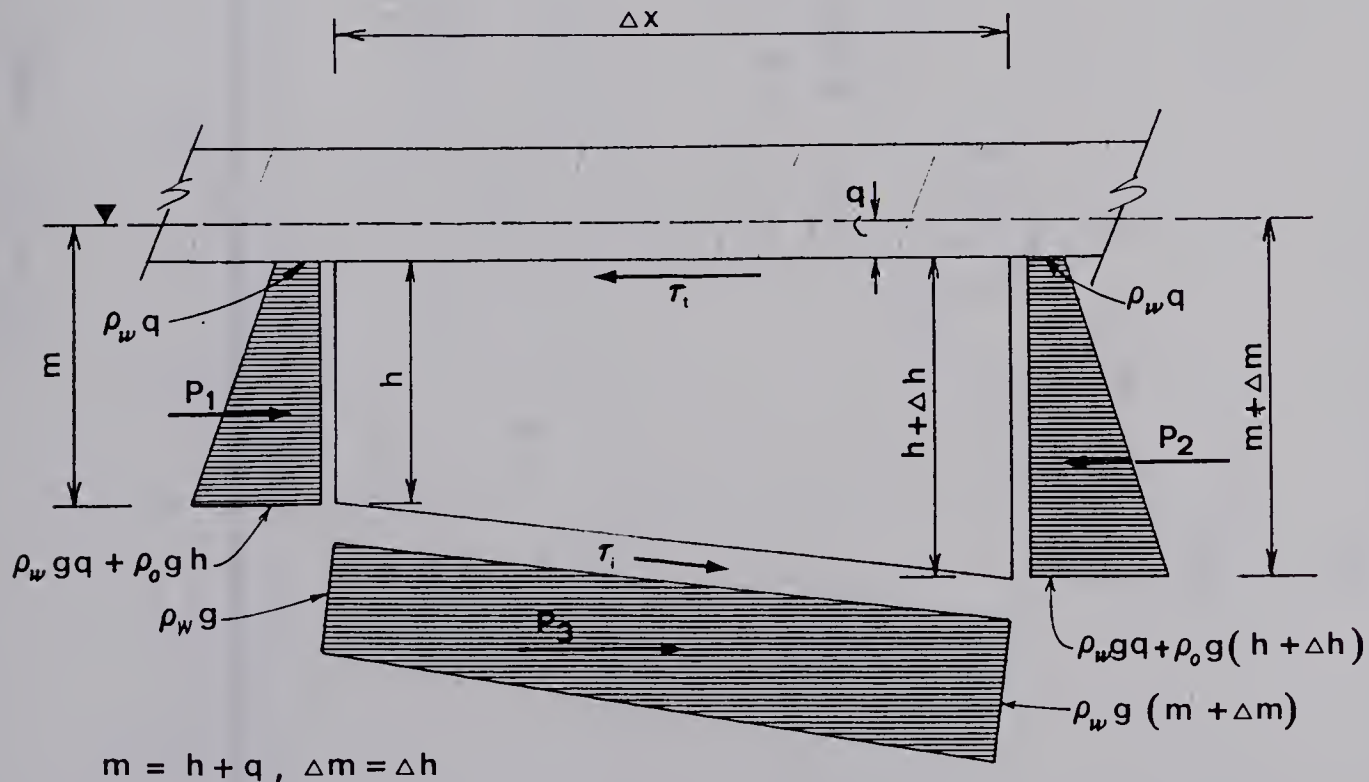
b) ICE COVERED CASE





$$\rho_w m = \rho_o h, \quad m = h \frac{\rho_o}{\rho_w}, \quad \Delta m = h \frac{\rho_o}{\rho_w}$$

### a) ICE FREE FORCE BALANCE



$$m = h + q, \quad \Delta m = \Delta h$$

### b) ICE COVERED FORCE BALANCE

FIGURE 4.2

FORCE BALANCE CONTROL ELEMENT



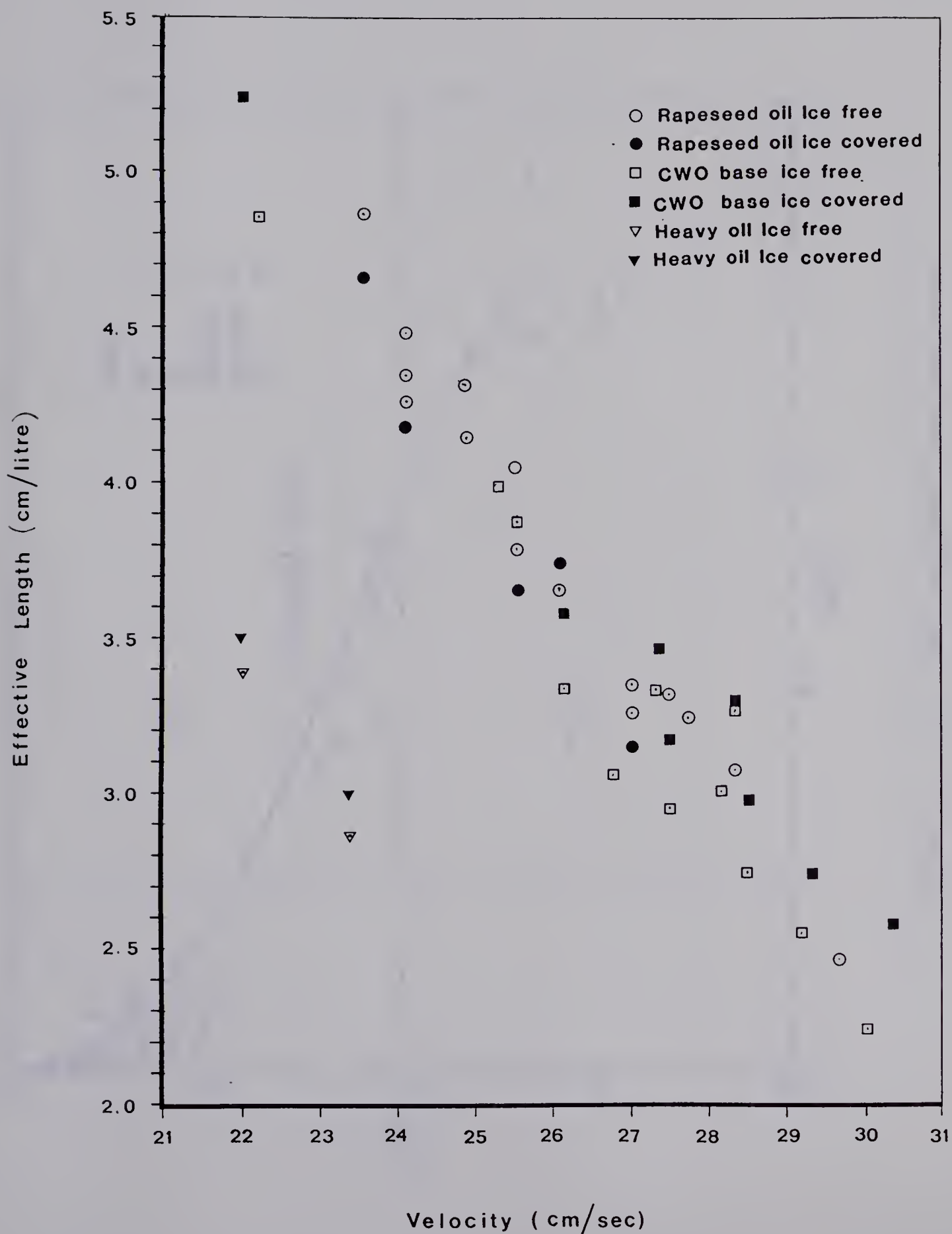


FIGURE 5.1 EFFECTIVE LENGTH



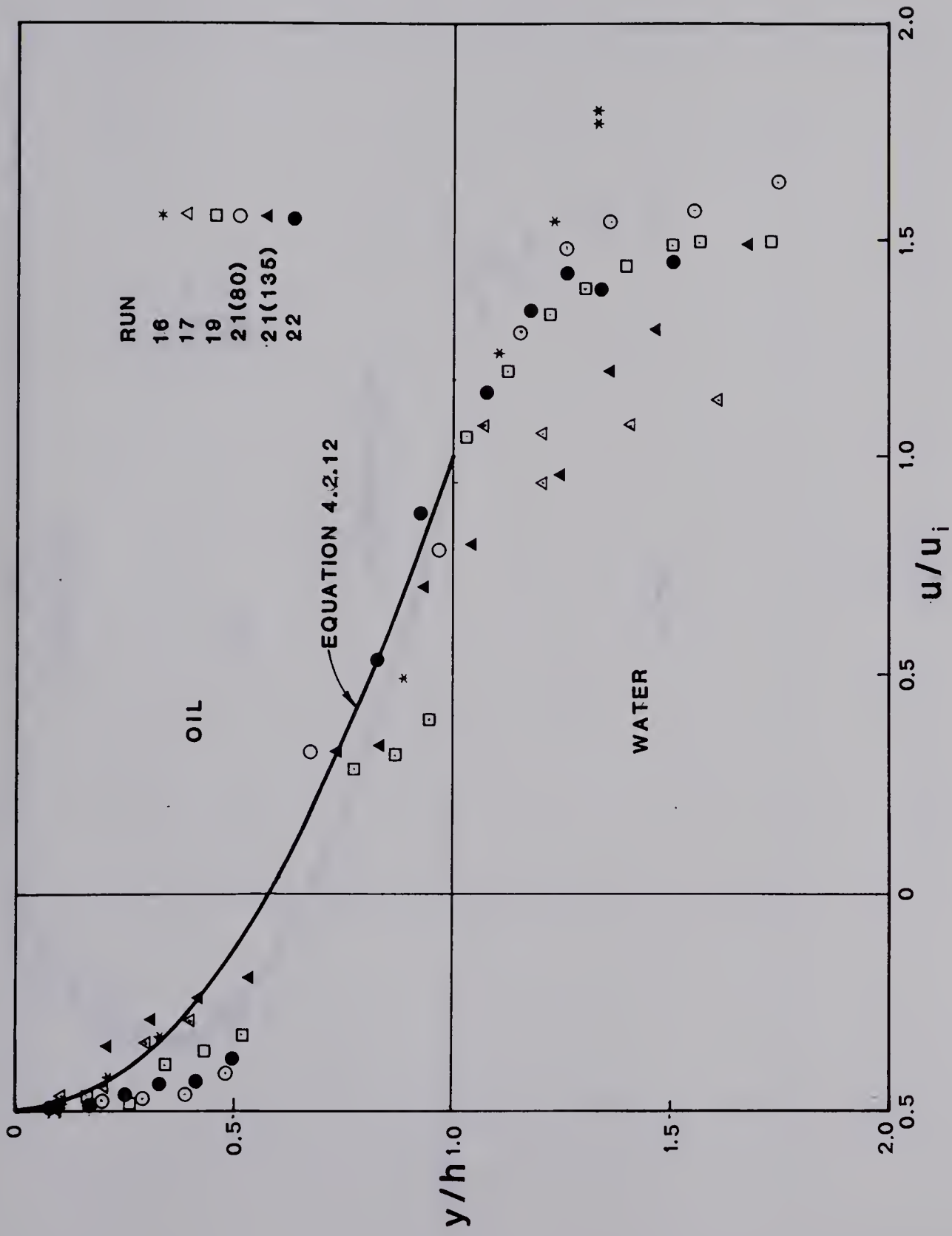
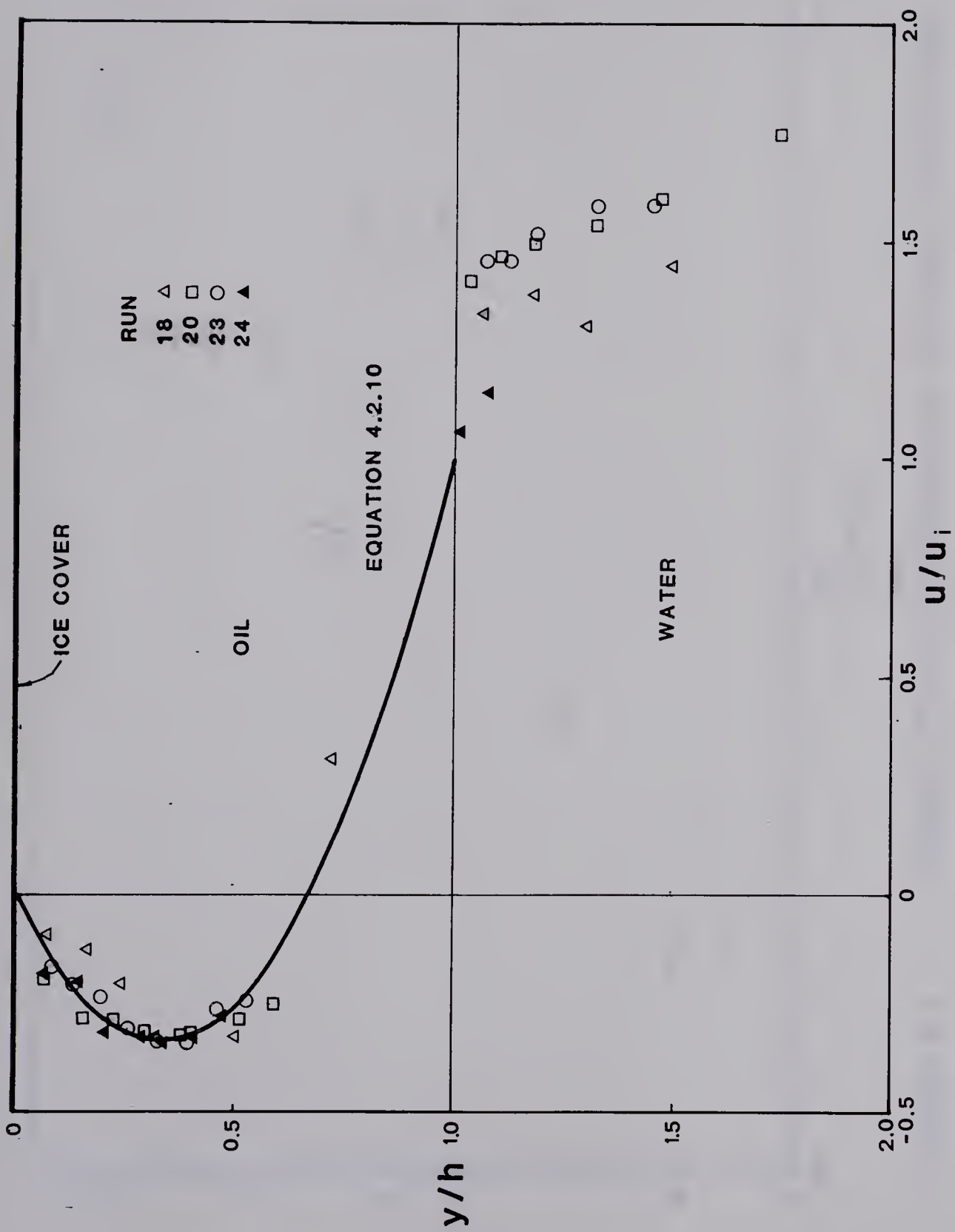


FIGURE 5.2 ICE FREE VELOCITY DISTRIBUTION





**FIGURE 5.3** ICE COVERED VELOCITY DISTRIBUTION



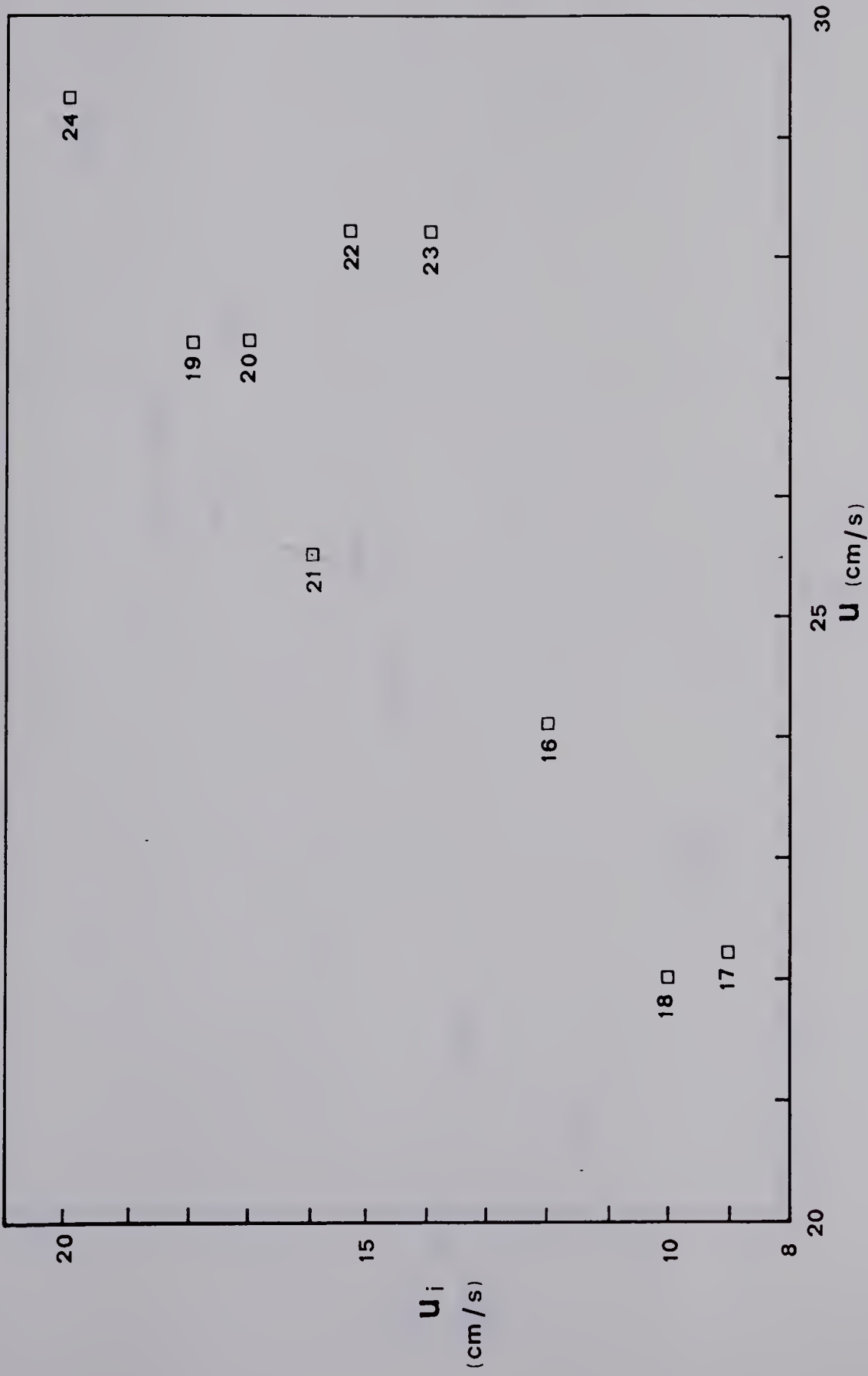


FIGURE 5.4 CORRELATION OF INTERFACIAL VELOCITY WITH FREE STREAM VELOCITY



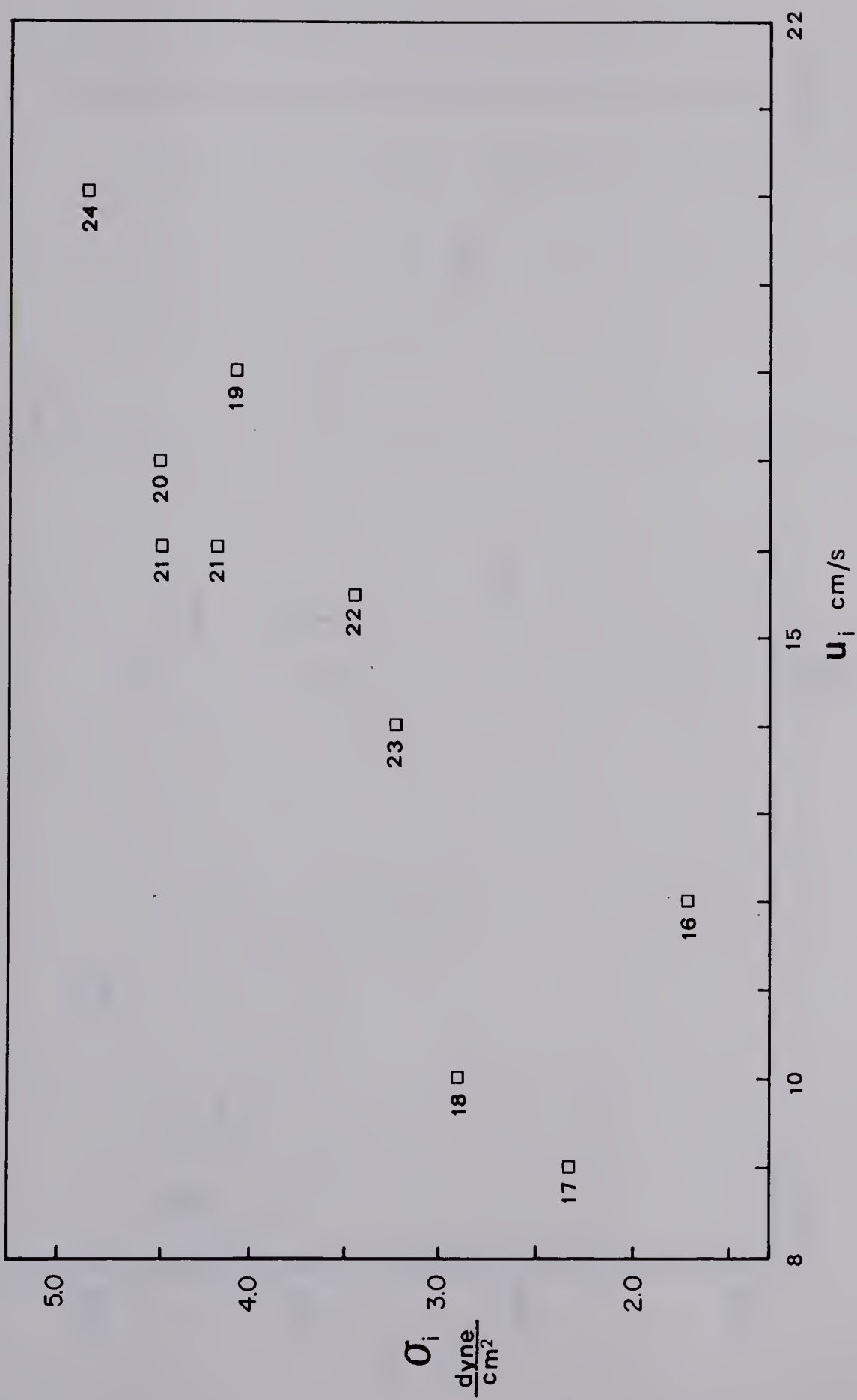


FIGURE 5.5

CORRELATION OF SHEAR STRESS WITH INTERFACIAL VELOCITY



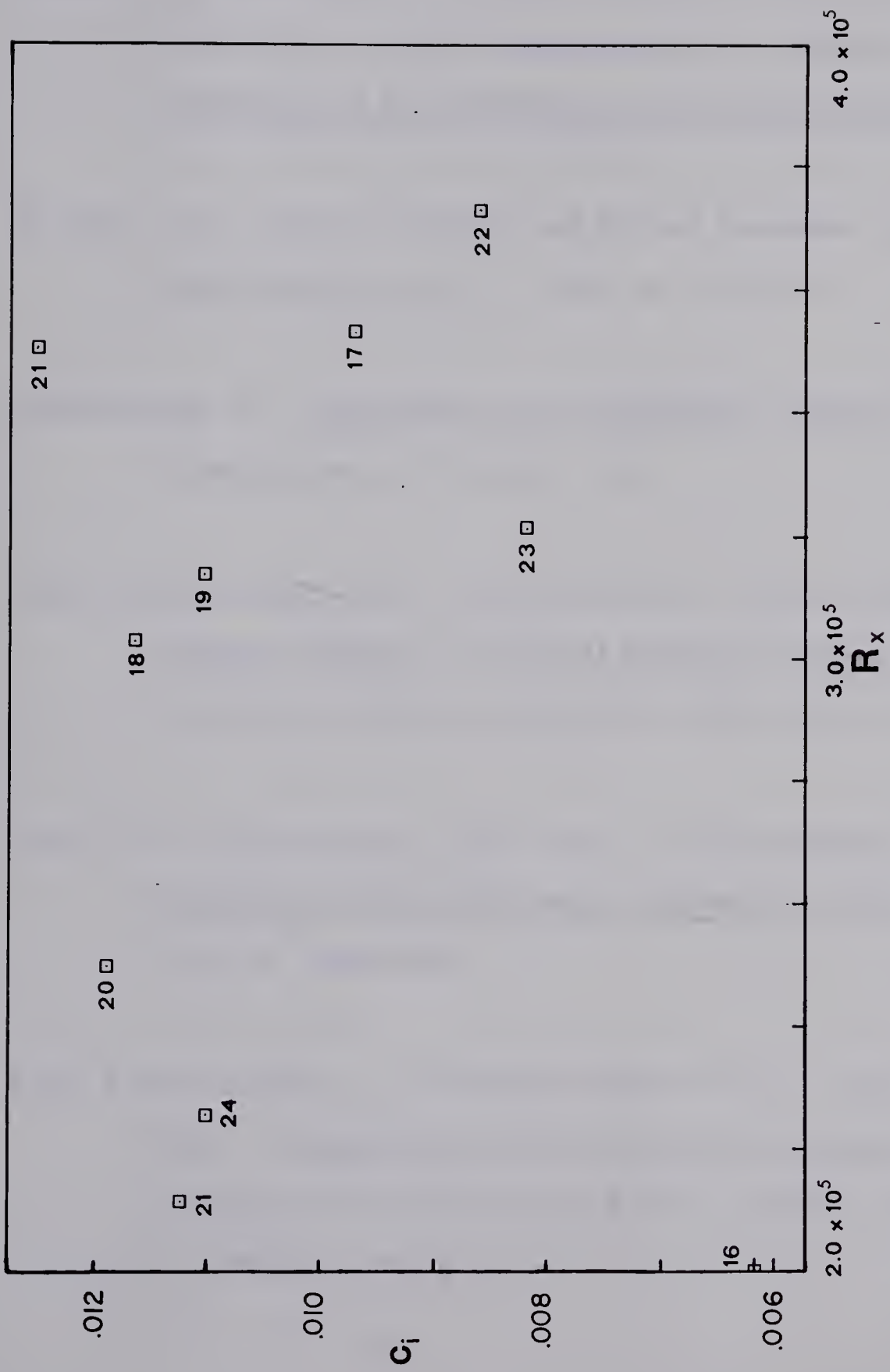


FIGURE 5.6 CORRELATION OF FRICTION COEFFICIENT WITH REYNOLD NUMBER



## BIBLIOGRAPHY

Agrawal, R.K. and Hale, L.A., "A New Criterion For Predicting Headwave Instability of an Oil Slick Retained by a Barrier", Proceedings of the 1974 Offshore Technology Conference, 1974.

Benjamin, T.B., "Gravity Currents and Related Phenomena, "Journal of Fluid Mechanics, Vol. 31, 1968, pp. 209-248.

Chandrasekhar, S., Hydrodynamics and Hydrodynamic Stability, Oxford University Press, 1961, Sec. 101.

Cross, R.H. and Hoult D.P., "Collection of Oil Slicks", Journal of the Waterways, Harbors and Coastal Engineering Division, ASCE, Vol. 97, No. WW2, Proc. Paper 8122, May, 1971, pp. 313-322.

Cross, R.H., and Hoult,D.P., "Oil Booms in Tidal Currents", Proceedings of the 12th Coastal Engineering Conference, ASCE, 1970, pp. 1745-1758.

Dick, T.M., Marsalek, J., "Interfacial Shear Stress in Density Wedges", Proceedings of the First Canadian Hydraulics Conference, The University of Alberta, Edmonton, May 10 and 11, 1973, pp. 176-191.



Drazin, P.G., "Kelvin - Helmholtz Instability of Finite Amplitude,"  
Journal of Fluid Mechanics, Vol. 42, 1970, pp. 321-335.

Hale, L.A., Norton, D.J. and Rodenberger, C.A., The Effects of  
Currents and Waves on an Oil Slick Retained by a Barrier,"  
Texas A&M Report to the Coast Guard Under Contract  
DOT-CG-23357A, 1974.

Ippen, A.T., Estuary and Coastline Hydrodynamics, McGraw-Hill Book  
Company, 1966.

Jones, W.T., "Instability at the Interface Between Oil and Flowing  
Water", Journal of Basic Engineering, ASME, Vol. 94, 1972,  
pp. 874-878

Keulegan, G.H., "Interfacial Instability and Mixing in Stratified  
Flows", Journal of Research of the National Bureau of  
Standards, Vol. 43, Nov. 1949, pp. 487-500.

Lamb, H., Hydrodynamics, Sixth Edition, Dover Publications, New York,  
1932.

Lau, Y. L., and Kirchefer, S.A., A Review of the dynamics of Contained  
Oil Slicks in Flowing Water, Canadian Centre for Inland  
Waters, Mar 1974



Lau, Y.L. and Moir, J., "Booms used for Oil Slick Control", Journal of the Environmental Engineering Division, ASCE, Vol. 105, No EE2, Proc. Paper 14530, April, 1979, pp 369 - 382.

Leibovich, S., "Oil Slick Instability and the Entrainment Failure of Oil Containment Booms," Journal of Fluids Engineering, ASME, Vol. 98, March 1970, pp. 98-105.

Lindenmuth, W.T., Miller, E.R., and Hsu, C.C., "Studies of Oil Retention Boom Hydrodynamics", U.S. Government, Dept. of Transportation, Report No. 714102/A/008, Dec. 1970.

Milgram, J.H. and Van Houten, R.J., "Mechanics of a Restrained Layer of Floating Oil Above a Water Current", Journal of Hydraulics, Vol. 12, No.3, July 1978, pp. 93-108

Mitra, A., and Greenberg, M.D., "Effect of a Wavy Bottom on Kelvin-Helmholtz Instability", Journal of Hydraulics, Vol. 8, No.2, April 1974, pp. 53-57.

Schlichting, H., Boundary Layer Theory, 6th Edition, McGraw Hill Book Company, 1968.

Turner, J.S., Buoyancy Effects in Fluids, Cambridge University Press, 1973.



Von Karman, T., "The Engineer Grapples with Nonlinear Problems",  
Bulletin of the American Mathematical Society, Vol. 46, Aug.  
1940, pp. 605-680.

Wicks, M., "Fluid Dynamics of Floating Oil Containment by Mechanical  
Barriers in the Precence of Water Currents", Proceedings of  
Joint Conference on Prevention and Control of Oil Spills,  
American Petroleum Institute, 1969, pp. 55-106.

Wilkinson, D.L., "Containment of Oil Slicks in the St. Lawrence River",  
National Research Council, Division of Mechanical  
Engineering, Report No. LTR-HY-16, Dec. 1971.

Wilkinson, D.L., "Dynamics of Contained Oil Slicks", Journal of the  
Hydraulic Division, ASCE, Vol. 98, No. HY6, Proc. Paper 8950  
June 1972, pp. 1013-1030.

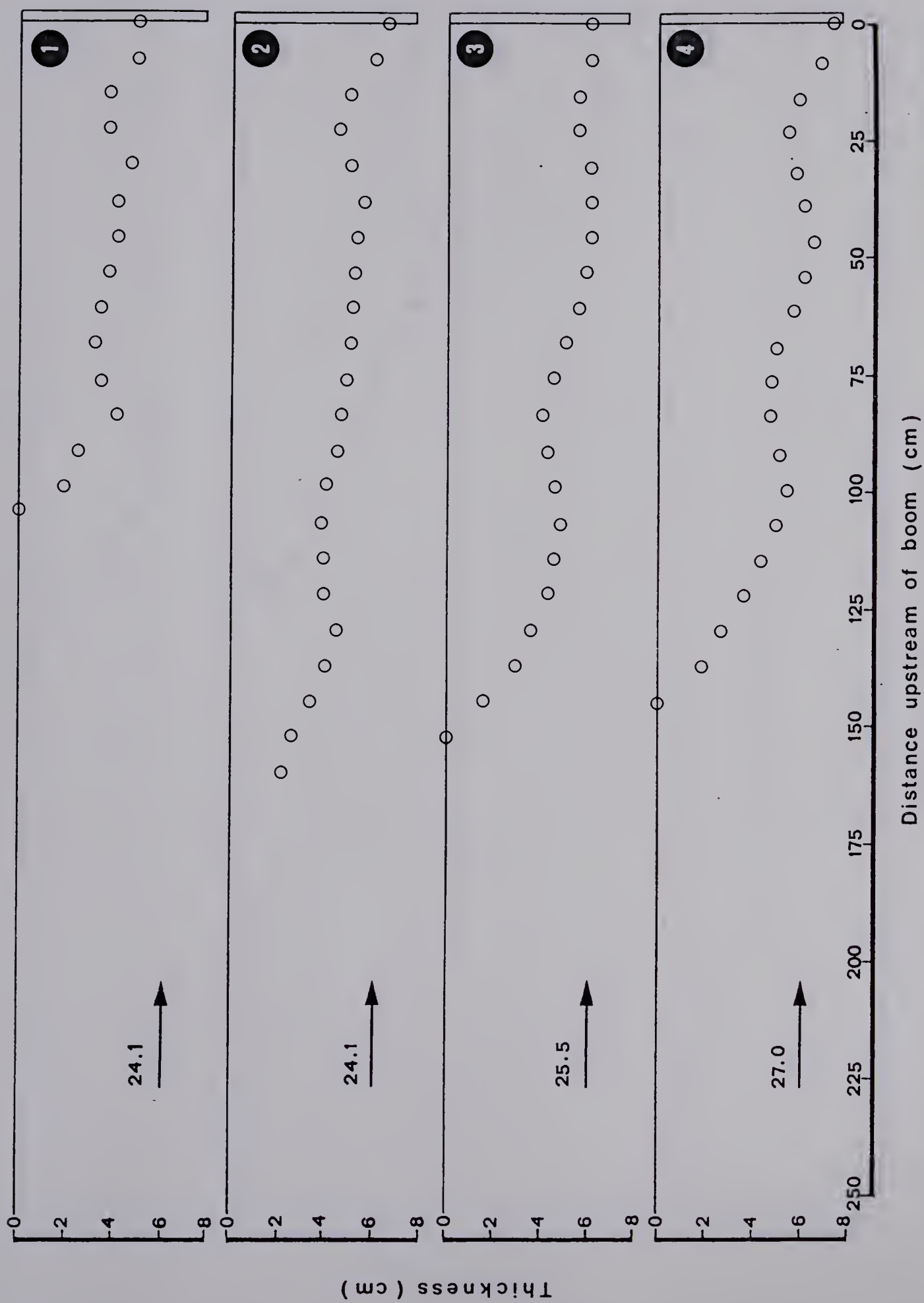
Wilkinson, D.L., "Limitations to Length of Contained Oil Slicks",  
Journal of the Hydraulics Division, ASCE, Vol. 99, No. HY5,  
Proc. Paper 9711, May 1973, pp. 701-712.

Yih, C.S., Non Homogeneous Fluids, The MacMillan Company, New York,  
1965.

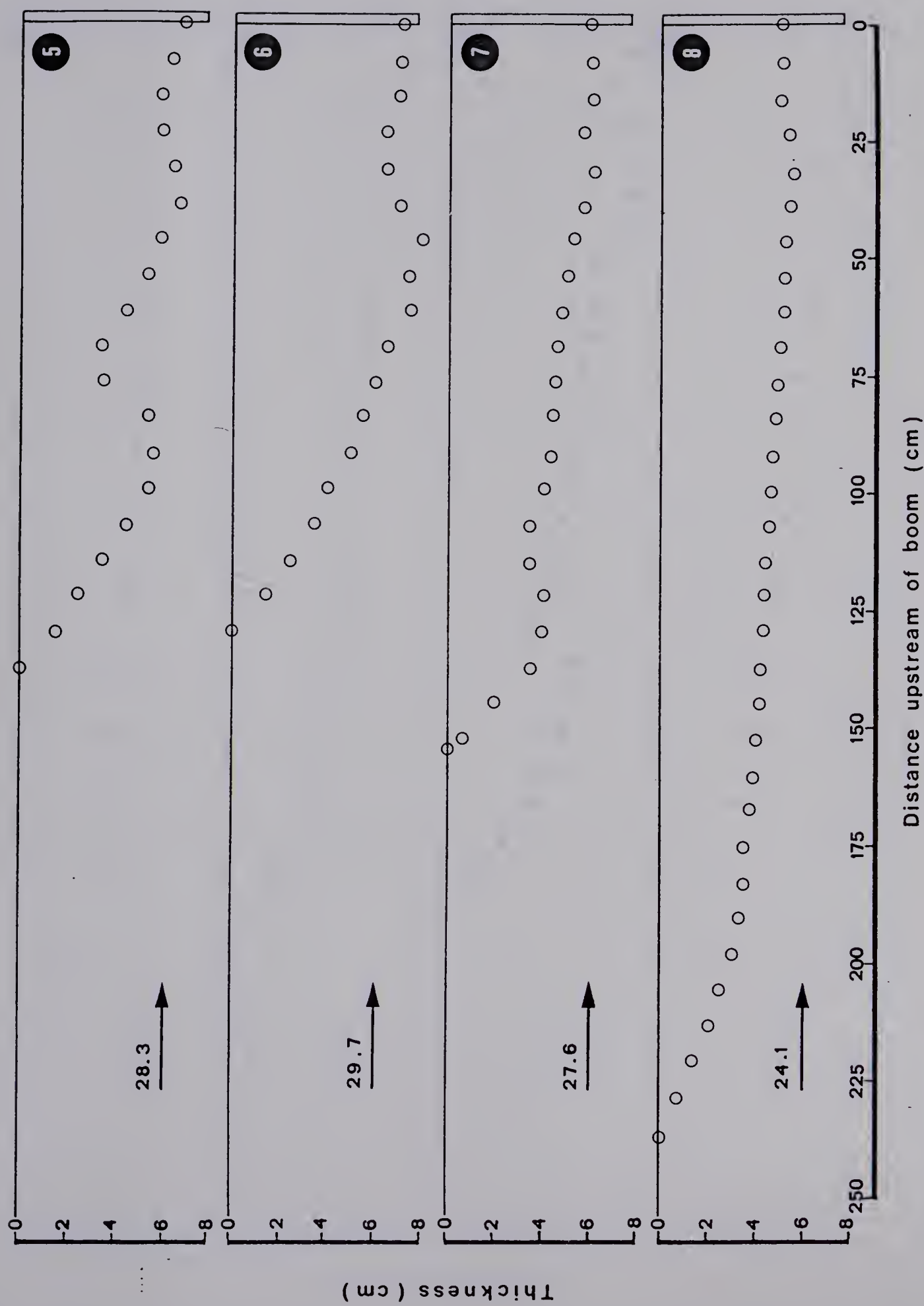


APPENDIX A  
OIL SLICK PROFILES

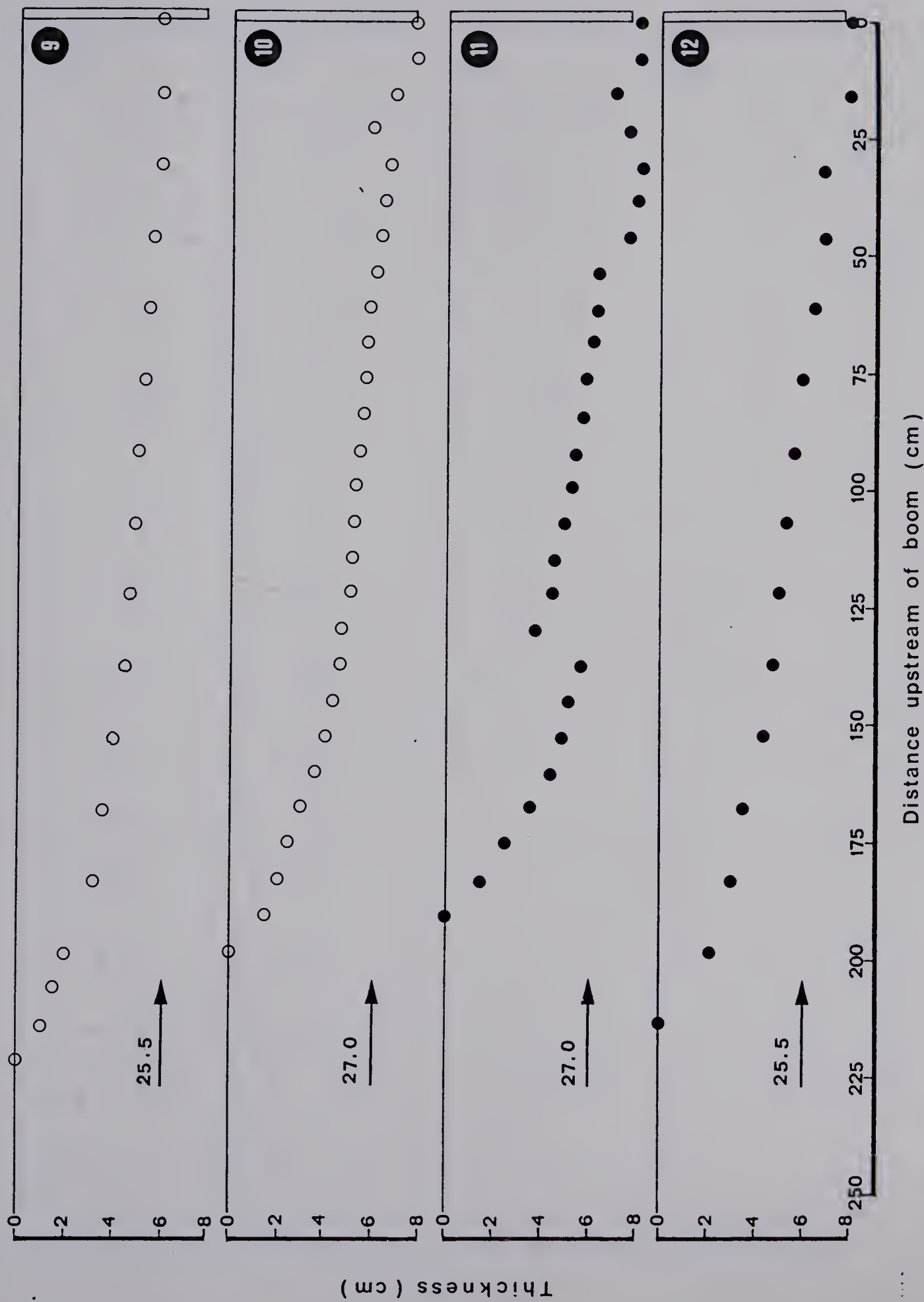




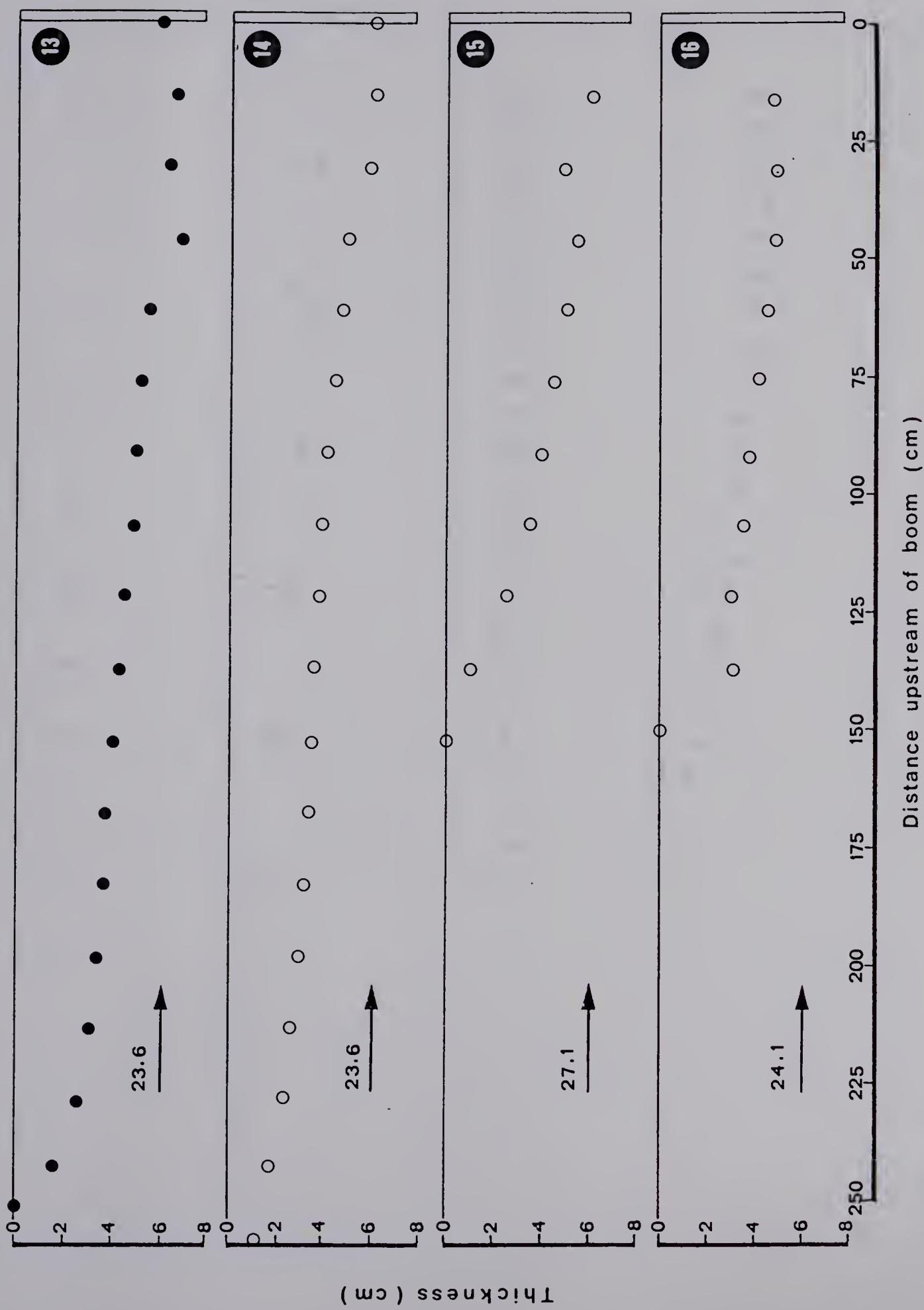




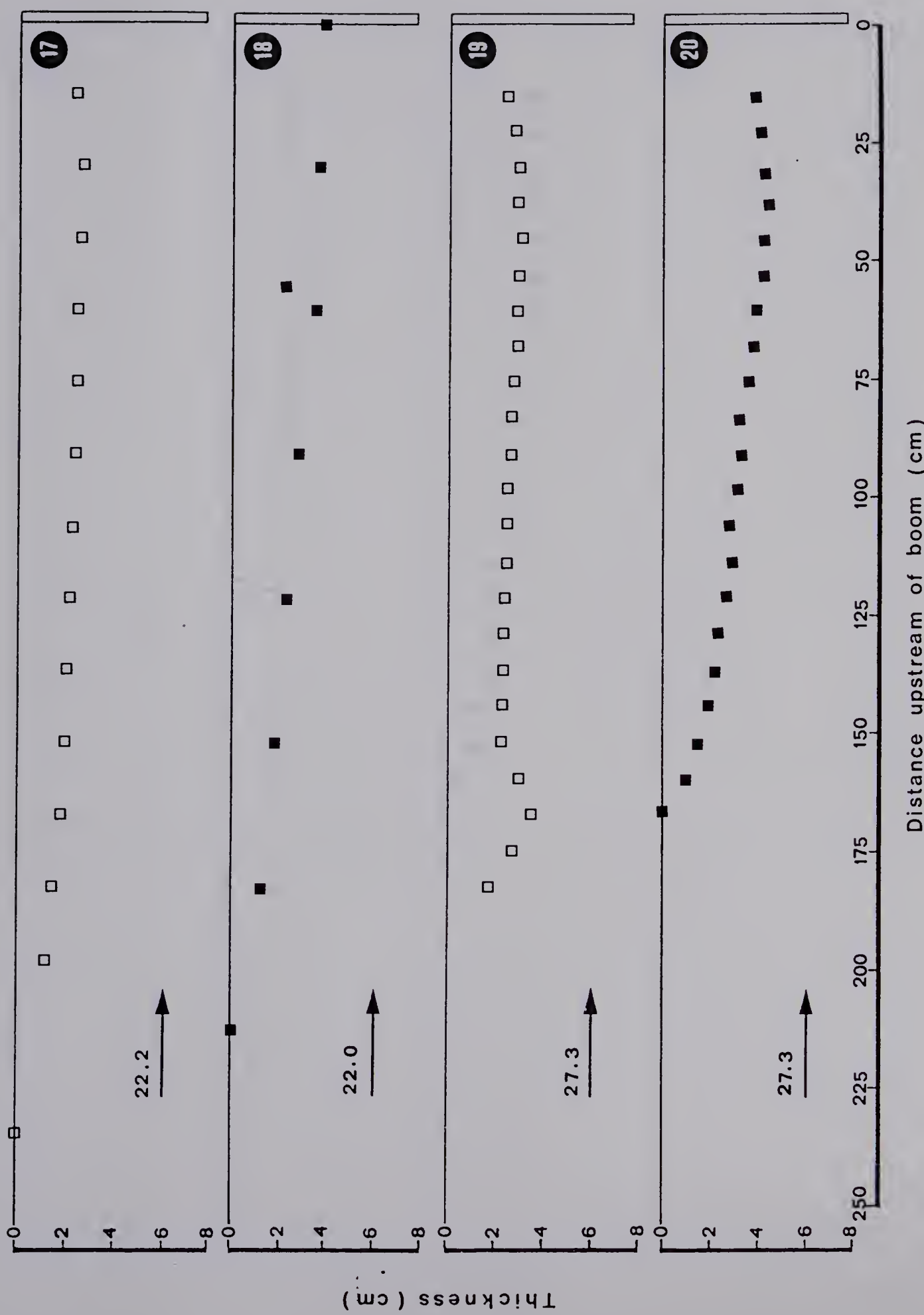




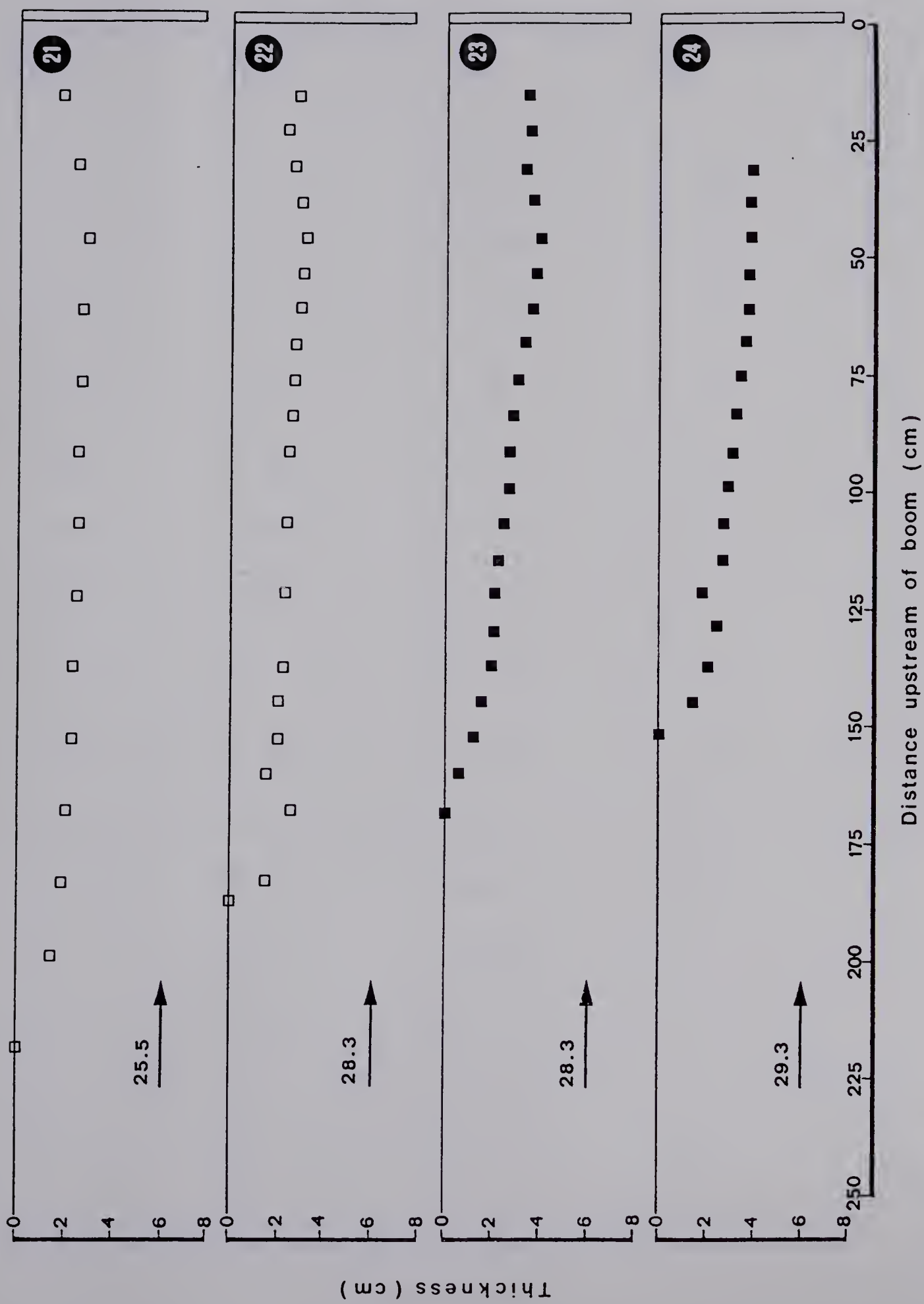




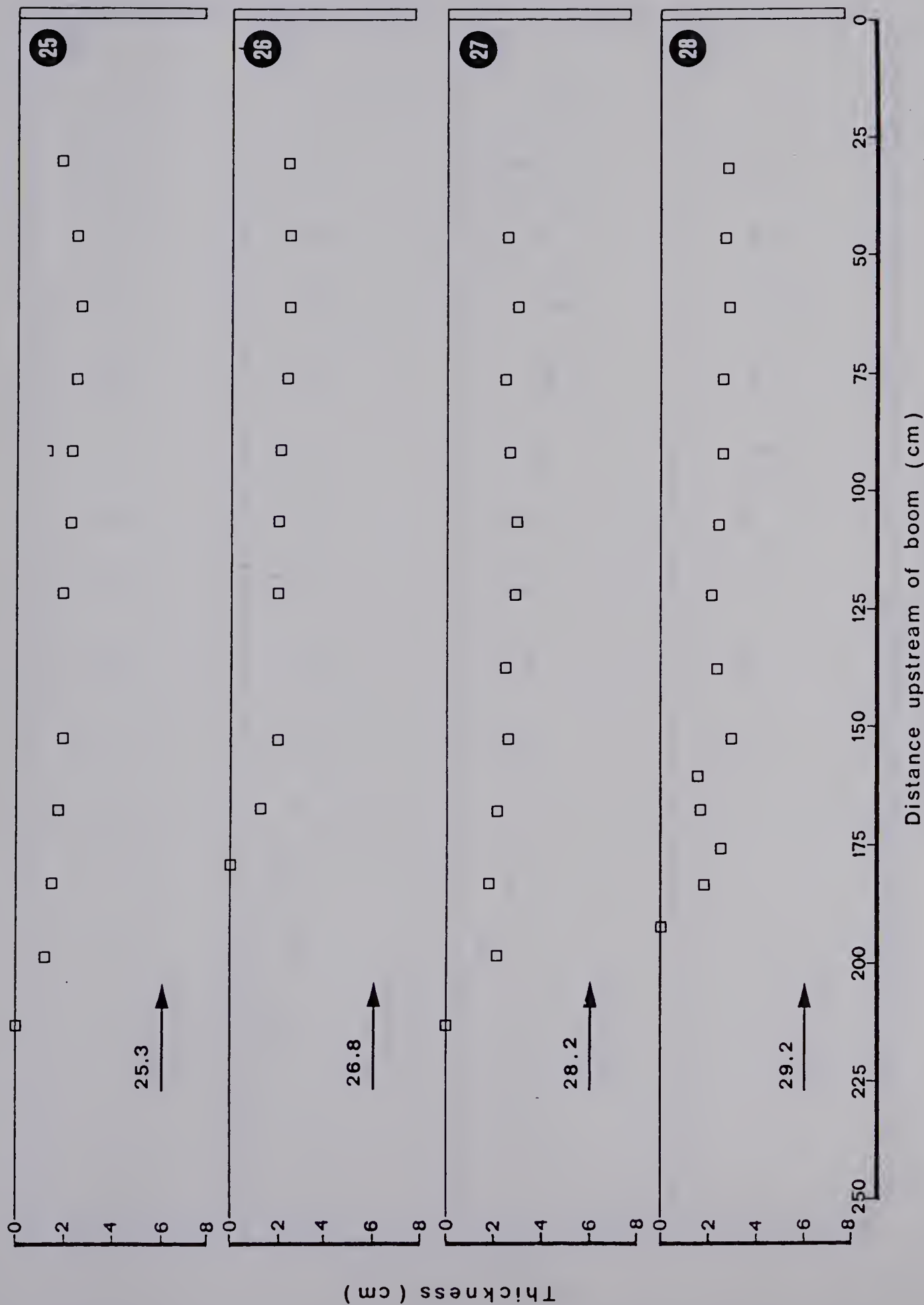




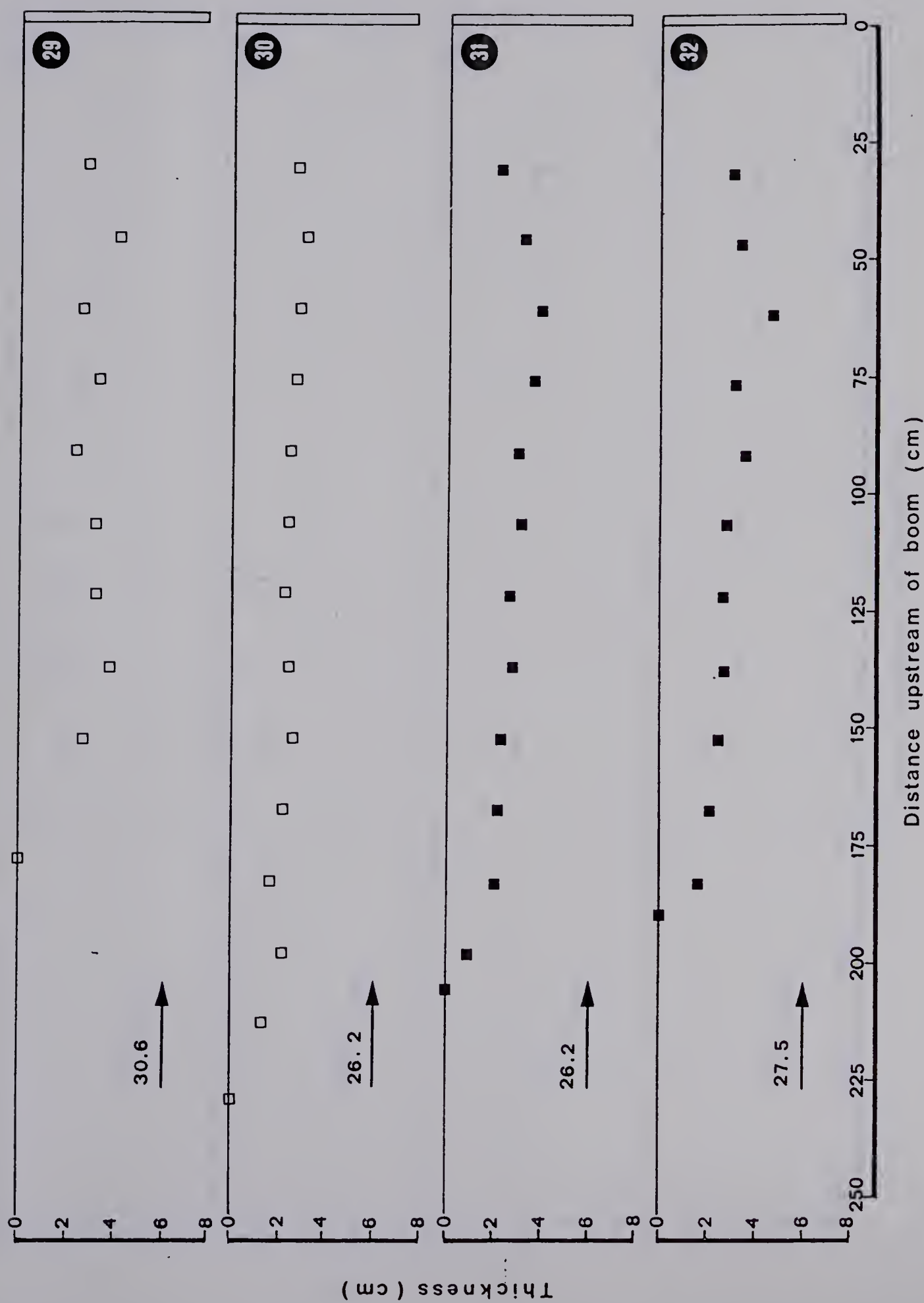




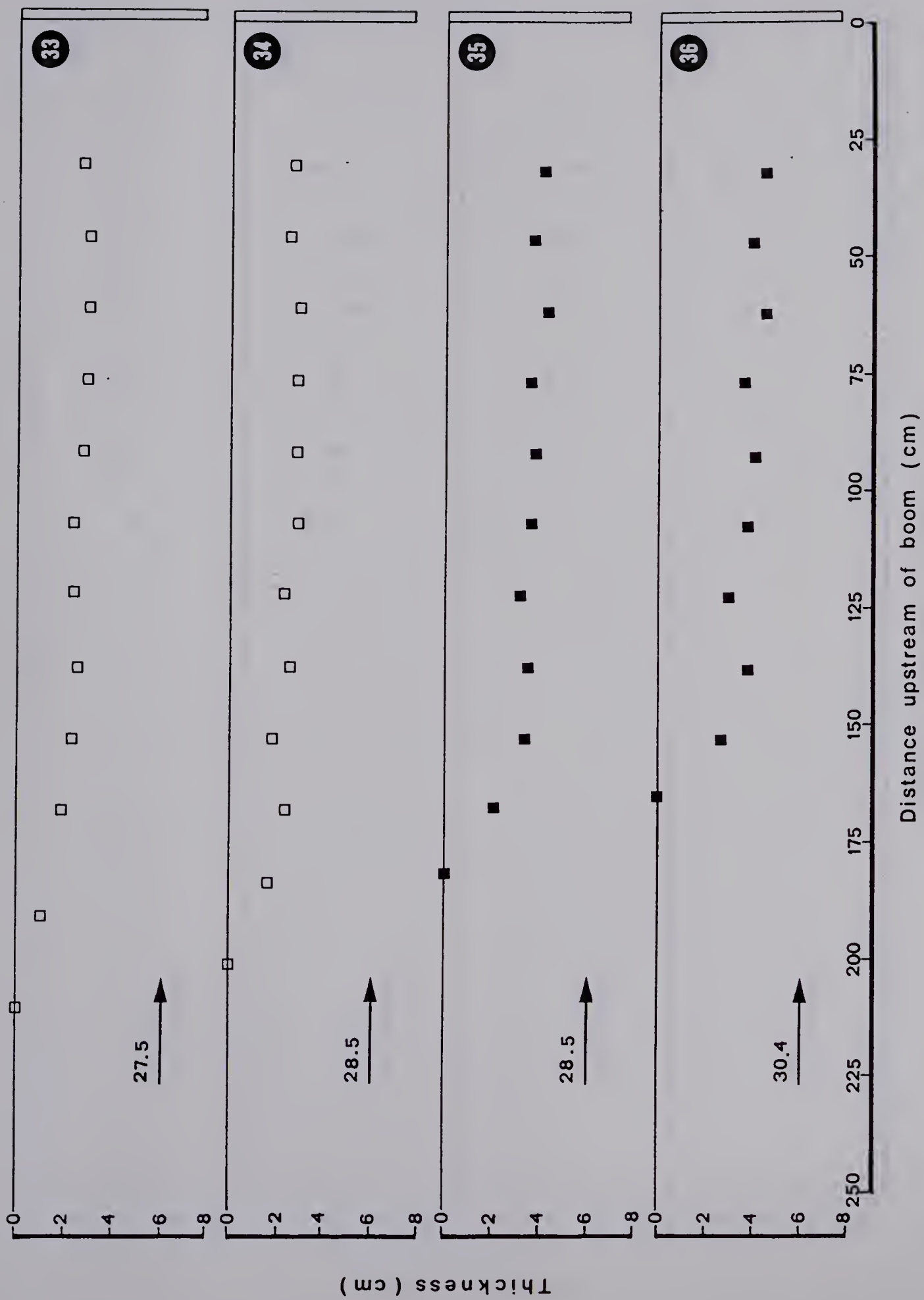




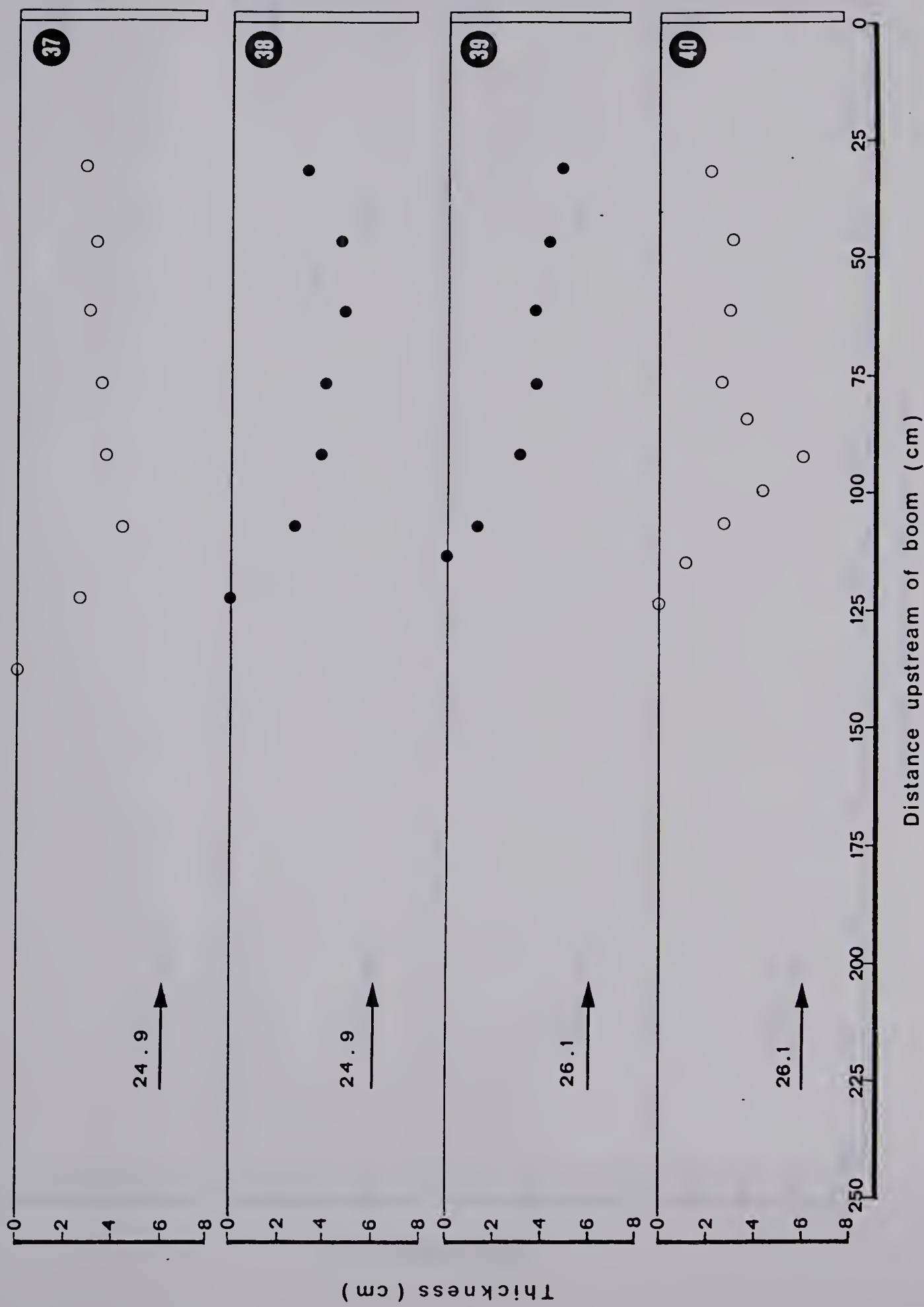




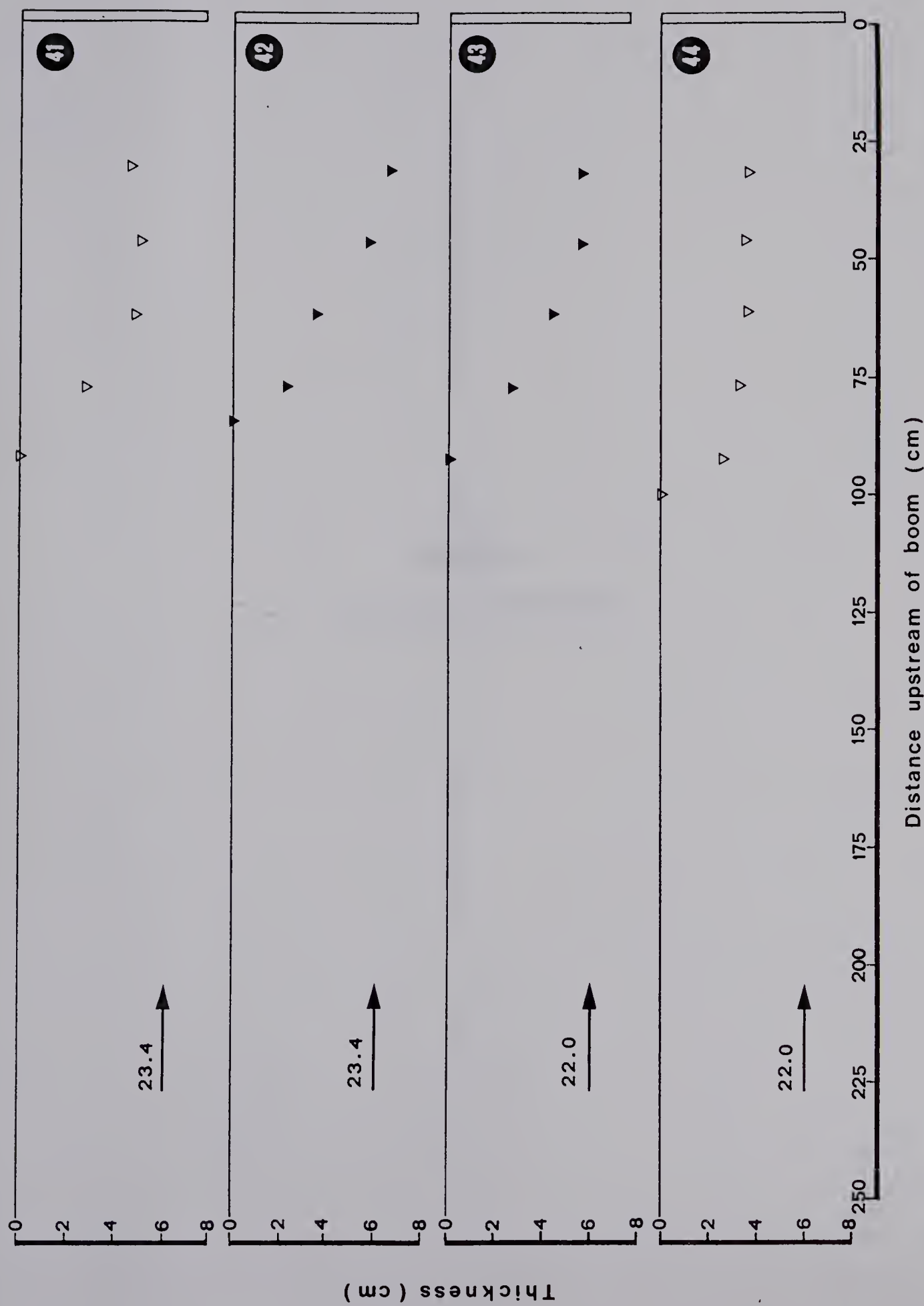








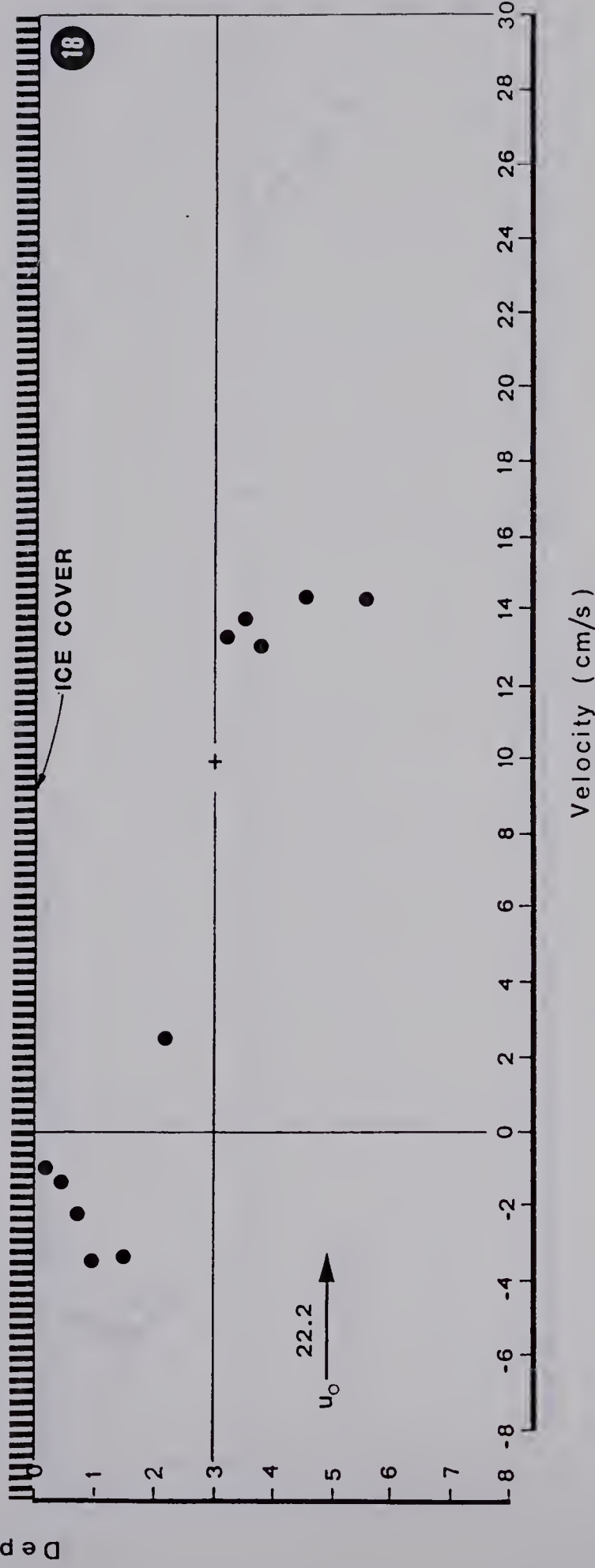
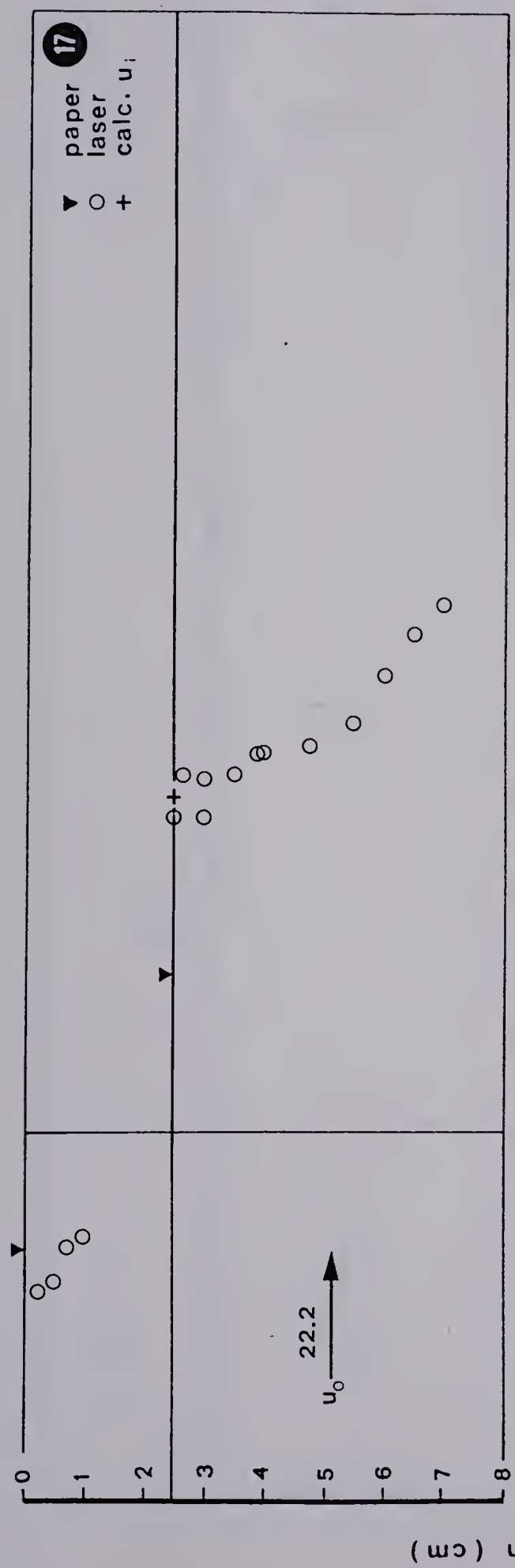




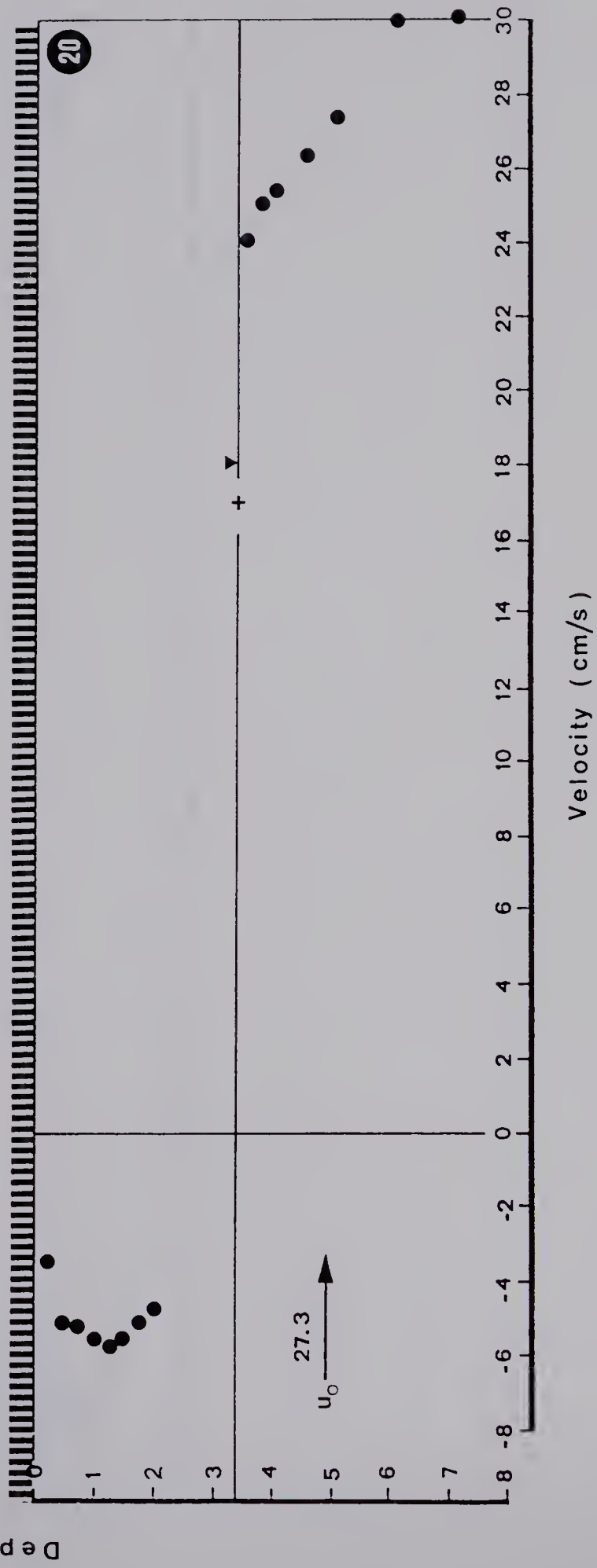
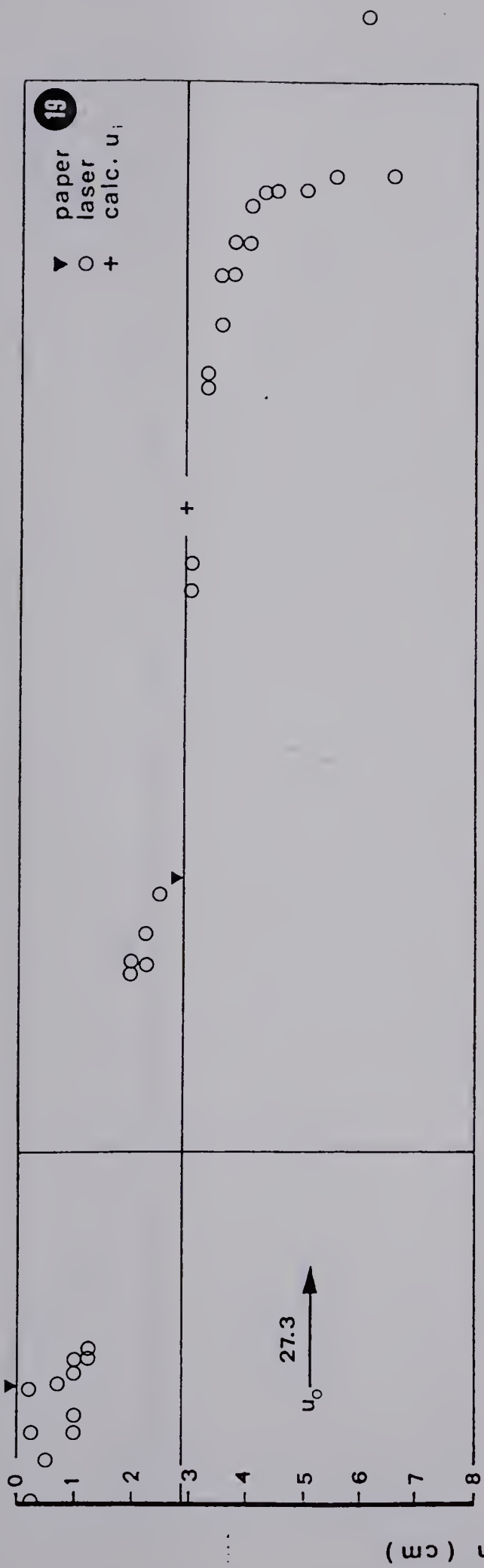


APPENDIX B  
OIL VELOCITY PROFILES

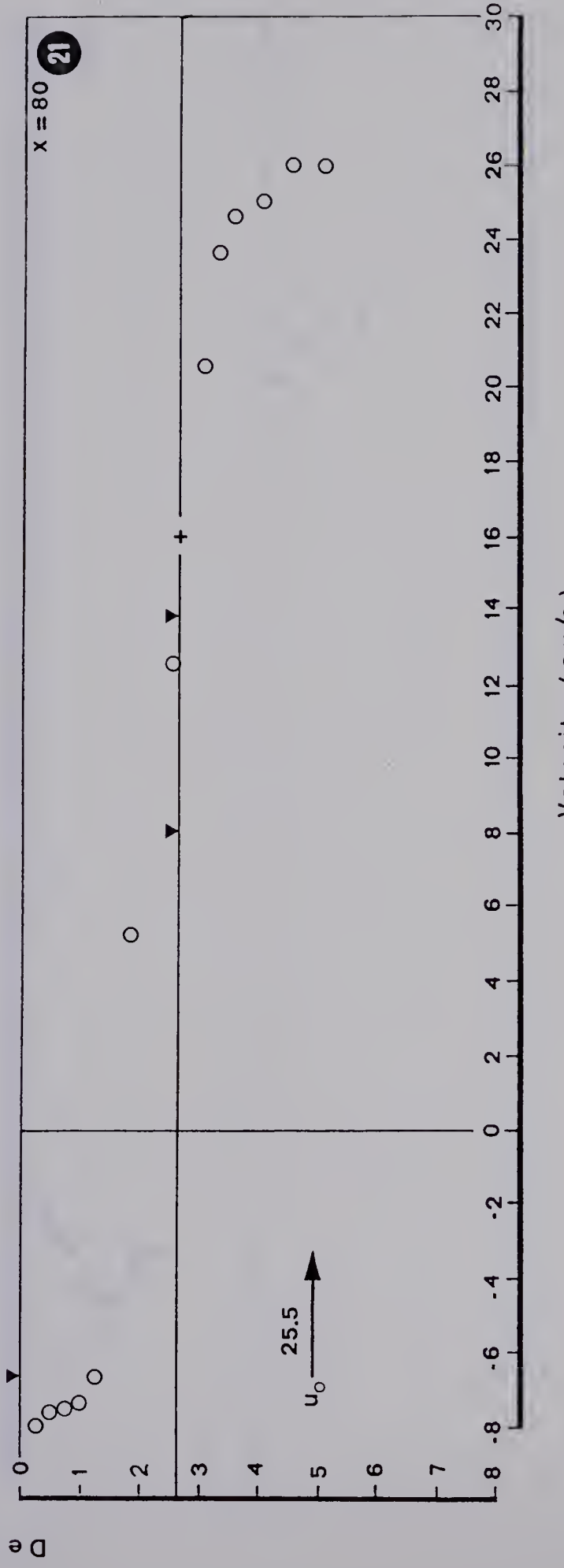
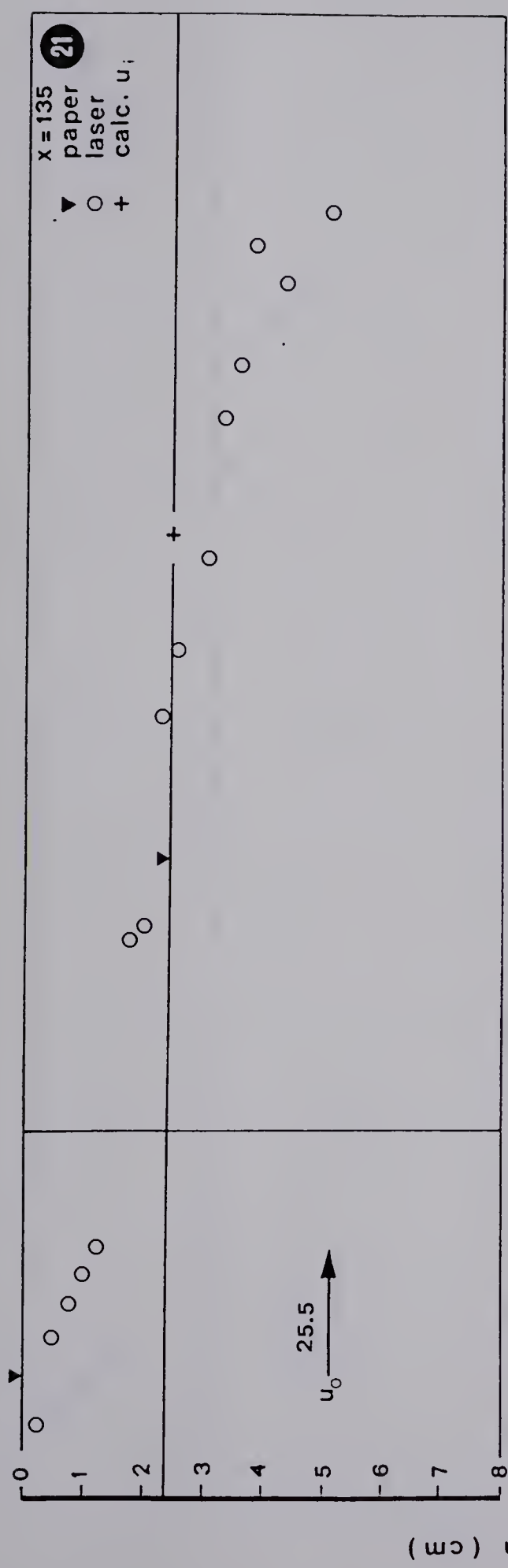




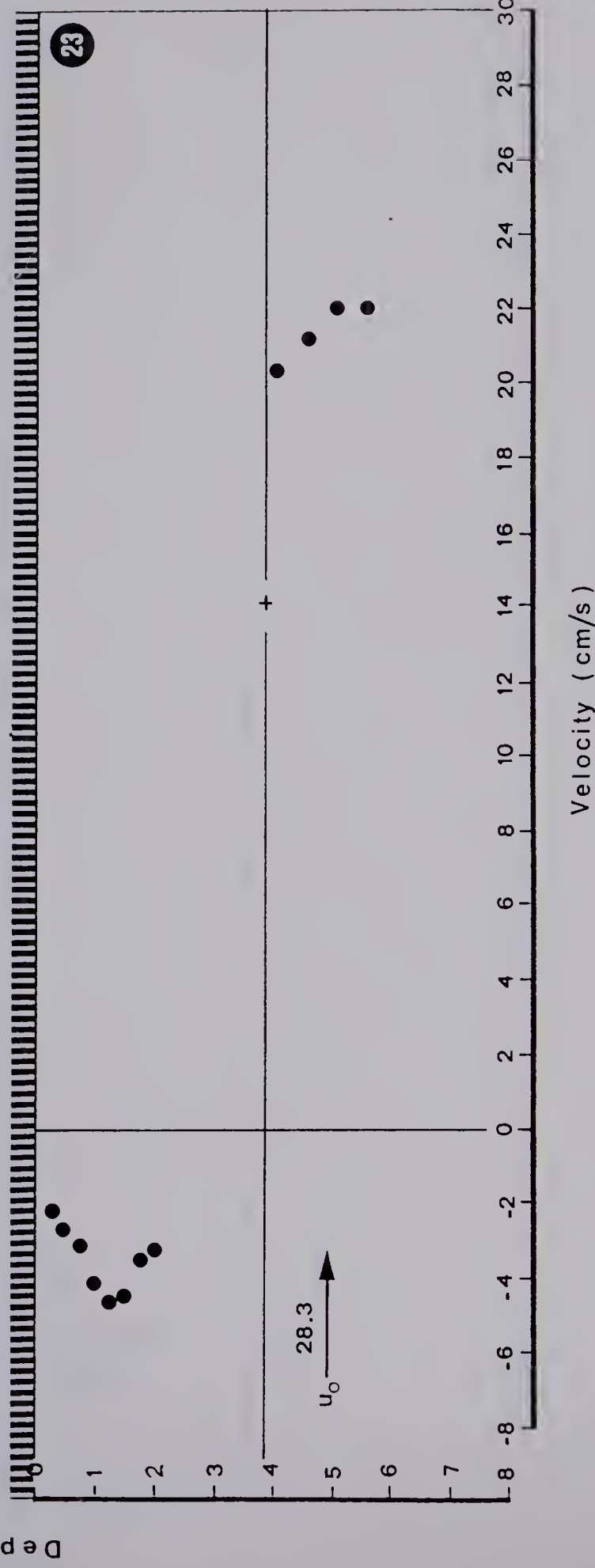
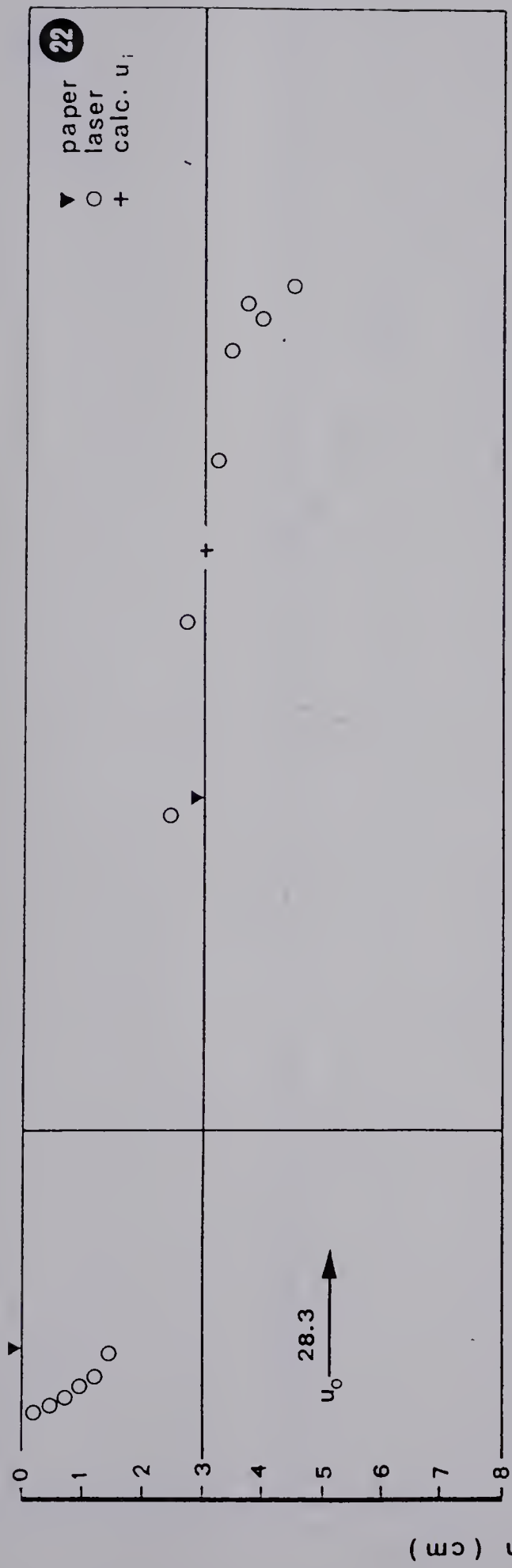




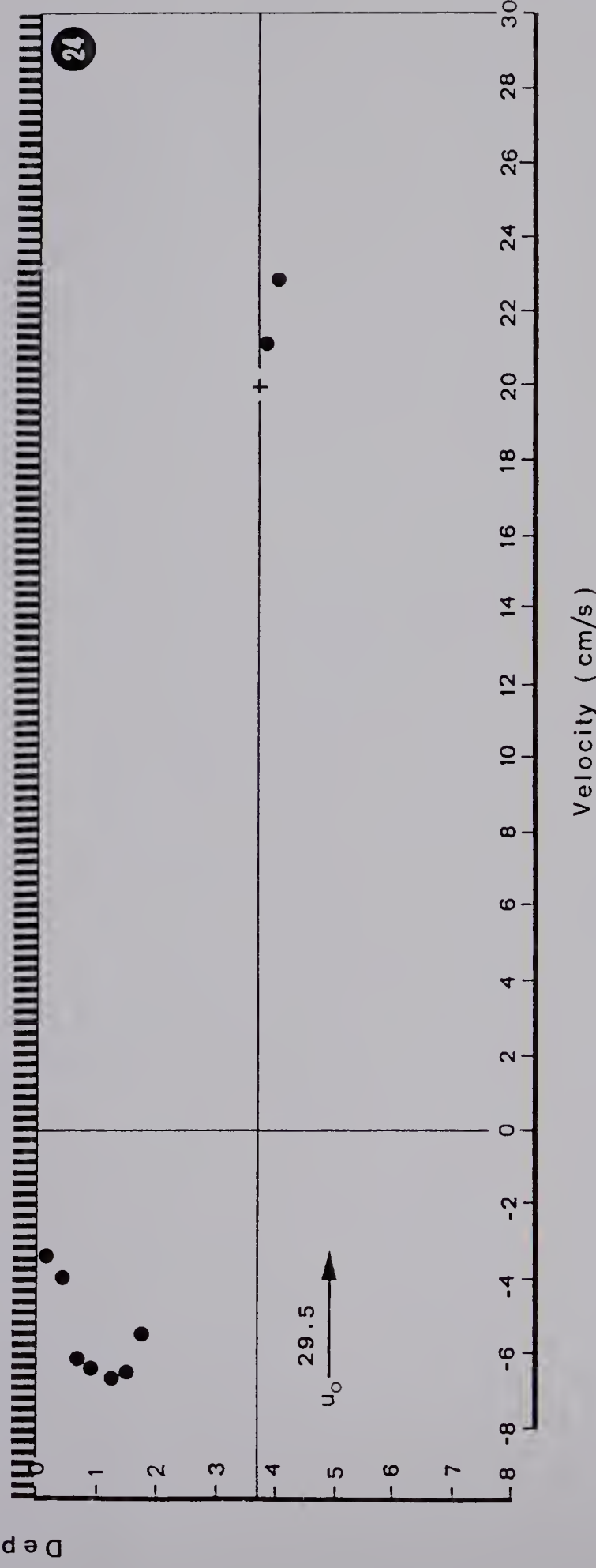
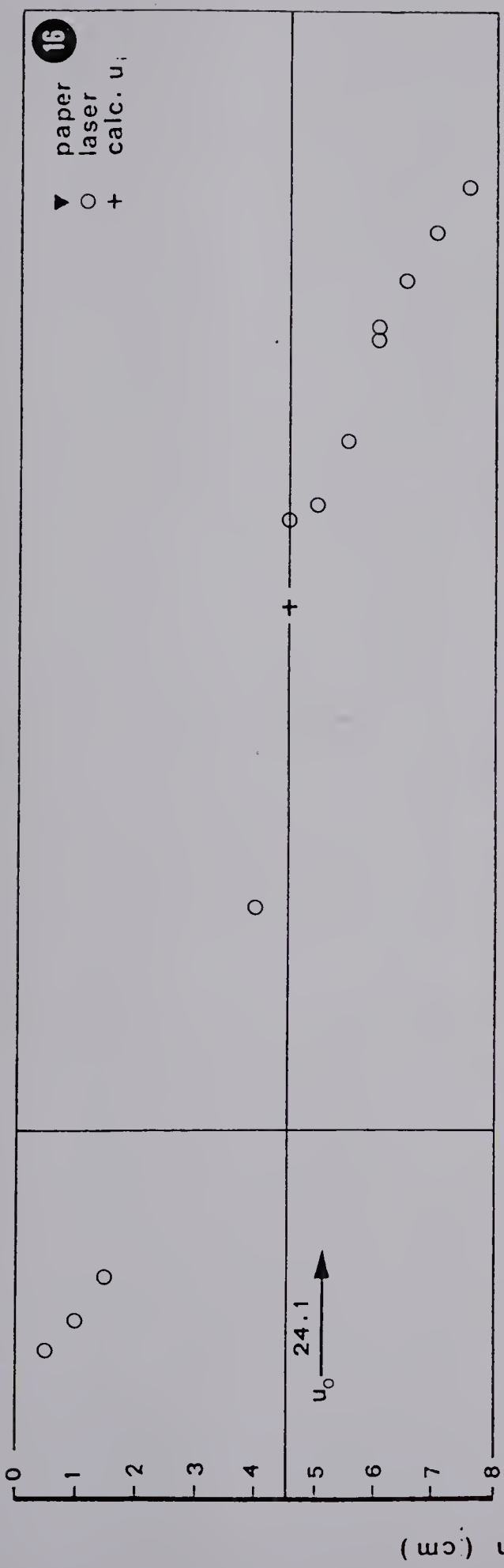




















**B30313**